5-22-2018

# Dynamic Properties of Local Memphis Area Loess

Efrem Weldegebriel Emhatsion

# DYNAMIC PROPERTIES OF LOCAL MEMPHIS AREA LOESS

By

Efrem Weldegebriel Emhatsion

A Thesis

Submitted in Partial Fulfillment of the

Requirement for the Degree of Master of Science

Major: Civil Engineering

The University of Memphis

May 2018

Dedicated To

My Parents, My Fiancée and

My Son

## ACKNOWLEDGMENTS

First and foremost, I would like to thank my advisor Dr. David Arellano for his guidance, support, valuable suggestions, and patience through the course of this thesis and for teaching several fine geotechnical courses.

I am also very grateful to my committee members: Dr. Roger Meier and Dr. Shahram Pezeshk for their advice and thorough review of this thesis. Thank you to the University of Memphis Civil Engineering Department for the financial support over the past two years.

Thanks are also extended to my fellow graduate students, Paras Panadi and Sudip Khadka, for the numerous discussions we shared. I would also like to express my appreciation to Dawit Mebrahtom, Ghezae Fisseha, and Tsehaye Habtom for reviewing my thesis. Finally, I want to thank my family and friends for their love, support, and encouragement.

## ABSTRACT

This study was motivated by the fact that the current practice for performing seismic site response analysis in the Memphis area uses shear modulus degradation and damping that are based on test results of soils obtained outside of the Memphis area. Memphis is located in the New Madrid seismic zone and is covered predominantly by loess soil. Loess has unique behavior from other soils. The purpose of the research is to determine the dynamic properties of Memphis area loess. In order to investigate the dynamic properties, remolded specimens with varying saturation levels and densities were prepared and tested using a resonant column and torsional shear device. Each specimen was tested at increasing confining stress and strain amplitudes.

Shear modulus degradation and material damping curves were developed to evaluate the parameters that affect the dynamic properties of loess. The influence of void ratio, confining pressure, coefficient of lateral earth pressure, and saturation on shear modulus and damping ratio were evaluated. The dynamic properties of loess soil was found to vary at low saturation, 23%, and remains the same from medium to high saturation levels, 36% to 74%. The effect of confining stress is found to be more pronounced at low saturation than at high saturation and the influence of void ratio is found to be insignificant. Shear modulus degradation of loess soil increases slightly but damping remains constant with the decrease of coefficient of lateral earth pressure. The test results were also compared with current shear modulus degradation and damping models. Seismic site response analysis was also performed to further compare the impact of using current models and this study test results on ground response.

**TABLE OF CONTENTS**

## LIST OF TABLES

## LIST OF FIGURES

# 1 INTRODUCTION

## 1.1 Background

Earthquakes generate ground shaking that may trigger landslides, liquefaction, and settlement that can result in tilting and collapse of structures. The nature and distribution of earthquake damage can be influenced by the soil-structure interaction, site conditions (such as soil deposits and topography), the path of the seismic wave (such as distance, and wave propagation, reflection, dispersion, or attenuation), and source conditions (such as type of fault, rupture process, and directivity effects). This study focuses on the site effects, i.e., characterization of local soil deposit.

The New Madrid Seismic Zone (NMSZ) is the most active earthquake region in the Central and Eastern United States (CEUS) (Tavakoli et al. 2010). It is located in the northern part of the Mississippi embayment, which comprises of parts of Illinois, Indiana, Missouri, Arkansas, Kentucky, Tennessee, and Mississippi (U.S. Geological Survey 1995). Memphis, located within the NMSZ, is covered predominantly by loess soil, an Aeolian (wind-blown) silt. The dynamic properties of sands and clays have been studied extensively (Hardin and Drnevich 1970; Dobry and Vucetic 1987; Darendeli 2001). However, there is a significant lack of information on the dynamic properties of loess soil. In this study, the dynamic properties of loess soil from Memphis area are investigated using a Resonant Column and Torsional Shear (RCTS) device.

The dynamic properties of soils are expressed in terms of shear modulus, G, and material damping, D. Shear modulus relates the change in shear stress to shear strain, and damping ratio is a measure of the dissipation of energy within soil. These two parameters can be determined in the laboratory or the field using various techniques. Maximum shear modulus, $G_{max,}$ which occurs at a very low strain level ($< 10^{-4}$ %) because shear modulus decreases with shear strain, is

very sensitive to specimen disturbance and testing conditions. Therefore, in practice, $G_{max}$ is determined from shear wave velocity, $V_s$, using in-situ tests. However, the strain-dependent shear modulus degradation, $G/G_{max}$, which describes the decrease of G with increasing shear strain, is very difficult to obtain in the field and is produced using laboratory tests (Ishihara 1996). A variety of laboratory techniques such as cyclic torsional shear tests, cyclic direct simple shear tests, cyclic triaxial tests, and resonant column tests are used for the measurement of shear modulus and damping. The resonant column testing method, ASTM D4015-15 is widely used for the evaluation of dynamic properties of soils and has been used in this study (ASTM 2016). It is based on harmonic excitation and determines the resonance by sweeping the frequency. Then, the shear modulus is calculated using the resonance and damping is computed using the free vibration decay and the logarithmic decrement method.

Dynamic soil properties, shear modulus and damping ratio, are affected by various factors such as strain amplitude, confining pressure, void ratio, overconsolidation ratio, loading frequency, temperature, and anisotropic stress (Hardin and Drnevich 1972). Darendeli (2001) concluded that confining stress and plasticity index have considerable influence on the shear modulus degradation and damping curves, but parameters such as frequency, number of cycles, overconsolidation ratio, void ratio, saturation degree, and grain characteristics have minimal effect. However, Dobry and Vucetic (1987) inferred that increase of void ratio increases shear modulus degradation in clay soils. Moreover, shear modulus degradation of loess soil is found to be dependent on saturation level (Jennings et al. 1997).

In this study, the dynamic properties of remolded Memphis area loess soil are determined using the RCTS and the effects of confining pressure, void ratio, saturation, and coefficient of

lateral earth pressure, k, are evaluated. The results of this study are also compared with the literature and site response analysis is performed to analyze the practical effect of the results.

## 1.2 Goal and Objectives of the Research

The overall goal of this study is to investigate the dynamic properties of Memphis area loess soil. The main objectives of this research include:

1. Investigate the influence of saturation on the dynamic properties of loess; i.e., shear modulus degradation and damping ratio.
2. Determine the influence of confining pressure on the dynamic properties of loess.
3. Determine the influence of void ratio on the dynamic properties of loess.
4. Examine the influence of coefficient of lateral pressure, K, on the dynamic properties of loess.
5. Compare the measured dynamic property values with current values, curves, and model values included in the literature.
6. Evaluate the influence of test results on seismic site response analysis.

## 1.3 Organization of the Thesis

This thesis is organized into six chapters. This introductory chapter, Chapter 1, describes the background on dynamic properties and presents the goal and objectives this study. Chapter 2 provides an overview of characteristics of loess soil and literature pertaining to the dynamic properties of soils including loess. Chapter 3 reviews the resonant column testing method and the GCTS resonant column and torsional shear device which is employed in this study. It also presents the experimental testing program and the specimen preparation procedure followed in this research.

Chapter 4 presents the results of resonant column tests performed on remolded Memphis area loess soil. The results are used to investigate the effects of saturation, confining stress, void ratio, and coefficient of lateral earth pressure on shear modulus degradation and damping ratio.

Chapter 5 compares the test results of this study with two widely used sets of curves, Darendeli (2001) and EPRI (1993). Another comparison is made with Chang (1992), the only other study carried out on Memphis area loess soil. The chapter also provides the seismic site response analysis that was performed using the test results. Finally, Chapter 6 discusses the main conclusions and recommendations for further research. Appendices A, B, and C presents the laboratory test results for characterizing the loess soil, resonant column test results, and design example, respectively.

# 2 LITERATURE REVIEW

## 2.1 Introduction

In this chapter, reviews of the characteristics of loess soil and the concept of dynamic properties of soils, as well as loess, is presented. Since shear modulus and material damping ratio are the most important dynamic properties of soils, a brief review of these theories is presented. Particular emphasis is placed on shear modulus degradation and damping curves and factors that affect dynamic properties of soils. The most common curves used in practice, EPRI (1993) and Darendeli (2001), are also discussed. A review of past studies dealing with loess soils that pertain to this research is also included in this chapter.

## 2.2 Characteristics of Loess Soil

Loess is wind-deposited sediment transported from the floodplains of glacial and other rivers after the glaciers melted during the arid and semi-arid periods following periods of Pleistocene continental glaciation. Loess typically consists predominantly of silt and a lesser quantity of clay and fine sand particles (Parsons et al. 2009).

Loess soil can be classified as clayey loess, silty loess, and sandy loess depending on the content of clay, silt, and sand. Coarser loess grains are angular with little rounding and polishing and composed of crystals of quartz, feldspar, volcanic ash shards, carbonates, and micas (Sartori 2000). Loess may not easily be distinguished from loess-like deposits (Kane 1968). Loess differs in proportions of silt, clay, sand, as well as color, porosity, strength, and plasticity from loess-like deposits. Typical loess is characterized by high porosity and a significant amount of macroscopic pores as a result of aeolian deposition. It can also have a high potential for consolidation, low stability, and high permeability. Typical loess has a pale yellow color, but

sometimes it may be grey, red or brown (Johnson et al. 2007). Due to the silty nature of loess, it is very vulnerable to erosion, wind, and seismic activity.

One of the unique aspects of loess is that the unsaturated shear strength of loess is derived primarily from cohesion between particles due to suction and bonding of soil particles provided by clay minerals and calcite (Johnson et al. 2007). Clay consists of minerals such as illite, montmorillonite, kaolinite, chlorite, and vermiculite. Calcite is formed by the flow and stagnation of hydrocarbon-bearing groundwater, precipitation, by weathering of calcareous shells and the presence of microorganisms. Secondary carbonate can also form calcite chemically from carbon dioxide present in soils and groundwater and the release of calcium during weathering of anorthite. Moreover, there are small amounts of minerals like pyrite, iron-oxides or -hydroxides and aluminum-hydroxides (Sartori 2000).

Unsaturated loess has high strength and the unique ability to stand and support loads on nearly vertical slopes. However, loess has low shear strength when it is saturated due to loss of suction and weakening of inter-particle cohesive bonds provided by clay mineral and calcite.

In West Tennessee, the liquid limit and plastic limit of loess generally ranges from 25-45 and 23-26 respectively, and plasticity index ranges from 5 to 25. The lower values are for sandy loess while the higher values are for clayey loess. The specific gravity ranges from 2.68 to 2.71. It has low sand content with less than 1% retained on a #200 sieve (Royster 1965; Sheeler 1968). Chang (1992) found that the Memphis loess has a composition of 75% silt and 25% clay, which can be classified as clayey silt (ML-CL). Also, the specific gravity ranged from 2.64 to 2.77, the void ratio from 0.469 to 0.931, and moisture content from 15 to 30%.

Adrian (2012) also studied two loess soils from Eagle Lake Wildlife Refuge south of Shelby Forest about a mile east of the Mississippi River, and from Fulton Wildlife Refuge along

the east bank of the Mississippi River west of Fort Pillow. Both sites are located just north of Memphis. His test results reveal that the soil from the Eagle Lake Wildlife Refuge has a plasticity index of 7; maximum dry unit weight of 18.83 KN/$m^3$ with an optimum water content of 14%; and is classified as CL-ML. On the other hand, the Fulton Wildlife Refuge soil differs slightly with a plasticity index of 13; maximum dry unit weight of 16.77 kN/$m^3$ at an optimum water content of 20% and is classified as ML.

The loess soil for this study is acquired from a bluff in Fulton Wildlife Refuge but at a different location from where Adrian (2012) obtained his samples. It was tested in the laboratory and is classified as low plasticity clayey silt, ML, with a plasticity index of 1, optimum water content 16.8% and maximum dry unit weight is 17.4 kN/$m^3$. A summary of particle size analysis, Atterberg limits, water content, and compaction test results are included in Appendix A.

## 2.3 Dynamic Properties of Soils

In seismic analysis, the dynamic properties of soil in the low (<0.001%) and medium (0.001 to 0.1%) strain range are essential. The severity of earthquake damage to structures is strongly influenced by the dynamic response of soils to cyclic loading. Dynamic analysis of any structure requires the determination of two important parameters; shear modulus and damping ratio. Shear modulus determines the deformation characteristics and is related to the soil stiffness while damping describes energy dissipation during cyclic loading (Das and Ramana 2011). A summary of shear modulus and damping is presented in the next sections.

### 2.3.1 Shear Modulus

Shear modulus, G, represents the ability of soil to resist shear deformation. It is defined as the ratio of shear stress ($\tau$) to shear strain ($\Upsilon$) (Das and Ramana 2011). When soil is excited by harmonic loading, the stress-strain response is linear for small strain ($\gamma \leq 0.001\%$) and nonlinear

for medium and large strain ($\gamma > 0.001\%$) as shown Figure 2.1. The cyclic response of a soil can be represented by a hysteresis loop for each period of the oscillation in the stress-strain diagram (Kavazanjian et. al, 1997). Figure 2.1 shows one complete period of oscillation. There are two types of shear modulus, the secant modulus, and the tangent modulus. The secant modulus or equivalent modulus is the slope of the line connecting the origin with the inversion point between loading and unloading, and it decreases as the level of strain increases as shown in Figure 2.1. The tangent modulus is the slope of the tangent line at any point on the stress-strain backbone curve. The backbone curve is the first loading curve that connects the load inversion points of oscillation. It has a hyperbolic shape. The maximum shear modulus ($G_{max}$) is equal to the tangent modulus in the low strain range (typically less than or equal to $10^{-4}$ %) or at the origin as shown in Figure 2.1.

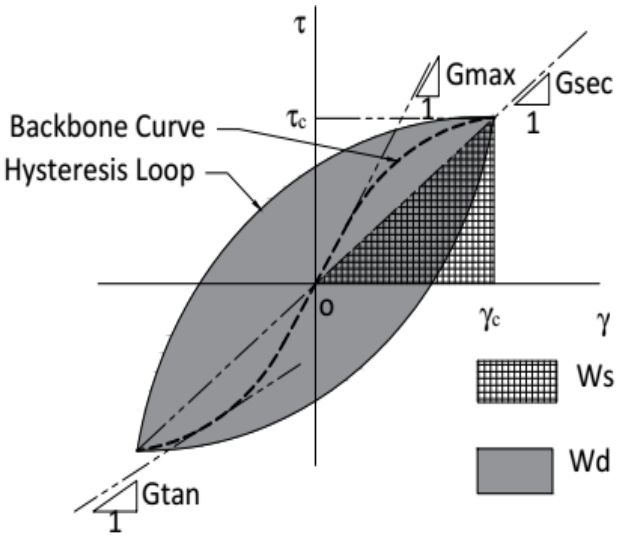


Figure 2.1: Typical hysteretic stress-strain response of soil subjected to cyclic loading (Kavazanjian et. al, 1997)

Maximum shear modulus, $G_{max,}$ is very sensitive to confining pressure, age, sample preparation, cementation, overconsolidation ratio, plasticity index, number of loading cycles and

stain rate (Kramer 1996). It can be measured by laboratory or in-situ tests. However, better accuracy is achieved by geophysical tests rather than laboratory tests for two reasons: (1) an undisturbed lab specimen is very difficult to achieve, especially of loess, due to inevitable disturbance from excavation, penetration, transportation and trimming process; (2) remolded specimens that are perfectly prepared with the same density, water content, and void ratio cannot replicate the microstructure of the in situ soil due to breakdown in material structure. Usually, insitu soils are stiffer due to geologic aging and cementation. Therefore, using laboratory measured normalized shear modulus reduction curves with an in-situ measured $G_{max}$ is a better way to find the value of shear modulus at any shear strain level. The shear modulus reduction curve describes the decrease of $G/G_{max}$ with increasing shear strain. The $G_{max}$ can be calculated from the field measured shear wave velocity and soil density as (Dobry and Vucetic 1987)

$$G_{max} = \rho . V_s^2 \tag{2.1}$$

where $G_{max}$ is maximum shear modulus, $\rho$ is the soil density in kg/m$^3$ and $V_s$ is the shear wave velocity in m/s.

Using the equivalent-linear analysis method (Kramer, 1996), the secant shear modulus ($G_{sec}$) can be determined for any point on the hysteresis loop as

$$G_{sec} = \frac{\tau}{\Upsilon_c} \tag{2.2}$$

where $\tau$ is shear stress, and $\Upsilon_c$ is strain amplitude at the inversion point as shown in Figure 2.1 and Figure 2.2(a).

In the absence of field tests, empirical relationships can be used to estimate $G_{max}$. Hardin and Drnevich (1970) proposed a relationship for the evaluation of maximum shear modulus for all soils by

$$G_{max} = 14760 \frac{(2.973 - e)^2}{1 + e} (OCR)^a \ \sigma_m^{1/2} \quad (2.3)$$

where $G_{max}$ is maximum shear modulus in psf,

*e* is void ratio,

*OCR* is over consolidation ratio,

*a* is a parameter that depends on the plasticity index and a is 0, 0.18, 0.3, 0.41, 0.48, 0.5 for PI 0, 20, 40, 60, 80 and >100 respectively, and

$\sigma_m$ is mean principal effective stress.

Shear modulus generally decreases with an increase of shear strain. Shear modulus degradation characterizes the change of shear modulus with an increase of shear strain. A plot of $G/G_{max}$ versus shear strain provides a modulus degradation curve as shown in Figure 2.2(b).

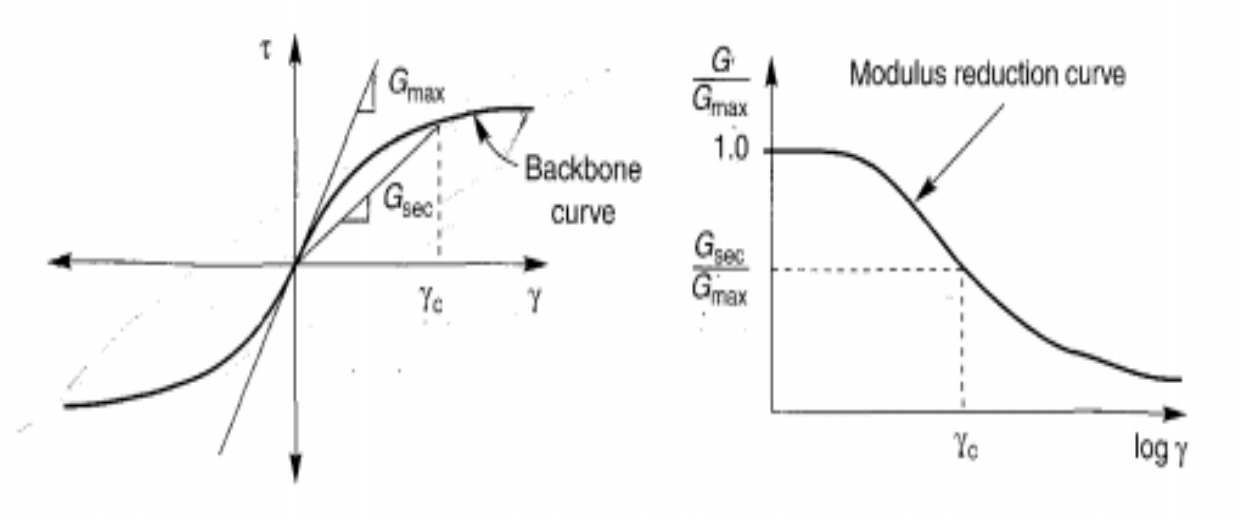


Figure 2.2: Typical (left) backbone curve and (right) shear modulus degradation curve (Kramer 1996).

### 2.3.2 Damping Ratio

Damping is a measure of energy dissipation or decrease of excitation over time. There are two types of damping: material damping and radiation damping. Material damping is the

dissipation of energy due to internal soil friction during each cycle of a given strain amplitude, whereas radiation damping is a dissipation of energy due to geometric spreading of the waves through space (Kramer 1996; Wu 2014). Material damping will be the focus of this study since it is predominant and is typically the only one considered in site response analysis.

Material damping occurs due to hysteretic damping and viscous damping (Kramer 1996). Hysteretic damping is caused by dry frictional resistance between soil particles and occurs in the nonlinear range of the strain threshold and is independent of the frequency of the loading, while viscous damping is caused by the movement of soil particles in a fluid medium and occurs in the linear range and is highly dependent on the frequency of the loading (Verruijt 2009). According to Verruijt (1994), hysteretic damping contributes more to soil damping than viscous damping and, therefore, hysteretic damping is a more accurate representation of the damping behavior of soils than viscous damping.

Material damping of soils is a function of the shear strain amplitude of the loading cycle, and not solely a function of the material (Ishihara 1996). Therefore, damping ratio expresses the level of damping in a system relative to critical damping. It is the ratio of the damping coefficient to the critical damping coefficient and is the key soil dynamic property to define damping provided by

$$D = \frac{C}{C_c} = \frac{C}{2\sqrt{Km}} \tag{2.4}$$

where $C$ is the damping coefficient, $C_c$ is the critical damping coefficient, $K$ is an elastic spring constant and $m$ is mass.

The critical damping corresponds to the limit between oscillatory motion and non-oscillatory motion. The system is over-damped for D > 1, critically damped for D = 1 and under

damped for D < 1. Damping ratio can also be determined from the area of the hysteresis loop, $W_d$, and the area of the triangle represented by $W_s$ shown in Figure 2.1 by (US DOT 1997)

$$D = \frac{W_d}{4\pi W_s} \tag{2.5}$$

where $W_d$ is the energy dissipated in one cycle of loading, which is equal to the area inside the hysteresis loop in Figure 2.1, and $W_s$ is the maximum strain energy stored during the cycle, which is equal to the area of the triangle in Figure 2.1.

Several factors can influence the damping ratio. It decreases with increasing effective confining stress, decreasing void ratio, increasing plasticity index, and cementation. It also increases with increasing strain rate whereas overconsolidation ratio (OCR) has no significant influence (Darendeli 2001; Vucetic and Dobry 1991; Hardin and Drnevich 1972). Figure 2.3 shows the effect of plasticity index on damping ratio (Vucetic and Dobry 1991). As shown in Figure 2.3, the damping ratio decreases as plasticity index increases.

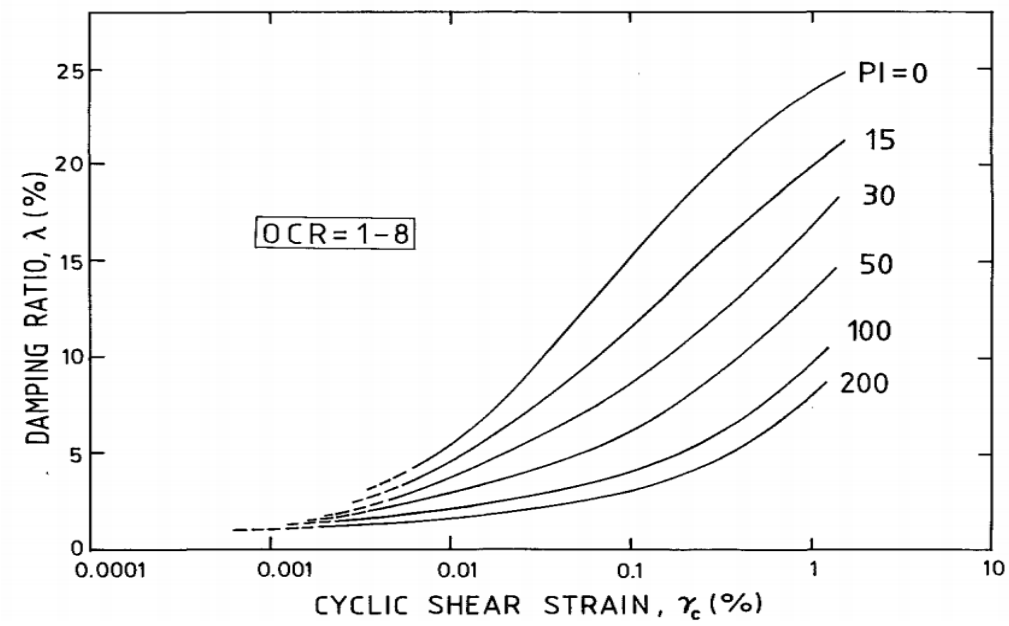


Figure 2.3: Damping ratio curves and soil plasticity for normally and overconsolidated Soils (Vucetic and Dobry 1991).

### 2.3.3 Shear Modulus Degradation and Material Damping Curves

The nonlinear behavior of dynamic soil properties is usually described by shear modulus degradation and damping curves. The shear modulus degradation curve is a representation of the secant shear modulus divided by the initial shear modulus, $G/G_{max}$ as a function of shear strain, while the damping curve describes the increase of D with increasing shear strain at a constant confining pressure. The variations of shear modulus and material damping ratio with increasing shearing strain are important for characterizing soil behavior during strong ground shaking. Soil behaves linearly under very small cyclic shear strain and nonlinearly when the strain reaches a threshold shear strain.

According to Vucetic (1994), there are two types of cyclic thresholds which represent boundaries of different cyclic behaviors: linear cyclic threshold shear strain ($\gamma_{tl}$), and volumetric cyclic threshold shear strain ($\gamma_{tv}$). The magnitudes of these threshold values, which are shown in Figure 2.4 and described in Table 2.1, are dependent on soil type. Figure 2.4 shows typical shear modulus reduction ($G_{SN}/G_{maxN}$ vs $\gamma_c$) and damping ($\lambda_N$ vs $\gamma_c$) curves and Table 2.1 explain the linearity, elasticity property, reduction of strength and suitable method of analysis for very small, small, and medium to large level of strains. The study summarized various prior studies done on $\gamma_{tv}$ of different soils and the range is from 0.005% to 0.27%. This cyclic threshold categorization enables selection of suitable methods of site analysis, i.e., linear, equivalent linear, or nonlinear method, for a given soil and anticipated level of cyclic shear strain.

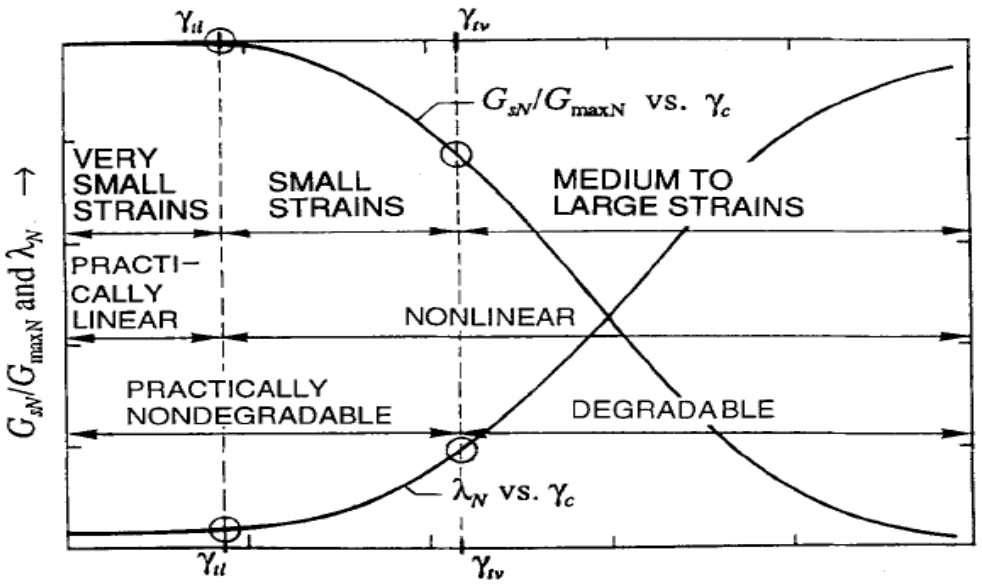


Figure 2.4: Shear modulus reduction and damping ratio vs. strain curves (Vucetic 1994)

Table 2.1: Practical ranges of strain amplitude for soil dynamics problems (Vucetic 1994)

| Range of $\Upsilon_c$ | | Linearity | Elasticity and Plasticity | Degradable for Fully Saturated Soils Cyclically Sheared in Undrained Conditions | Suitable Method of Analysis |
|---|---|---|---|---|---|
| Very small | $0 < \Upsilon_c \leq \Upsilon_{tl}$ | Practically linear | Practically elastic | Essentially non-degradable | Linear Elastic |
| Small | $\Upsilon_{tl} < \Upsilon_c \leq \Upsilon_{tv}$ | Nonlinear | Slightly elastoplastic | Practically non-degradable | Equivalent Linear |
| Medium to Large | $\Upsilon_c > \Upsilon_{tv}$ | Nonlinear | Elastoplastic | Degradable | Nonlinear |

Various researchers such as Hardin and Drnevich (1972); Seed and Idriss (1970); Vucetic and Dobry (1991); EPRI (1993); and Darendeli (2001) developed curves and empirical relationships that are widely used in practice to estimate the shear modulus and damping. Hardin and Drnevich (1972) used the hyperbolic model in their relationship to describe nonlinear soil behavior under cyclic loading. The hyperbolic model assumes that the stress-strain curve of soil can be represented by a hyperbola asymptotic to the maximum shear stress. The hyperbolic form can be expressed as

$$\frac{G}{G_{max}} = \frac{1}{1 + {\Upsilon}/{\Upsilon_r}} \tag{2.6}$$

where G is shear modulus, $G_{max}$ is maximum shear modulus at very small strains, $\Upsilon$ is shear strain and $\Upsilon_r$ is the reference strain defined as the shear strength divided by $G_{max}$. The damping curve is related to shear modulus degradation as

$$D = D_{min}\left(1 - \frac{G}{G_{max}}\right) \tag{2.7}$$

where D is damping and $D_{min}$ is minimum damping at very large strains

Figure 2.5 shows the Electric Power Research Institute (EPRI) empirically derived shear modulus and damping curves for Eastern North America (ENA) (EPRI 1993b). These are the most widely used curves for seismic analysis. Although the EPRI curves are based on extensive test data of California and Taiwan soils, many other studies have found a difference in curves due to soil type and geological formation (Dobry and Vucetic 1987; Ishibashi and Zhang 1993; and Stokoe et al. 1999). A summary of the factors affecting shear modulus and damping ratio is included in the next section of this thesis. The variations of curves have initiated the necessity of investigating the stress-strain behavior of local soils and developing new ones. This study begins the development of shear modulus and damping curves for Memphis area soils.

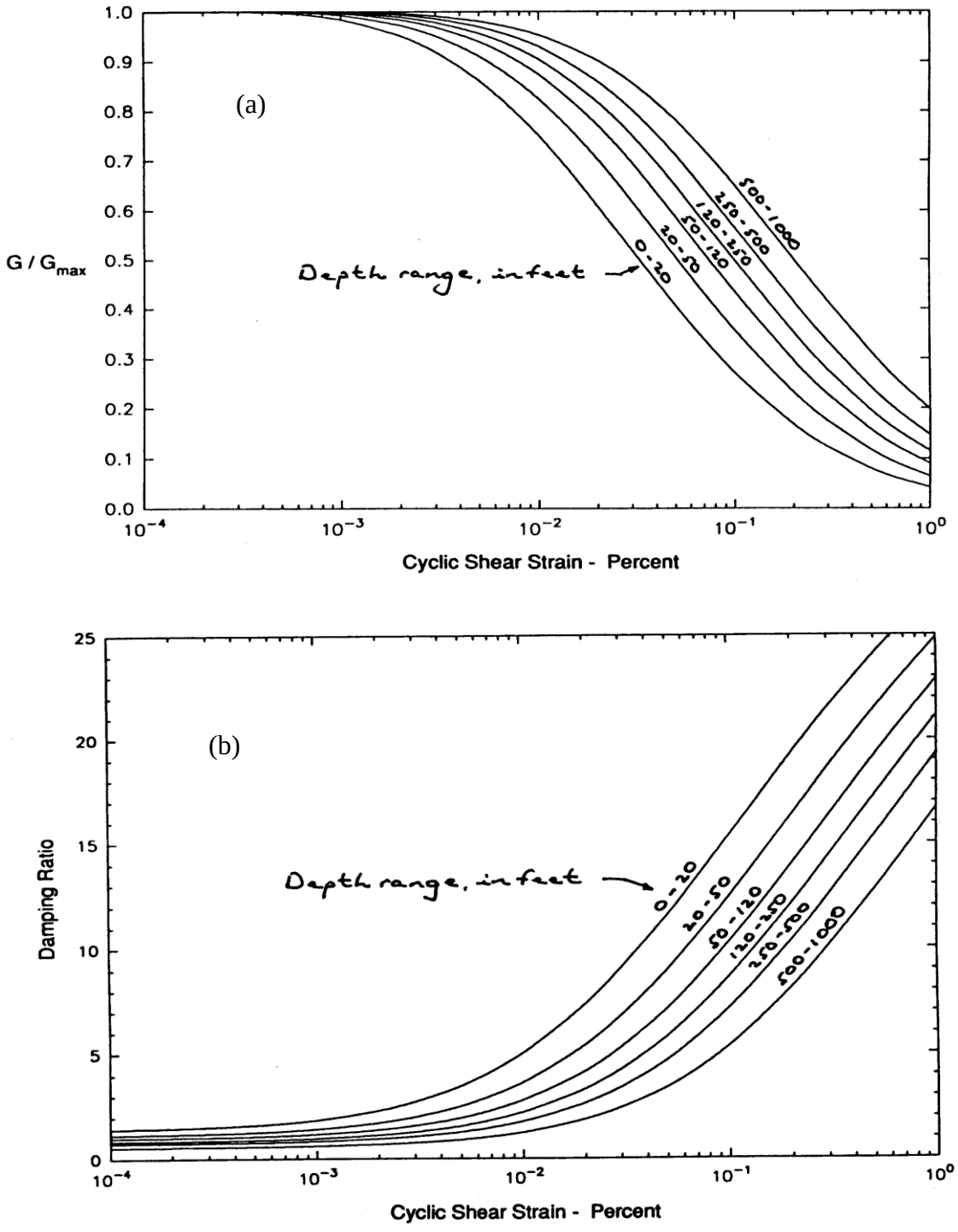


Figure 2.5: Variation in (a) shear modulus reduction, and (b) material damping curves for generic Eastern North America (ENA) sites with depth (EPRI 1993b)

Darendeli (2001) revealed that the simple hyperbolic model of Equation 2.6 has poor fit to actual test data. He improved the fit by integrating a curvature coefficient and established a modified hyperbolic model as

$$\frac{G}{G_{max}} = \frac{1}{1 + (\gamma/\gamma_r)^a} \tag{2.8}$$

where a is second curve-fitting variable called the curvature parameter equal to 0.919, $\Upsilon_r$ is strain at $G/G_{max} = 0.5$ and it can be related to soil plasticity, overconsolidation and confining pressure as

$$\gamma_r = (0.0352 + 0.001 * PI * OCR^{0.3246})\sigma_o{}'^{0.3483} \tag{2.9}$$

where $\sigma_o$' is mean effective confining pressure (atm), PI is soil plasticity (%), and OCR is overconsolidation ratio.

Darendeli (2001) also determined the damping by adjusting the damping from the Masing relationship and adding minimum damping function as

$$D_{Adjusted} = b * (\frac{G}{G_{max}})^{0.1} * D_{Masing} + D_{min} \tag{2.10}$$

where $D_{Adjusted}$ is scaled and capped material damping ratio (%)

b is a scaling coefficient given by

$$b = 0.6329 + (-0.1069) * ln(N) \tag{2.11}$$

where N is number of loading cycles

$D_{min}$ is the small-strain material damping ratio (%)

$$D_{min} = (0.8005 + 0.0129 * PI * OCR^{-0.1069}) * \sigma_0^{-0.2889} * [1 + 0.291 * ln(frq)] \tag{2.12}$$

$$D_{Masing} = c_1 D_{Masing,a=1.0} + c_2 D_{Masing,a=1.0}{}^2 + c_3 D_{Masing,a=1.0}{}^3 \ (\%) \tag{2.13}$$

$$D_{Masing,a=1.0} = \frac{100}{\pi}\left(4\frac{\gamma - \gamma_r\, ln\left(\frac{\gamma+\gamma_r}{\gamma_r}\right)}{\frac{\gamma^2}{\gamma+\gamma_r}} - 2\right) \quad (\%) \tag{2.14}$$

$$c_1 = 1.1143a^2 + 1.8618a + 0.2523 \tag{2.15}$$

$$c_2 = 0.0805a^2 + 0.0710a + 0.0095 \tag{2.16}$$

$$c_3 = 0.0005a^2 + 0.0002a + 0.0003 \tag{2.17}$$

Darendeli analyzed data obtained from 110 specimens of clay, silt and sand soils and investigated the parameters that affect dynamic properties. He showed that the confining stress and plasticity index had considerable influence on the shear modulus degradation and damping curves and developed a set of curves at varying confining stresses (0.25, 1.0, 4.0, 16 atm) and plasticity indices (0, 15, 30, 50, 100). Other parameters that have a minimal effect include frequency of loading, number of loading cycles, overconsolidation ratio, void ratio, saturation degree, and grain characteristics. Figure 2.6 shows shear modulus degradation and damping curves for PI = 0 and these curves will be compared with the curves developed as part of this study for Fulton loess.

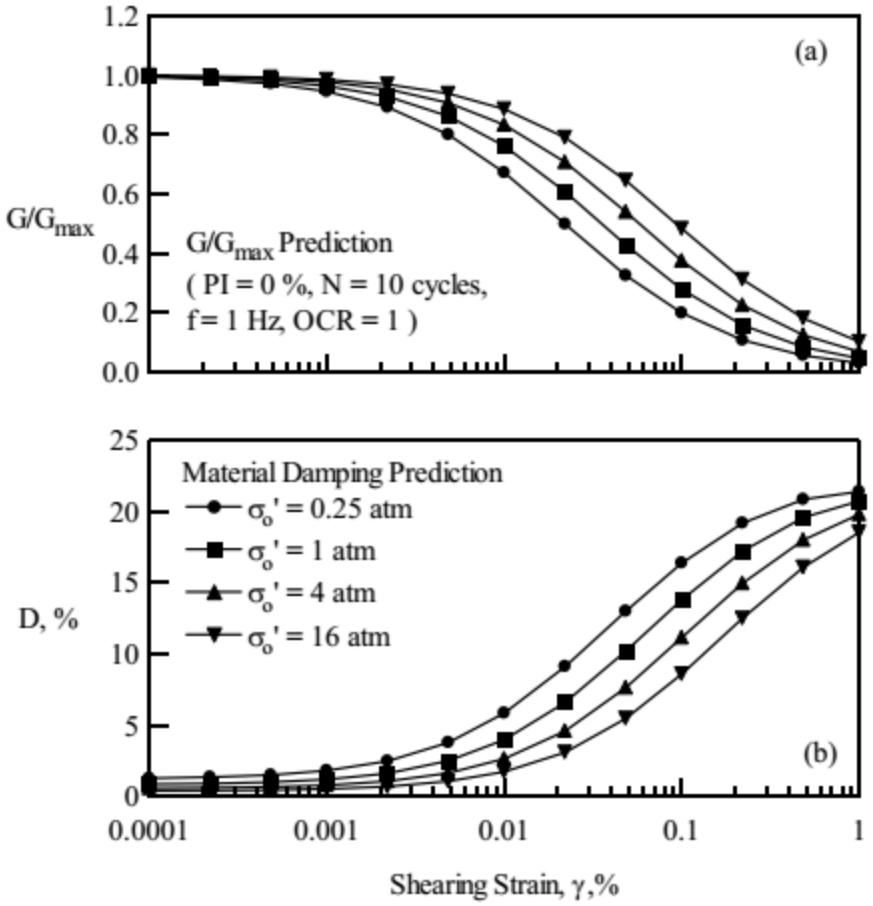


Figure 2.6: Effect of mean effective stress on (a) normalized modulus reduction and (b) material damping curves of a non-plastic soil (Darendeli 2001).

### 2.3.4 Factors Affecting the Shear Modulus and Damping Ratio

The non-linear hysteretic characteristics of soil under cyclic loading can be affected by the insitu condition and natural environment of the soil, i.e., soil density, soil structure and angularity, plasticity, void ratio, gradation, confining pressure, OCR, cementation and geologic age, water content and saturation and loading condition factors such as strain amplitude, strain rate and number of loading cycles (Çabalar 2009; Darendeli 2001; Kim et al. 1991).

Some of the factors mentioned above and their influence on soil stiffness have strong correlations with one another. The effect of the number of loading cycles on the soil stiffness

only becomes apparent for strain amplitudes over a certain threshold (Pinto 2012). The effect of these factors is also dependent on soil type. Moreover, the effect of overconsolidation is more pronounced on high plasticity soils than non-plastic soils. For a normally consolidated soil, magnitude and duration of confining pressure have a larger effect on clayey soils than on sandy soils (Darendeli 2001). Table 2.2 includes a summary of factors that influence shear modulus, shear modulus degradation and damping ratio of clay soil (Dobry and Vucetic 1987).

Table 2.2: Effect of increase of various factors on $G_{max}$, $G/G_{max}$, and D of normally consolidated and moderately overconsolidated clays (Dobry and Vucetic, 1987)

| Increasing Factor | Maximum Shear Modulus ($G_{max}$) | Shear Modulus Degradation ($G/G_{max}$) | Damping Ratio (D) |
|---|---|---|---|
| Confining pressure ($\sigma$) | increases with $\sigma$ | stays constant or increases with $\sigma$ | stays constant or decreases with $\sigma$ |
| Void ratio (e) | decreases with e | increases with e | decreases with e |
| Geological age (t) | increases with t | may increase with t | decreases with t |
| Cementation (c) | increases with c | may increase with c | may decrease with c |
| Overconsolidation ratio (OCR) | increases with OCR | not affected | not affected |
| Plasticity index (PI) | increases with PI if OCR>1; stays about constant if OCR is 1 | increases with PI | decreases with PI |
| Cyclic strain $\gamma_c$ | ---- | decreases with $\gamma_c$ | decreases with $\gamma_c$ |
| Strain rate, $\dot{\gamma}$ (frequency of loading) | increases with $\dot{\gamma}$ | G increases with; $G/G_{max}$ probably not affected if G and $G_{max}$ are measured at the same $\dot{\gamma}$ | stays constant or may increase with $\dot{\gamma}$ |
| Number of loading | decreases after N cycles of large $\gamma_c$ but recovers with time | decreases after N cycles of large $\gamma c$ ($G_{max}$ measured before N cycles) | not significant for moderate $\gamma_c$ and N |

## 2.4 Dynamic Properties of Loess

A large part of the world is covered with loess soil including Asia, Europe, and North America. In the United States, a significant area includes loess soil, as shown in Figure 2.7. The Mississippi Embayment, including the City of Memphis, is overlaid by a layer of loess. The thickness can reach up to 20 m near the Mississippi River and progressively thins eastward for about 70 miles (Moore 1994).


Figure 2.7: Map showing the distribution of loess (orange) in North America (USGS 2016)

The effect of different parameters on the dynamic properties of loess soil has been studied by various researchers such as (Karam et al. 2009; Jennings et al. 1997; Chang 1992; Mosallamy et al. 2014). Jennings et al. (1997) examined the influence of saturation and confining stresses on shear modulus of sandy loess and clayey/silty loess using the Stokoe

resonant column and torsional shear device on undisturbed samples. Figure 2.8 shows the normalized shear modulus results of sandy loess and clayey loess at different saturation levels in relation to the Seed and Idriss (1970) upper and lower bound curves for sand. As illustrated in the figure, the $G/G_{max}$ of the clayey loess is found to be dependent more on the saturation conditions of the soil than on the applied confining stresses, while the sandy loess shear modulus variations were more stress-dependent with no clear relation to the change in saturation. They also concluded that the damping ratio is more sensitive to saturation in clayey loess than sandy loess.

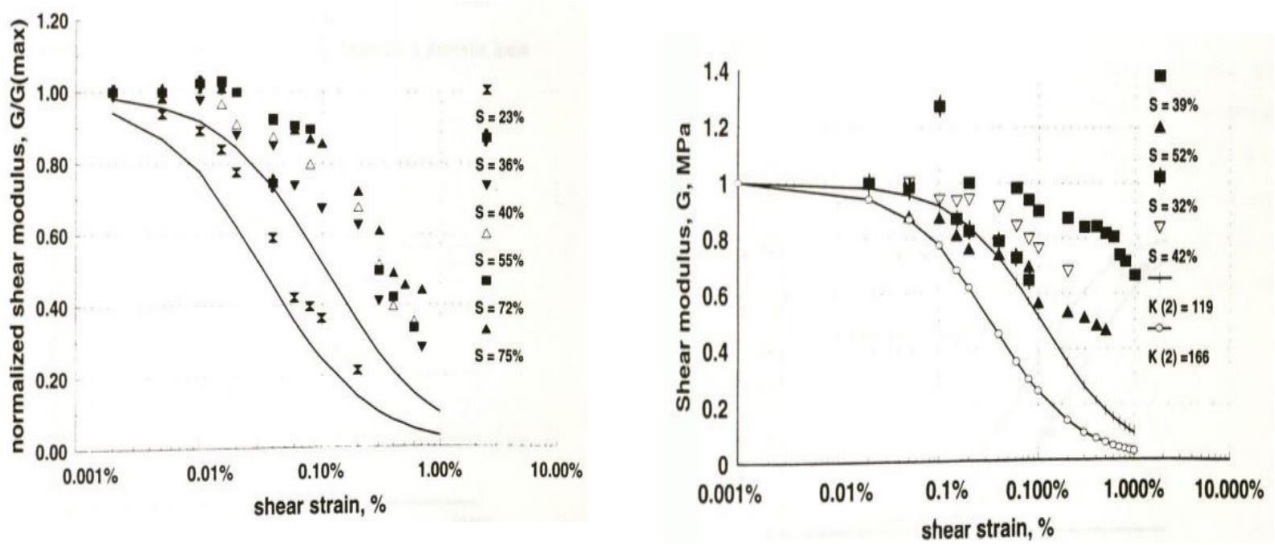


Figure 2.8: Effect of saturation on the normalized shear modulus reduction curve for (left) sandy loess and (right) clayey/silty loess (Jennings 1994).

Mosallamy et al. (2014) also did an extensive experimental study on the factors that affect dynamic properties of loess found in Egypt using a resonant column. They found that shear modulus increases with confining pressure and the rate of increase was higher at low stresses and lower relative densities. Moreover, an increase in the silt content decreased the shear modulus but had no effect on damping ratio at constant confining stress and relative density. The shear modulus also increased with an increase in relative density.

Published data on the dynamic properties of Memphis area loess is currently limited. Chang (1992) did tests for two Memphis soils (sandy loess and clayey/silty loess) on undisturbed samples using a resonant column device. The sandy loess was retrieved from Collierville, TN area, and the clayey loess was from Peabody, Memphis area. The tests were done under confining stresses of 5, 10, 20, and 40 psi. The study compared the results with the Mash Program, Hardin equation, Edil and Luh equation, and Iwasaki and Tatsuoka equation (Chang 1992). The study concluded that the Memphis loess has a lower shear modulus than is predicted by the available relationships under confining pressure of less than 15 psi. Figure 2.9 shows the shear modulus degradation curves of two Memphis loess soils in comparison to available curves. The study also concludes that the nonlinear cyclic behavior of Memphis clayey loess soils is different from clay soils of other regions in that the clayey loess behaves more like a cohesionless granular soil than a typical cohesive soil as shown in Figure 2.9(B) (Chang 1992).

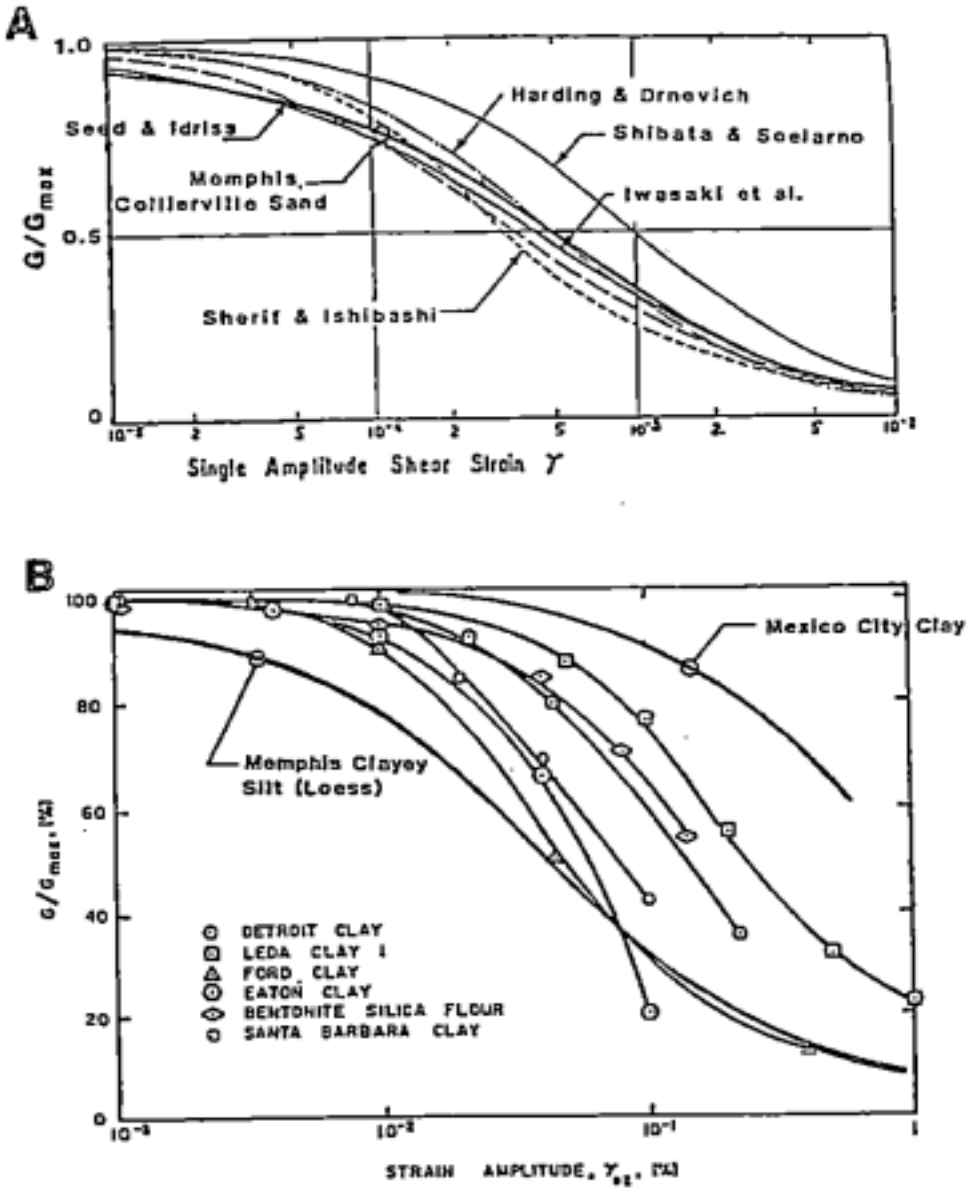


Figure 2.9: Comparison of shear modulus reduction curves for (A) sandy loess and (B) clayey loess (Chang 1992).

In summary, Memphis loess behaves differently from other region's soils. Furthermore, the previous study on Memphis loess lacks the effect of moisture content on the cyclic response of the soil though it has a more pronounced effect than confining stress in clayey/silty loess soil as discussed in this section. The soil that was investigated in this study was classified as silty loess, ML, according to a Unified Soil Classification System (USCS). A summary of physical

property tests of the soil is included in Appendix A. The effect of different ratios of horizontal and vertical stress as defined by the coefficient of lateral earth pressure has also been ignored in all studies by testing the soil with equal confining stress in all directions. But soils may exist at different vertical and horizontal stresses. In summary, the effects of moisture content (saturation) and coefficient of lateral earth pressure on the dynamic properties of loess will be investigated in addition to void ratio and confining pressure.

## 2.5 Summary

In this chapter, a review of the physical characteristics of loess soil is presented. Literature regarding the dynamic properties of soil, i.e., shear modulus, damping, and shear modulus degradation, is also provided. Moreover, factors that influence the dynamic properties of soil and models used in the current state of practice are discussed. Finally, experimental research results regarding loess soil around the world and Memphis specifically are summarized.

# 3 TEST EQUIPMENT AND METHODOLOGY

## 3.1 Introduction

This chapter reviews the resonant column testing method and the GCTS resonant column and torsional shear device that is employed in this study. The resonant column test is a widely used laboratory test for measuring the dynamic properties, i.e., shear modulus and damping ratio, of soil specimens at low to medium strains. In this method, a cylindrical, solid or hollow, specimen is excited by a harmonic torsional load at the top. The resonant frequency is then measured to calculate the shear modulus, and the damping is determined from free vibration decay or frequency sweep response. The specimen can be tested under all-around stress confinement as well as under an applied vertical stress if desired.

This chapter also presents the experimental procedure used in this study. The steps employed in preparing test specimens and conducting resonant column tests are presented.

## 3.2 Resonant Column and Torsional Shear Equipment

The resonant column, RC, is an instrument used to measure dynamic soil properties based on wave propagation theory. It is a relatively non-disruptive laboratory test that has been used to determine the shear modulus and damping ratio of soil and rock at small to medium strains since the early 1930's (Drnevich 1978). The test is carriedout by applying a torsional or longitudinal vibration at an increasing frequency to determine the first mode resonant frequency or frequency at resonance of a specimen. In the 1970's a torsional shear device was added to the resonant column apparatus for testing soil specimens. The torsional shear device applies torsional vibration at a constant low frequency (Isenhower and Stokoe 1981). Thus, the difference between a typical resonant column test and a torsional shear device is that the former tests samples at a range of frequencies while the latter tests at a single frequency. Also, since the

torsional shear device conducts tests typically at high strain, the specimens may become remolded or disturbed,

In this study, a resonant column and torsional shear device, RCTS, (GCTS TSH-100) is used. This RCTS applies a constant amplitude torsional excitation over a range of frequencies or a single frequency. Figure 3.1 shows a schematic diagram of a resonant column. The apparatus is known as a fixed-free longitudinal apparatus because the specimen is only fixed at the bottom but free at the top.

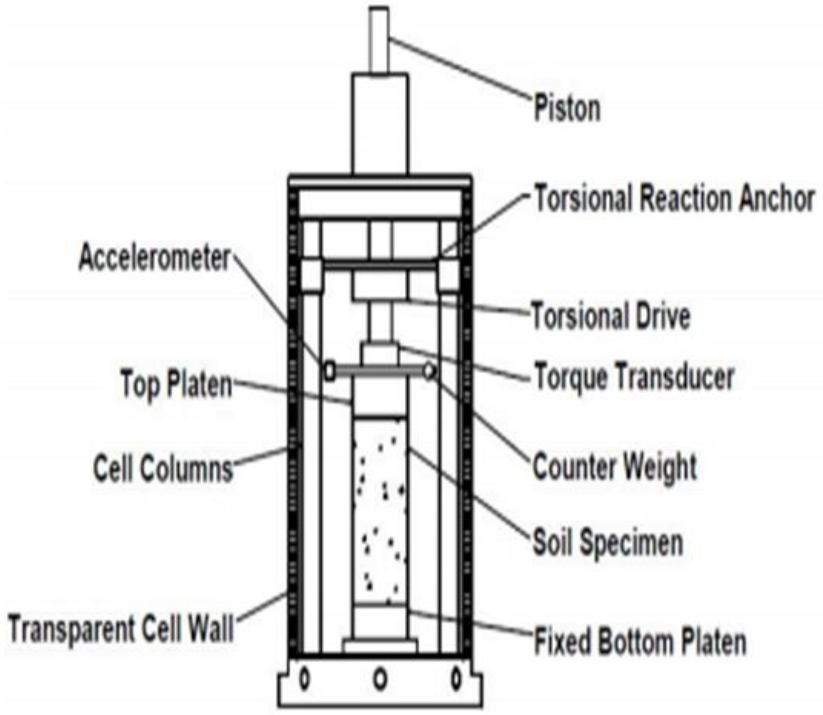


Figure 3.1: Schematic diagram of Resonant Column (GCTS 2007).

The solution for non-linear vibration is extremely complex, hence, the resonant column method is based on the more simplistic one-dimensional wave equation mechanics derived from the theory of linear-elastic vibration. This limits the resonant column test to medium and low strain amplitudes even when the apparatus is capable of measuring larger strains. Figure 3.2

shows the typical strain limit range of the resonant column and most other common dynamic testing devices with respect to strain amplitude. The resonant column can give accurate results in the range of 0.0001 to 0.01% strain

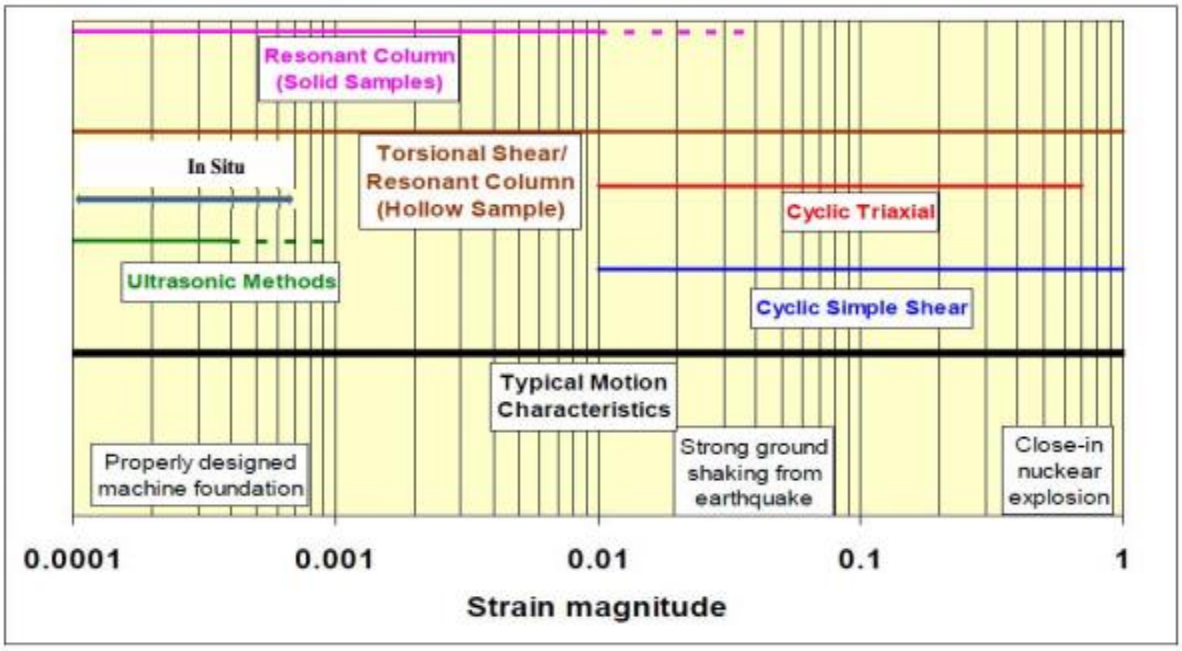


Figure 3.2: Typical strain level associated with different laboratory and field testing (GCTS 2012)

### 3.2.1 Components of the GCTS Resonant Column Apparatus

The main components of the GCTS Resonant Column and Torsional Shear (RCTS) apparatus are shown in Figure 3.3 and include the main cell, servo-controller, data acquisition system, computer with data acquisition system software, and pressure panel.

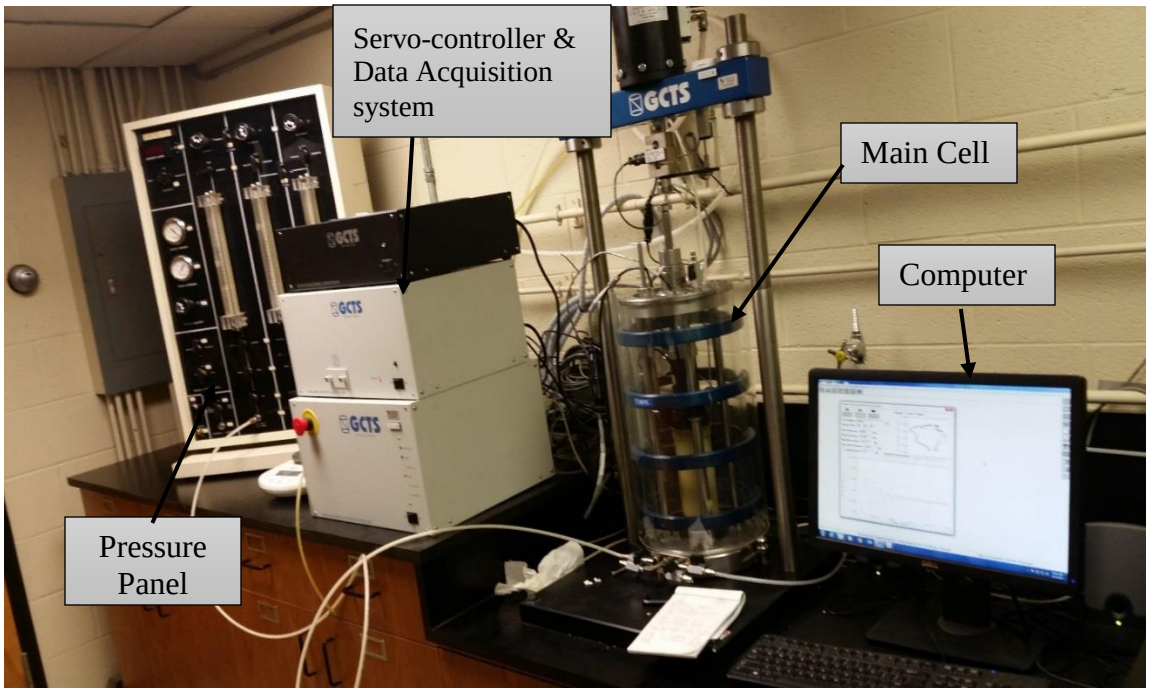


Figure 3.3: Resonant Column setup

The main cell consists of most of the components shown in Figure 3.1 such as the lower platen and upper platen, torque motor, deformation sensors, and cell wall. The lower platen is fixed while the upper platen is free to rotate and is attached to the torque motor. The torque motor is an electromagnetic loading system mounted on the cell with tie rods and is free to move vertically to accommodate large axial deformations. It has a torque capacity of 2.3 N-m and 300 Hz frequency. The RCTS is also equipped with two primary deformation sensors. It includes an accelerometer and proximitor for measuring torsional strains. However, only one can be selected to measure torsional strains during a given test. In general, the accelerometer provides more precise torsional strain measurements than the proximitor. Therefore, the accelerometer is used in this study. The second crucial deformation sensor is the axial displacement sensor for measuring axial strain. Both torsional and axial sensors are attached to the top platen as indicated in Figure 3.1.

The main cell is enclosed by an air-tight reinforced acrylic plastic cell wall that provides the capability of applying all-around confining stress to the specimen with air pressure. The cell wall is made of transparent acrylic plastic and is reinforced with four columns of external stainless-steel reinforcement which is capable of withstanding a maximum confining air pressure of 1000 kPa.

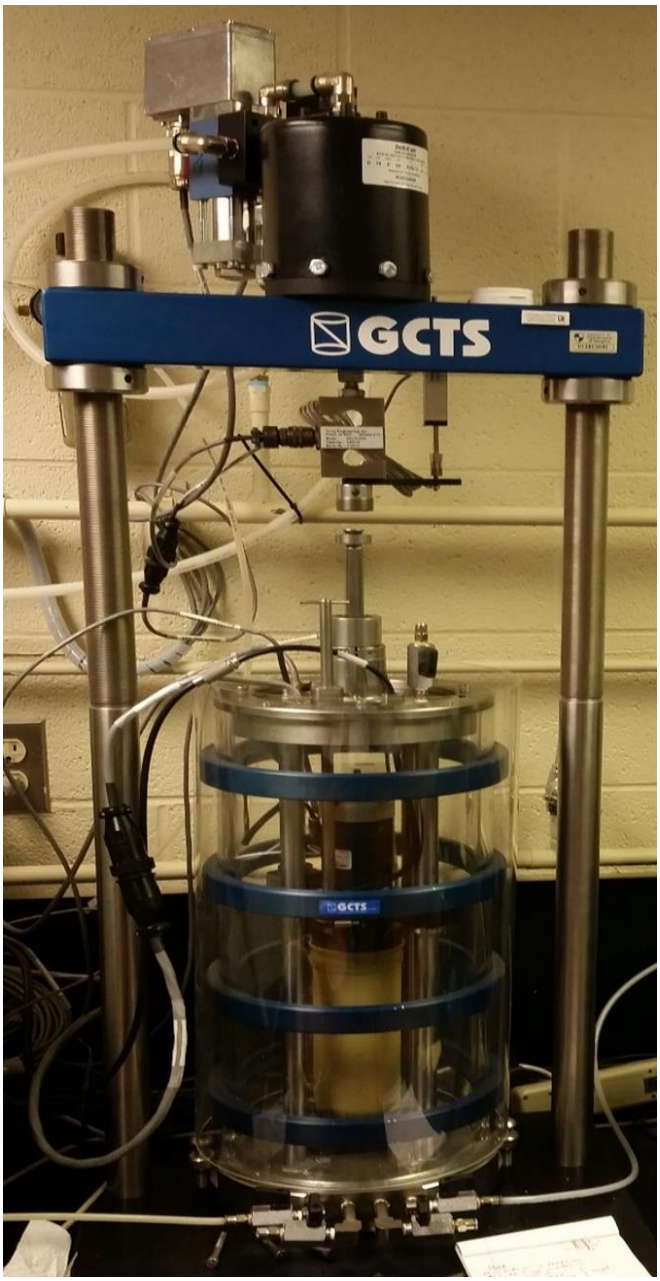


Figure 3.4: Photograph of GCTS Resonant Column & Torsional Shear Equipment

The digital servo-controller and acquisition system, SCON-1500, is used to activate and control the resonant column as well as to store the output from the transducers. The configuration settings are performed in the CATS software. The CATS software initiates, controls, and ends the test. It also collects the output from the SCON-1500. The initial input data that the CATS software requires includes specimen height, diameter and weight and then the software automatically calculates the following parameters from the test results: resonant frequency (Hz), maximum shear strain (fraction or %), shear wave velocity (m/sec), shear modulus (MPa), damping ratio (%), predominant frequency, and natural frequency (Hz). Predominant frequency is an average frequency that is calculated using a Fast Fourier Transform analysis of the free vibration data. Figure 3.5 presents a screenshot photo of a typical CATS software display.

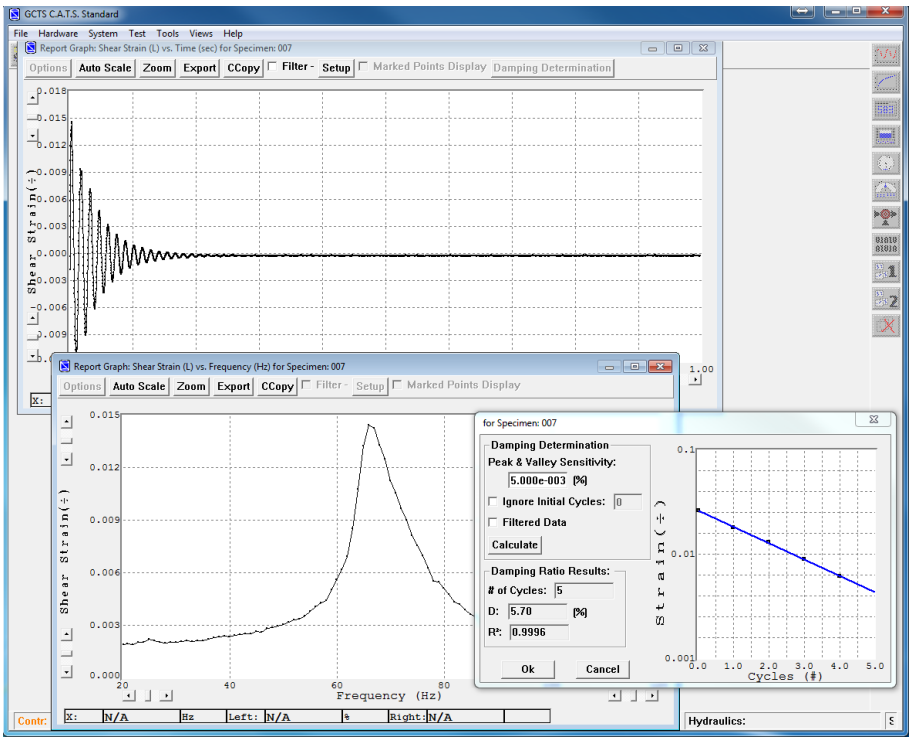


Figure 3.5: Screen shot of CATS software

The pressure panel controls the supply air pressure through a triaxial-type drainage system at the top and bottom of the RC cell. In this study, a DGSI pressure panel is used for

controlling the supply air pressure as shown in Figure 3.3 on the left side. The RCTS is also equipped with an axial load actuator for applying a vertical deviator load on the specimen while testing. Thus, the RCTS has the capabilities to test specimens under all-around confining stress as well as with additional vertical deviator stress.

### 3.2.2 Shear Strain

The amount of shear strain in a solid cylindrical specimen, when torsionally excited in the resonant column device, varies from zero at the center to a maximum value at the periphery as shown in Figure 3.6. For the fixed-free longitudinal apparatus used in this study, the maximum shear strain occurs at the top of the specimen. The shear strain at a given frequency is determined by

$$\gamma(r) = \frac{r\theta_{max}}{h} \tag{3.1}$$

where r is the radial distance from the soil column axis, $\theta_{max}$ is the maximum angle of twist, and h is specimen height as illustrated in Figure 3.6.

As shown in Figure 3.6 and indicated by Equation 3.1, the shear strain at the top of the specimen varies with radial distance from the center of the specimen. Therefore, it is convenient to represent the shear strain with an average equivalent shear strain, $\gamma_{eq}$. Generally, $r_{eq}$ is assumed as 2/3 $r_o$ for solid specimens with radius $r_o$. But, Chen and Stokoe (1979) found $r_{eq}$ varied from $0.82r_o$ for a peak shear strain below 0.001% to 0.79 $r_o$ for peak shear strain of 0.1%. In the CATS software, the $r_{eq}$ default value is 0.707 $r_o$ (GCTS 2007). The overall maximum shear strain incurred by the specimen during a test that consists of a range of frequencies is the largest average equivalent shear strain in the frequency sweep or range.

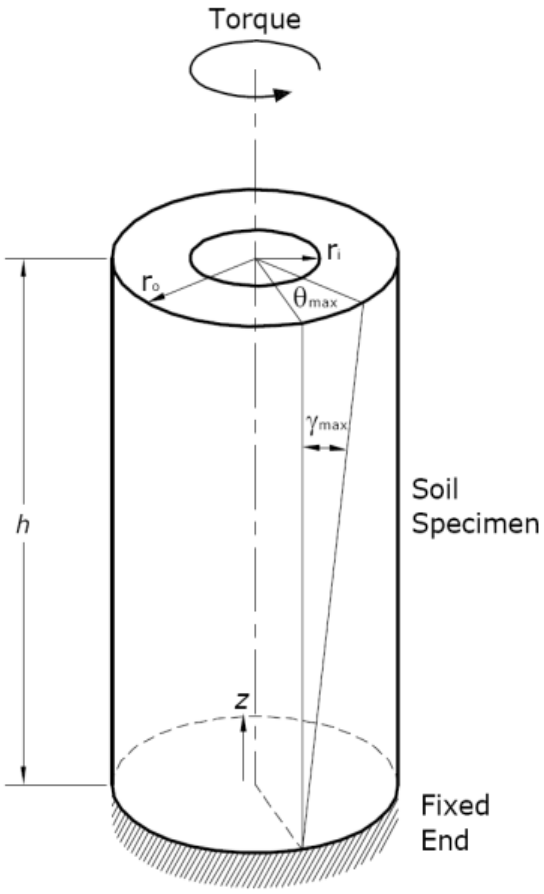


Figure 3.6. Shear Strain in soil specimen (GCTS 2007).

### 3.2.3 Shear Modulus and Damping

In the GCTS RCTS apparatus, the RC test is conducted by applying a constant amplitude torsional excitation over a range of frequencies to the top of the specimen by an electromagnetic loading system and a response curve, strain vs frequency, is measured. The shear wave velocity, $V_s$, is obtained by measuring the first mode frequency, also called the frequency at resonance, using Equation 3.2 (GCTS 2007)

$$\frac{I}{I_o} = \frac{wh}{V_s} tan(\frac{wh}{V_s}) \tag{3.2}$$

where *I* is the mass moment of inertia of the soil column, $I_0$ is the mass moment of inertia of the drive system including the top cap, *w* is the natural/resonant frequency of the specimen (rad/sec), and *h* is the height of soil specimen. Then, the maximum shear modulus is determined by

$$G_{max} = \rho V_s^2 \tag{3.3}$$

where ρ is the density of the specimen.

Damping is obtained either from the free vibration-decay method or half-power bandwidth method. The free-vibration decay determines the damping from the free vibration response after forced vibration is removed, assuming viscous damping. Thus, the resulting damping will depend on the underdamped behavior the soil specimen will exhibit as shown in Figure 3.7.

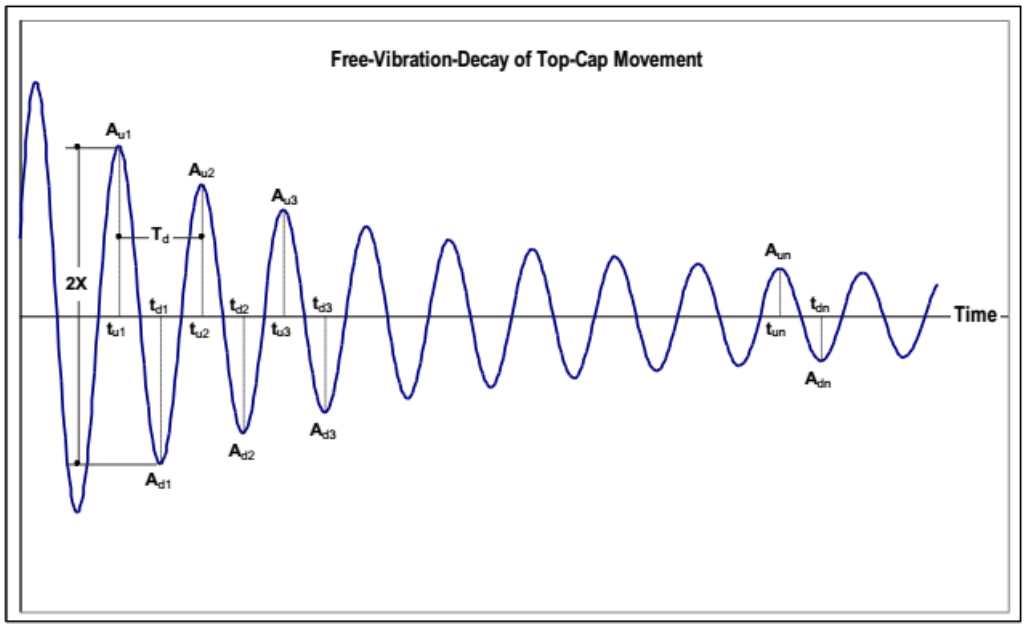


Figure 3.7. Free-vibration decay (GCTS 2007).

The free vibration damping ratio is calculated as

$$D = \sqrt{\frac{\delta^2}{4\pi^2 + \delta^2}} \tag{3.4}$$

where $D$ is the viscous damping ratio, and $\delta$ is the logarithmic decrement given by

$$\delta = ln\frac{x_n}{x_{n+1}} \tag{3.5}$$

where $x_n$ is the peak displacement at the nth cycle, and $x_{n+1}$ is the peak displacement at the n+1th cycle.

In the CATS software, the free vibration decay damping ratio is determined using the free vibration data of a resonant column test right after the test or later from the test data file. A least squares analysis is used to determine the slope of the line by graphically assessing the shear strain vs. cycles graph as shown in Figure 3.8. The user controls the number of cycles used for damping determination by setting the peak and valley sensitivity value as illustrated in Figure 3.8. The GCTS (2007) manual recommends at least three, but no more than ten, cycles should be used for the damping ratio determination from the free vibration data. It has an option to ignore the initial cycles if these cycles do not follow the general degradation trend of the other cycles as shown in Figure 3.8 in which the first cycle is ignored.

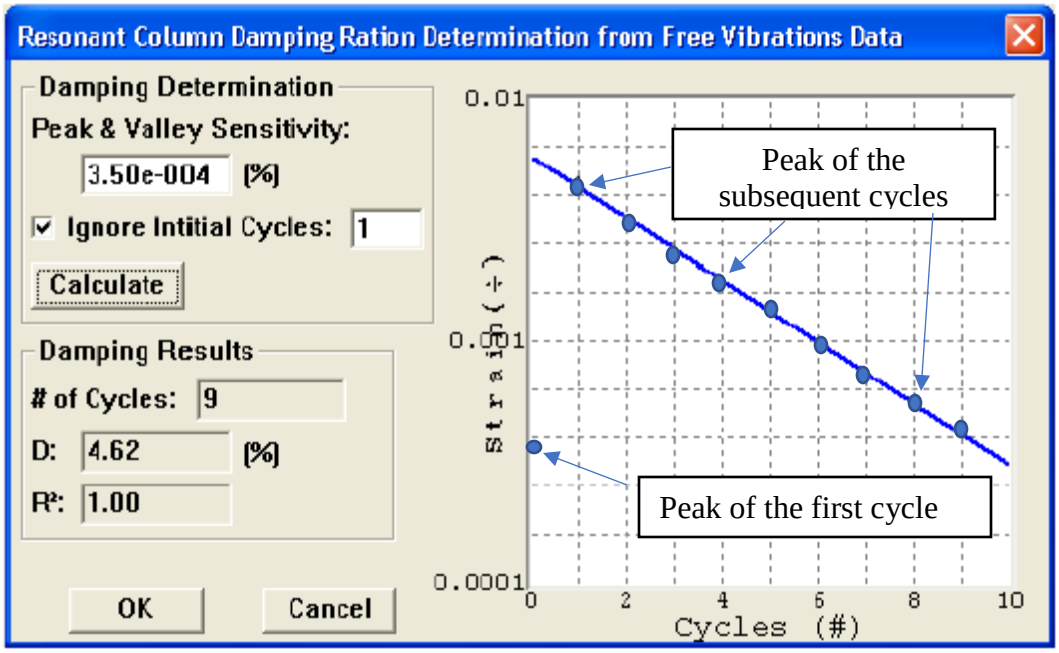


Figure 3.8: Resonant Column Specimen Damping Determination small Peak & Valley sensitivity value selected.

The half-power bandwidth method determines damping based on the width of the frequency response curve near resonance as shown in Figure 3.9. According to this method, the frequencies corresponding to amplitude A, $f_1$ and $f_2$, are obtained from the frequency sweep i.e., the range in frequencies, and the damping is calculated as

$$\delta = \frac{\pi(f_2^2 - f_1^2)}{2f_r^2}\sqrt{\frac{x^2}{x_{max}^2 - x^2}}\frac{\sqrt{1-2D^2}}{1-D^2} \tag{3.6}$$

where $\delta$ =logarithmic decrement,

$f_1$ = frequency below the resonance where the strain amplitude is A,

$f_2$ = frequency above the resonance where the strain amplitude is A,

$f_r$ = resonant frequency,

$D$ = material damping,

$x_{max}$ = maximum strain ($A_{max}$), and

$x$= strain corresponding to $f_1$.

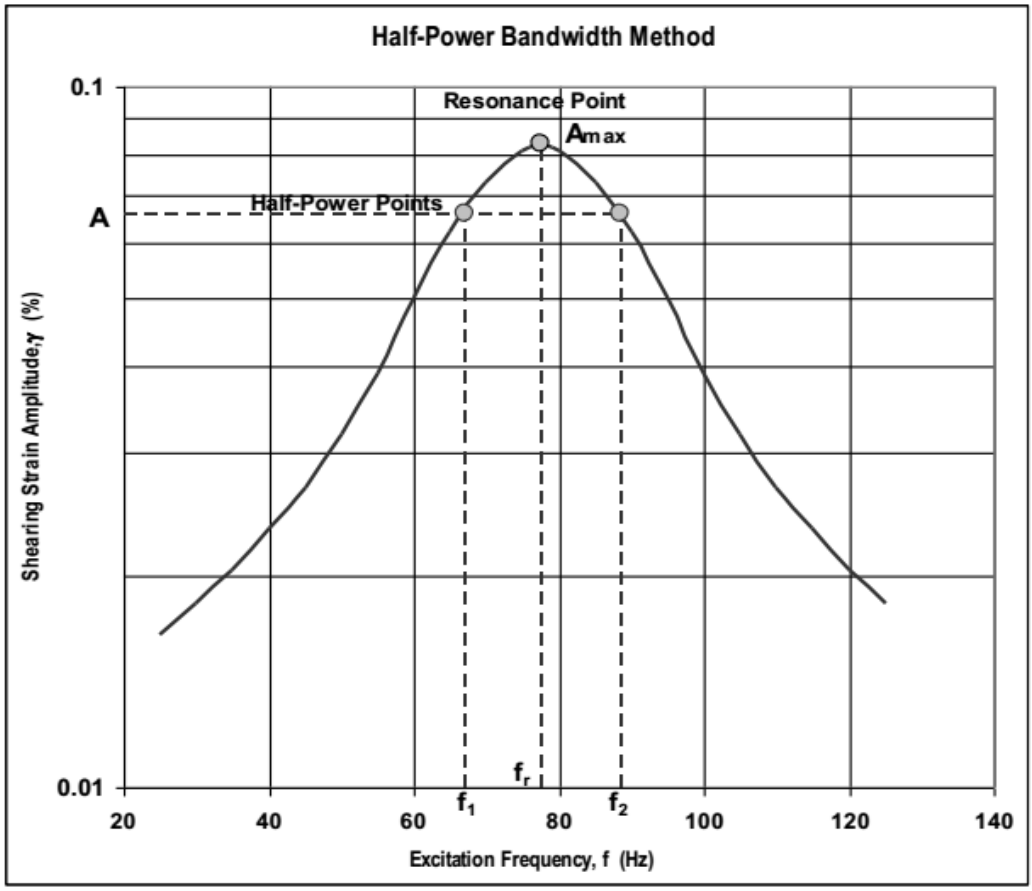


Figure 3.9: Material damping from Half-Power Bandwidth Method (GCTS 2007).

Equation 3.6 can be simplified when the amplitude A is $\frac{A_{max}}{\sqrt{2}}$ and the the damping is small as

$$\delta \cong \frac{\pi(f_2 - f_1)}{f_r} \tag{3.7}$$

Then, the damping ratio can be expressed as

$$D \cong \frac{(f_2 - f_1)}{f_r} \tag{3.8}$$

The CATS software sometimes fails to provide damping results in the half-power bandwidth method. In the Free Vibration Decay, the CATS software allows the user to assess

and make changes in the number of cycles to be considered as well as the initial cycles to be ignored. Therefore the Free Vibration Decay method is used to determine damping ratio in this study.

### 3.2.4 Calibration of Resonant Column and Torsional Shear Apparatus

The calibration of the GCTS Resonant Column system is performed using a metallic specimen assuming zero, or close to zero, damping and a constant torsional stiffness, k. From Newton's second law, the mass moment of inertia, *I*, is related to the resonant frequency, ω, as

$$I = \frac{k}{\omega^2} \tag{3.9}$$

The moment of inertia, *I*, includes the mass moment of inertia of the driving system (motor, proximitor, and accelerometer) and the mass moment of inertia of the calibration specimen. The recommended procedure to find the mass moment of inertia of the driving system, $I_o$, is to perform two resonant column tests with metal calibration specimens, one by itself and the other with added mass, as shown in Figure 3.10, and find the resonant frequency of each test. The first test without the added mass can be solved as

$$I_o + I_{cal} = \frac{k}{{\omega_1}^2} \tag{3.10}$$

where $I_o$ is the mass moment of inertia of the drive system, $I_{cal}$ is the mass moment of inertia of the calibration specimen, and $\omega_1$ is the resonant frequency of the calibration specimen without the added mass.

The second test with the added mass can be solved as

$$I_o + I_{cal} + I_{mass} = \frac{k}{{\omega_2}^2} \tag{3.11}$$

where $I_{mass}$ is the mass moment of inertia of the added mass, and $\omega_2$ is the resonant frequency of the calibration specimen with the added mass.

The mass moment of inertia of the driving system, $I_o$, can be determined by combining Equations 3.10 and 3.11 as shown by Equation 3.12:

$$I_o = \frac{(I_{cal} + I_{mass})\omega_2{}^2 - I_{cal}\omega_1{}^2}{\omega_1{}^2 - \omega_2{}^2} \tag{3.12}$$

The calibration specimen is made of 6061-T6 aluminum with a mass density of 2.7 g/cm$^3$, a shear modulus of 26.0 GPa, and a mass moment of inertia of 82 kg.mm$^2$. The added-mass is made of 303 stainless steel with a mass density of 7.7 g/cm$^3$ and a mass moment of inertia of 472.5 kg.mm$^2$.

In this study, to calibrate the Resonant Column, two tests were performed, first without the added- mass and then with the added mass. The resonant frequency results with and without added mass are found to be $\omega_1$ = 76 Hz, and $\omega_2$ = 59.8 Hz, respectively.

Then, the mass moment of inertia of the driving system, $I_o$, was determined using Equation 3.12 and found to be 686.05 kg.mm$^2$. To check if the calibration result is accurate, an additional test was done on the calibration specimen without the added mass, and the shear modulus was found to be 26.1 GPa. This result is in agreement with the given shear modulus of the specimen of 26.0 GPa, signifying that the RC was successfully calibrated.

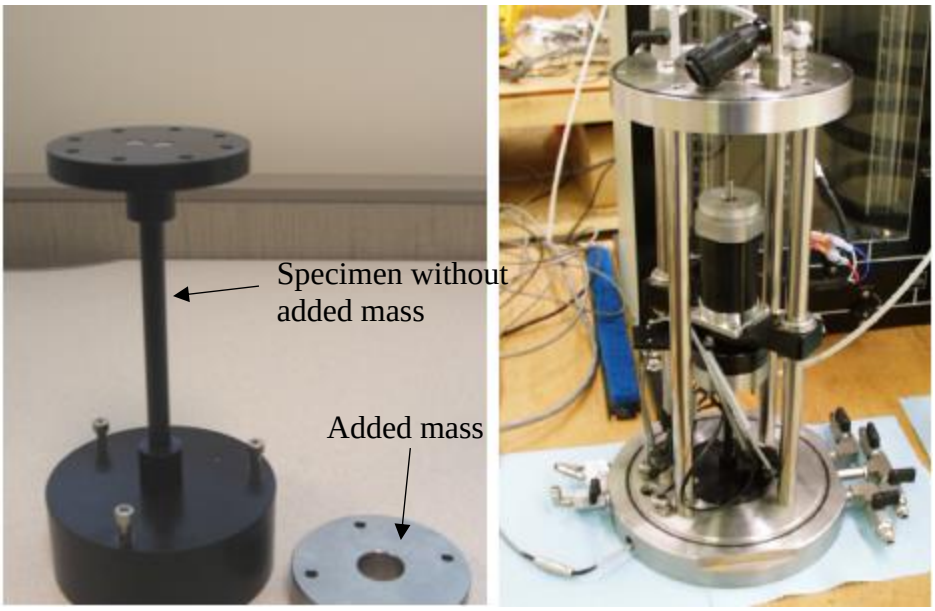


Figure 3.10: Calibration specimen (left) calibration test setup with added mass (right).

### 3.3 Methodology and Experimental Procedure

The experimental procedure includes obtaining soil samples from the field, characterizing the soil, preparing specimens, performing resonant column tests, analyzing the test results, and comparing the test results with test data reported in the literature. Both disturbed and intact loess soil samples were acquired from a bluff located at Fulton Wild Life Refuge, north of the city of Memphis. The disturbed sample was scraped from the bluff with a shovel, collected in buckets and transported to the laboratory. The undisturbed block samples were obtained by cutting cubical specimens, about 25cm wide, from the bluff with a pick per ASTM D7015−13. Due to the high moisture content, some of the block samples fell apart and it was only possible to obtain two intact block samples. The block samples were then covered with three layers of wax and cheesecloth and enclosed in a plastic bag per ASTM D4220/D4220M−14 to avoid loss of moisture then transported to the lab in wooden boxes.

A summary of the laboratory tests for classifying and characterizing the loess which included sieve analysis, hydrometer analysis, Atterberg limits and compaction tests are included

in Appendix A. The soil is classified as a low plasticity silt, ML, based on the Unified Soil Classification System with 0% sand, 83% silt, and 17% clay. The soil is considered silty loess. Atterberg limit tests indicate that the soil has a liquid limit of 30 and plasticity index of 1. Compaction tests were also conducted based on the ASTM D 698 procedure and a maximum dry unit weight of 17.4 kN/m$^3$ was obtained at an optimum water content of 16.8%. The specimen preparation and resonant column testing are described in the next sections.

### 3.3.1 Specimen Preparation

Soil specimens can be prepared from disturbed samples by remolding in the laboratory or from undisturbed soil samples by trimming. Remolded soil specimens lose the in-situ structure and properties of the soil while undisturbed specimens recovered from a Shelby tube or the block sampling method retain the in-situ structure of the soil.

There are various methods of preparing remolded specimens in the laboratory such us slurry consolidation, air pluviation, compaction, and undercompaction (Lade 2016). The slurry consolidation method is used for preparing clay specimens. Specimens are prepared by mixing clay powder with water and consolidating the slurry in a tank to the desired pressure or density. The air pluviation method is used for preparing sand specimens. Air pluviation of sand simulates sedimentation of sand deposits, and the specimen is made by raining the sand slowly from a fixed height. The compaction method is used to prepare both clay and sand specimens by static or dynamic compaction. Static compaction is performed by placing an amount of moist soil in a mold and compressing it statically to the desired pressure or density. Dynamic compaction is performed by applying a dynamic load with a falling mass. Ladd (1978) revealed that in the static and dynamic compaction methods the lower lifts receive additional compactive energy from successive higher lifts making the sample non-uniform in density from top to bottom. To

counter this problem, Ladd (1978) proposed the undercompaction method. In this method, each layer is compacted to a lower density than the final desired value by a predetermined amount, which is defined as the percent undercompaction ($U_n$). The bottom layer has the maximum $U_n$ value, and linearly decreases to the top layer which is usually zero. Typically for sands, the $U_n$ value for the bottom layer ranges between zero for the preparation of dense specimens to about 15% for the preparation of very loose specimens.

Another important factor that should be taken into account is the effect of molding water content on the structural arrangement of the soil. Initial molding water content influences the soil structure of remolded specimens despite having the same density, void ratio, soil texture, and mineralogy. Studies suggest that clay soils compacted on the dry side of the optimum moisture content exhibit a random arrangement while clay soils compacted on the wet side of optimum moisture content exhibit a more oriented arrangement of particles as illustrated in Figure 3.11. As a result, the engineering behavior of specimens prepared on the wet side versus the dry side of optimum can vary (Alonso et al. 2013; Maleki and Bayat 2012; Wen and Yan 2014; Jiang et al. 2016). Cetin et al. (2007) and Mitchell and Soga (2005) inferred that the major factor of fabric formation for a compacted fine-grained soil is the strain induced by the compaction rammer rather than the molding water content. In the case of compacting dry of optimum moisture content, there is less penetration of the rammer, which creates a random arrangement of particles.

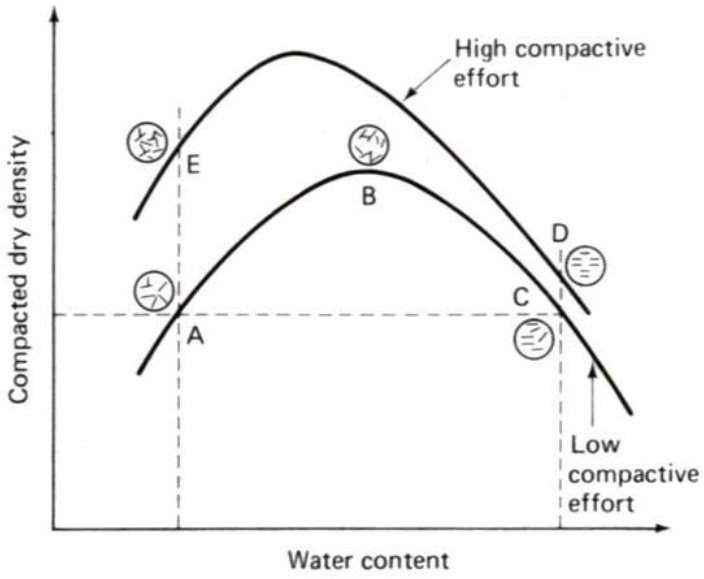


Figure 3.11: Effect of water content on soil structure (Lambe and Whitman 1979).

Many studies show that molding water content affects dynamic soil behavior. It affects the stiffness, shear wave velocity, and maximum shear modulus (Mancuso et al. 2002; Salem 2007; Sawangsuriya et al. 2008). However, the molding water content has no or insignificant influence on the normalized shear modulus degradation and damping curves (Wu 2014; D'Onofrio and Penna 2003; Fleureau et al. 2001; Kim et al. 2003). This result is similar to the effect of overconsolidation and aging, which influences the maximum shear modulus but has minimal effect on shear modulus degradation and damping curves. Therefore, in this study of loess, the molding water content effect on the normalized shear modulus degradation and damping curves is ignored.

In this study, static compaction is selected for preparing remolded specimens due to its repeatability and uniformity of density throughout the height of a specimen. To prepare a specimen, a soil sample is first mixed properly with a predetermined quantity of water, and then the soil sample is placed in a sealed plastic bag and allowed to reach water equilibrium for 24 hours. Then the specimens are compacted using static compaction method in a 72.5-mm-

diameter, 147.6-mm-high mold using a triaxial test device loading frame as illustrated in Figure 3.12. To get relatively uniform density along the height of the specimen, samples are prepared by using five lifts having the same weight of soil and compacting each layer to an equal height by applying a constant compaction displacement rate of 1.0 mm/min.

(a) (b)

Figure 3.12: (a) Triaxial loading system used for specimen compaction and (b) full specimen prepared by static method.

Undisturbed specimens are prepared by trimming the block sample with a wire saw. The GCTS resonant column requires a 70-mm-diameter and 140-mm-height solid specimen. Trimming to the desired size was difficult due to breakage of the loess. Consequently, it was only possible to prepare one intact specimen.

### 3.3.2 Testing Program

One of the objectives of this thesis is to determine the influence of saturation, confining pressure, void ratio, and coefficient of lateral earth pressure on the dynamic properties of loess,

i.e., shear modulus degradation and damping ratio. To examine the effect of saturation the remolded soil specimens were prepared at systematically varied degrees of saturation. Specimens prepared below 23% saturation were prone to cracks, and above 75% the specimens slumped or couldn't support their self-weight after being extruded from the compaction mold. Hence, five specimens were prepared at 23, 36, 48, 61, and 74% saturation and 0.87 void ratio. The effect of confining stress was also investigated by testing each specimen at 25, 50, 100, 200 and 400 kPa confining stress. The loess soil in the Memphis area extends to a depth of about 20 m, equivalent to a vertical stress of about 400 kPa. To investigate the effect of void ratio, two specimens at 0.7 void ratio, 60% and 76% saturation, were also prepared. At a void ratio of 0.7, preparation of specimens with a degree of saturation less than 60% was impossible due to load limitations of the triaxial loading system. Moreover, specimens were tested at a coefficient of lateral earth pressure, $K_o$ of 1 and 0.8. A trial test was carried out at K of 0.6, but the specimen failed due to excessive crack development. For a K of 0.8 the specimen remained intact during testing. At a K of 1, the test was performed by applying uniform air pressure around the specimen. To achieve a K of 0.8, an additional static vertical deviator load was applied to the top of the specimen. Table 3.2 provides a summary of the specimen preparation and test conditions evaluated in this study.

Table 3.1: Test Matrix

| Void Ratio (e) | Saturation, $S_r$ (%) | Confining Pressure, σ (kPa) | Coefficient of Lateral Earth Pressure, K |
|---|---|---|---|
| 0.7 | 60 | 25, 50, 100, 200 and 400 | 1 and 0.8 |
| | 76 | 25, 50, 100, 200 and 400 | 1 and 0.8 |
| 0.87 | 23 | 25, 50, 100, 200 and 400 | 1 |
| | 36 | 25, 50, 100, 200 and 400 | 1 and 0.8 |
| | 48 | 25, 50, 100, 200 and 400 | 1 and 0.8 |
| | 61 | 25, 50, 100, 200 and 400 | 1 and 0.8 |
| | 74 | 25, 50, 100, 200 and 400 | 1 and 0.8 |
| In-situ conditions of undisturbed specimen | | 25, 50, 100, 200 and 400 | 1 |

### 3.3.3 Test Procedure

After compacting the specimen, it was extruded using a manual extruder and then sealed with a rubber membrane. The specimen was then placed in the resonant column with the membranes secured to the top and bottom platen with O-rings. The cell wall of the resonant column was assembled and the external cables are connected. Once the system was assembled, 25 kPa of air pressure was applied within the cell to confine the specimen. The test was performed without allowing air or water to dissipate. Therefore, the test was considered as undrained test. A resonant column test was then performed by applying 0.01 pfs. Pfs stands for percent full scale and 1.0 pfs is equivalent to 0.02 N-m of torque or 0.1 volts. The 0.01 pfs torque can produce 0.00001 to 0.0001% strain. A series of tests were then performed by slowly increasing the torque until the strain level reaches 0.1% to produce the dynamic curve of the soil.

As the test is a non-destructive test, the same specimen was used to test at higher confining stresses. Therefore, the confining stress was increased from 25 kPa to 50 kPa, and another series of tests were performed. Before the resonant column test, the specimen was

confined for 40 minutes to eliminate the effect of disturbance from the previous test. This process was repeated for 100, 200, and 400 kPa confining pressure. Note that for testing at K=1 condition, no deviator stress was applied and the specimen was tested under the all-around confining stress. After testing at 400 kPa was completed, the same specimen was then tested at a K of 0.8 to investigate the effect of coefficient of lateral earth pressure on the dynamic response of the loess soil. For 100 and 200 kPa confining stresses, an additional deviator stress of 25 and 50 kPa, respectively, was applied to attain the desired K of 0.8. To investigate if overconsolidation (OCR) influences the shear modulus degradation and damping results while testing for K, a preliminary test was performed at 100 and 200 kPa confining stress after testing the same specimen at 25, 50, 100, 200, and 400 kPa, consecutively. Figures 3.13(a) and (b) show shear modulus degradation results for OCR equals 4 and 2. The figures show that OCR does not have influence on the dynamic properties of loess. Therefore, the effect of OCR while testing the same specimen for K of 0.8 by applying additional deviator stress is ignored in this study.

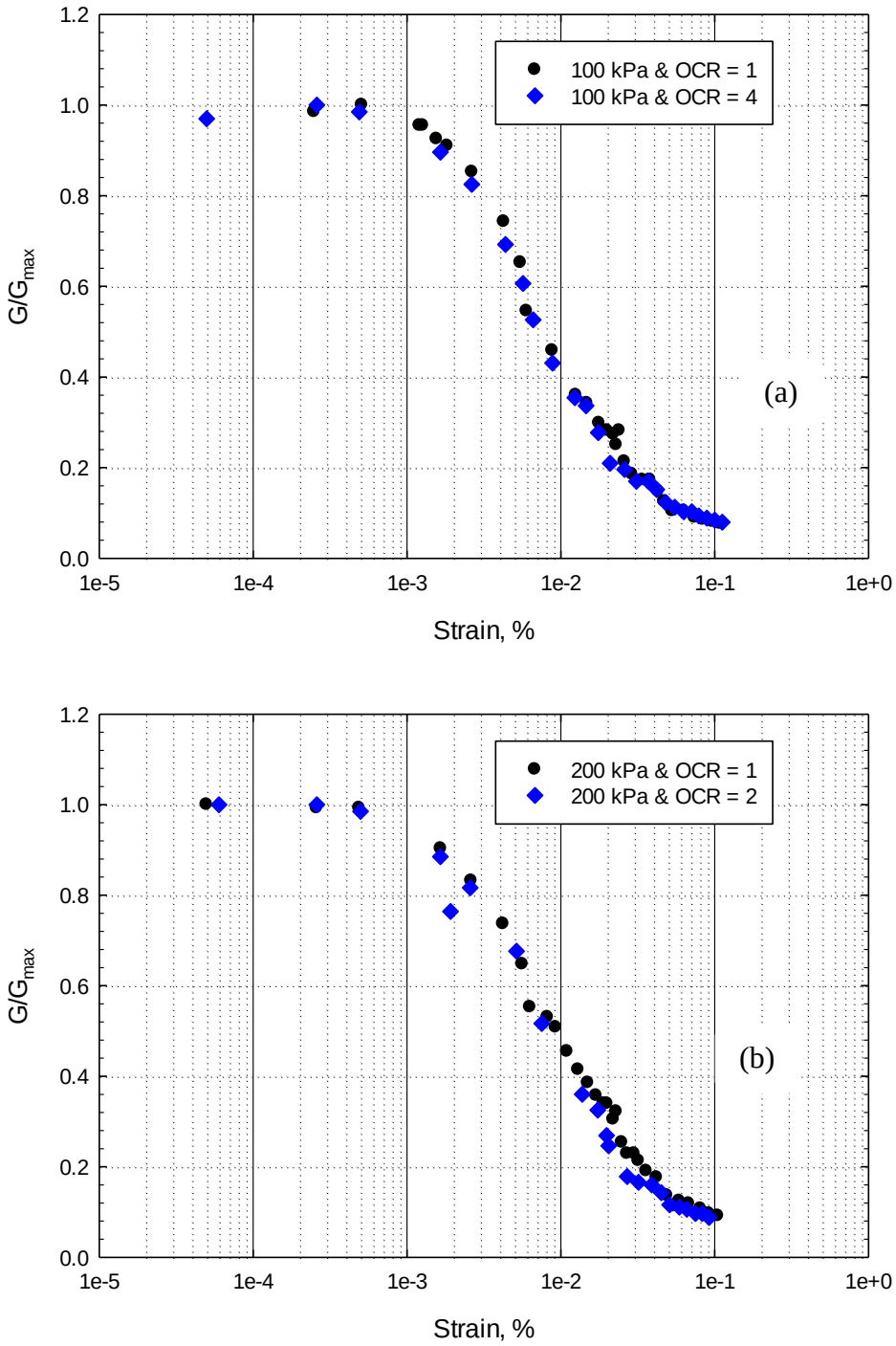


Figure 3.13: Effect of Overconsolidation ratio at (a) 100 and (b) 200 confining stresses.

After completing the test, the free vibration decay damping ratio was calculated from the free vibration data for the specimen. Finally, the test results of shear modulus and damping ratio

were retrieved, and curves for $G/G_{max}$ and D were then developed. The analysis of the test results is presented in the next chapter.

## 3.4 Summary

In this chapter, an overview of the resonant column & torsional shear (RCTS) testing method that includes the theoretical background and calibration is presented. This chapter also discusses the specimen preparation and testing procedure employed in this study.

# 4 PRESENTATION OF RESULTS

## 4.1 Introduction

This chapter presents the results of the resonant column tests performed on remolded and intact Memphis area loess soil. Five specimens were prepared at 0.87 void ratio and varying saturation levels of 23%, 36%, 48%, 61%, and 74%. Two specimens were also prepared at 0.7 void ratio with 60% and 76% saturation. An undisturbed specimen prepared by trimming from a block sample was also tested. The results, which are presented in this chapter, are used to investigate the effects of saturation, confining stress, void ratio, and coefficient of lateral earth pressure on shear modulus and damping.

## 4.2 Effect of Saturation

In order to investigate the effect of saturation on the dynamic properties of loess, remolded specimens of Fulton loess at 0.87 and 0.7 void ratio were prepared as described in Section 3.3.1. As shown in the test matrix of Table 3.2, five specimens with 0.87 void ratio and varying saturation levels of 23%, 36%, 48%, 61%, and 74% were tested. Moreover, two specimens with 0.7 void ratio at 60% and 76% saturation were also tested. Remolded specimens below 60% saturation at 0.7 void ratio could not be prepared due to the limitations of the triaxial loading system that was used to prepare the specimens, as described in Section 3.3.1. The load required to compact specimens below 60% saturation at a void ratio of 0.6 was higher than the maximum capability of the triaxial loading system.

All specimens were tested at 25, 50, 100, 200, and 400 kPa confining stress using the test procedure described in Section 3.3.2. Figures 4.1 through 4.9 summarize the resonant column test results and all test results are presented in Appendix B. Each figure includes shear modulus degradation, $G/G_{max}$, as a function of shear strain as the top figure and damping ratio as a

function of shear strain as the bottom figure. The GCTS CRTS device sometimes fails to accurately measure and gives a very low shear modulus at small strain as shown in Figure 4.4(a) and have been ignored in the test results.

Figures 4.1(a) and 4.2(a) provide a comparison of shear modulus degradation, $G/G_{max}$, as a function of shear strain at 25 and 100 kPa confining stress, respectively, at a void ratio of 0.87. The $G/G_{max}$ at 23% saturation is found to be noticeably lower than the others. But for saturation levels greater or equal to 36%, the $G/G_{max}$ curves appear to be more in agreement. Similar results were obtained at confining stresses of 50, 200, and 400 kPa as shown in Figures B.1 to B.3. The results obtained at 23% saturation in this study are similar to those of Jennings et al. (1997) on sandy loess in which a lower $G/G_{max}$ was obtained at a lower degree of saturation, as discussed in Section 2.4 and Figure 2.8(a).

Another comparison of test results is also made on the 0.7 void ratio specimens prepared at 60 and 76% saturation in Figure 4.3(a). Contrary to the trend at 0.87 void ratio, in which $G/G_{max}$ at 61% and 74% saturation are in agreement, there is a variation in $G/G_{max}$ at the lower void ration of 0.7 between the 60% and 76% saturation. The $G/G_{max}$ of the 60% saturation specimen at 100 kPa confining stress is noticeably lower than the 76% saturation specimen as shown in Figure 4.3(a). Given that the 60% and 76% are the only specimens prepared at 0.7 void ratio, not enough data are available in this study to fully evaluate the effect of saturation with varying void ratios and more tests are required to evaluate the effect of saturation at a higher density.

Figures 4.1(b) and Figure 4.2(b) present damping ratio, D, as a function of shear strain at 25 and 100 kPa confining stress, respectively. As with the results of shear modulus degradation, the damping results for 23% saturation are not in agreement with the damping curves at other

saturation levels tested. The damping ratios at 23% saturation are slightly higher than the damping ratios at degrees of saturation between 36% and 74%, though the difference is not uniform at all confining stresses. At 25 kPa the 23% saturation has higher damping at shear strains greater than $10^{-3}$%. Whereas, at the other confining stress the 23% saturation has slightly higher damping as shown in Figure 4.2 and Figures B.1 to B.3. Also, for saturation greater or equal to 36%, the variation of damping curves appears to be more in agreement.

In summary, the results shown in Figures 4.1 and 4.2 suggest that the dynamic properties, i.e., shear modulus degradation and damping ratio, of loess are different at the lower saturation level of 23% compared to the higher saturation levels between 36% and 74%. This observation led to a hypothesis that the dynamic properties of loess soil vary at low saturation of 23% but remains the same from medium to high saturation levels of 36% to 74%. However, as noted in Section 3.2, the specimen preparation procedure can yield inherent physical differences between specimens such as varying silt- versus clay-particles, density, and saturation. These inherent physical differences between specimens can possibly influence the dynamic property results shown in Figures 4.1 and 4.2. Therefore, to determine if the variance in the shear modulus degradation and damping ratio curves are greatly influenced by inherent physical differences between specimens or if indeed the hypothesis that dynamic properties of loess will vary between low saturation of 23% and medium to high saturation levels of 36% to 74% is valid, additional specimens were tested.

The additional testing program to validate the hypothesis consisted of preparing four additional specimens at each degree of saturation of 23% and 61%. The specimens have a void ratio of 0.87 and are tested at 25, 50, 100, 200, and 400 kPa confining stress. The $G/G_{max}$ test results of the five specimens prepared at 61% saturation and void ratio of 0.87 are depicted in

Figures 4.4(a) and 4.5(a) at 25 and 100 kPa confining stress, respectively. Similar results for $G/G_{max}$ were obtained at the other confining stresses of 50, 200, and 400 kPa as shown in Figures B.4 through B.6. In these figures, it can be seen that the $G/G_{max}$ has a small variation though the specimens were prepared at the same saturation and void ratio. The damping results also showed small variations with more scatter as illustrated in Figures 4.4(b) and 4.5(b). Similar results for D were obtained at the other confining stresses of 50, 200, and 400 kPa as shown in Figures B.4 through B.6. Similarly, the five test results of 23% saturated specimens presented in Figures 4.6 and 4.7 exhibited small variations of $G/G_{max}$ and damping. The results in Figures 4.4 through 4.7 suggest that the slight differences in dynamic properties between 36% and 74% saturation, observed in Figures 4.1 through 4.3, may not be due to the effects of saturation but may be caused by inherent soil differences between specimens. Therefore, the test results appear to support the hypothesis that the dynamic properties of loess will vary between low saturation of 23% and medium to high saturation levels of 36% to 74% and that at medium and higher saturation levels (S>36%), the dynamic properties are independent of saturation levels.

Figures 4.8(a) and 4.9(a) provides a comparison of $G/G_{max}$ between 23% and 61% saturation for 100 kPa and 200 kPa, respectively. The figures show that there is a distinct difference in $G/G_{max}$ between 23% and 61% saturated specimens. The 61% saturation has a higher $G/G_{max}$ than the 23% specimens especially at shear strains greater than $10^{-3}$ at 100 kPa confining stress and $10^{-4}$ at 200 kPa confining stress. Similar results are shown in Figures B.4 through B.6.

Figures 4.8(b) and 4.9(b) provides a comparison of D between 23% and 61% saturation for 100 kPa and 200 kPa confining stress, respectively. The difference in D is not as distinct as for $G/G_{max}$ because of the scatter of the test results. In addition to the inherent differences in

physical properties between specimens, the analysis method associated with determining damping from free vibration decay in resonant column tests can be contributing to the scatter in the damping results. The free vibration method calculates the damping ratio by determining the average slope of the free vibration decay using least squares analysis as summarized in Section 3.2.3. If the free vibration decay contains cycles that do not follow the predominant trend, especially the initial and the middle cycles, the method gives a less accurate estimate of average damping ratio. The CATS software has a provision for ignoring initial cycles that do not follow the trend as shown in Figure 3.6, but there is no provision to ignore the cycles that do not follow the trend in the middle. This results in an inaccurate determination of damping ratio that contributes to the scatter in D as shown in Figures 4.1(b) through 4.9(b). However, the overall comparison indicates that damping is slightly higher at 23% saturation than at 61% at shear strain less than $10^{-2}$%. Therefore, it can be concluded that dynamic properties of loess soil varies between low and high saturation levels.

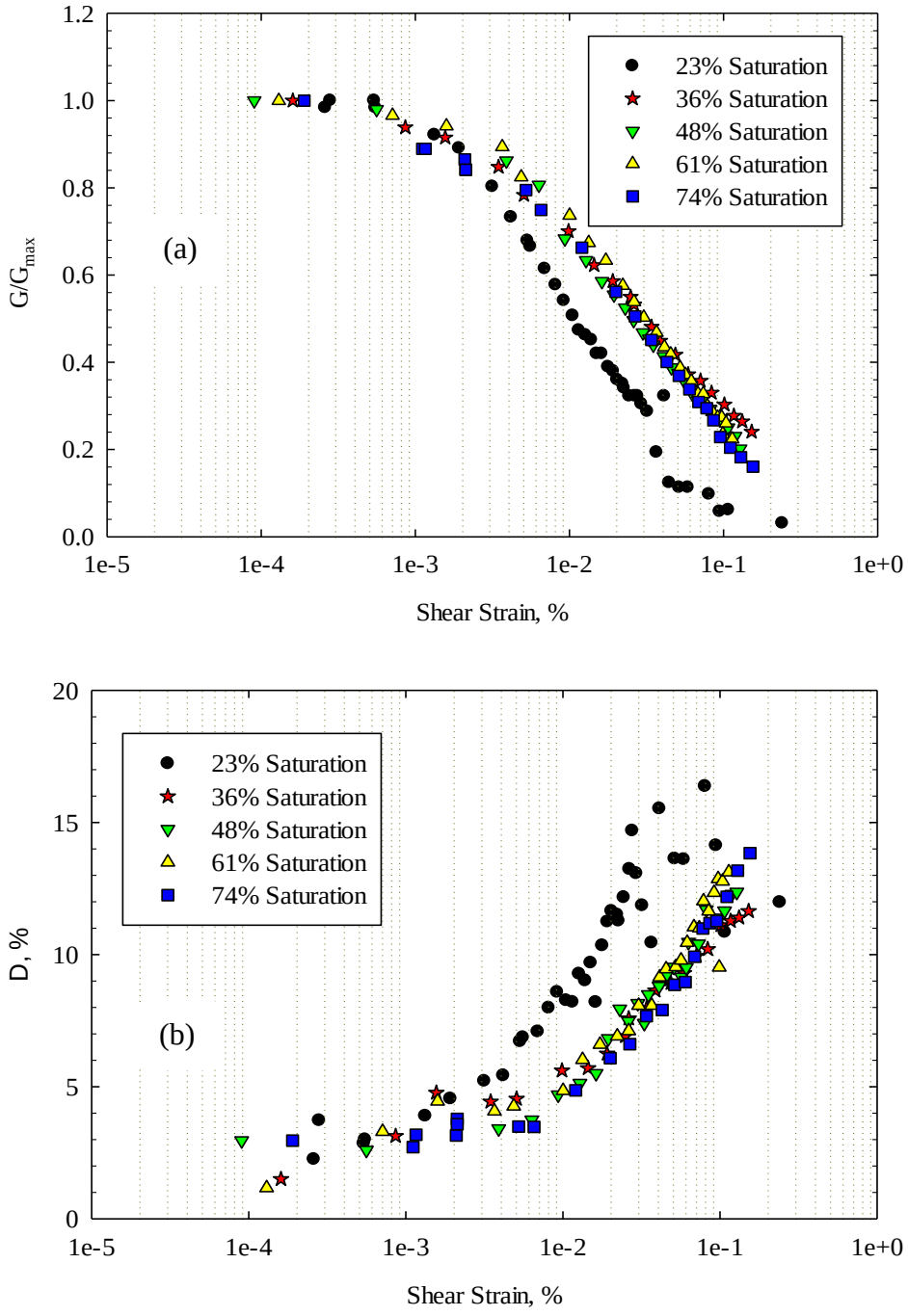


Figure 4.1: Effect of saturation on (a) shear modulus degradation and (b) damping of 0.87 void ratio specimen at 25 kPa confining stress

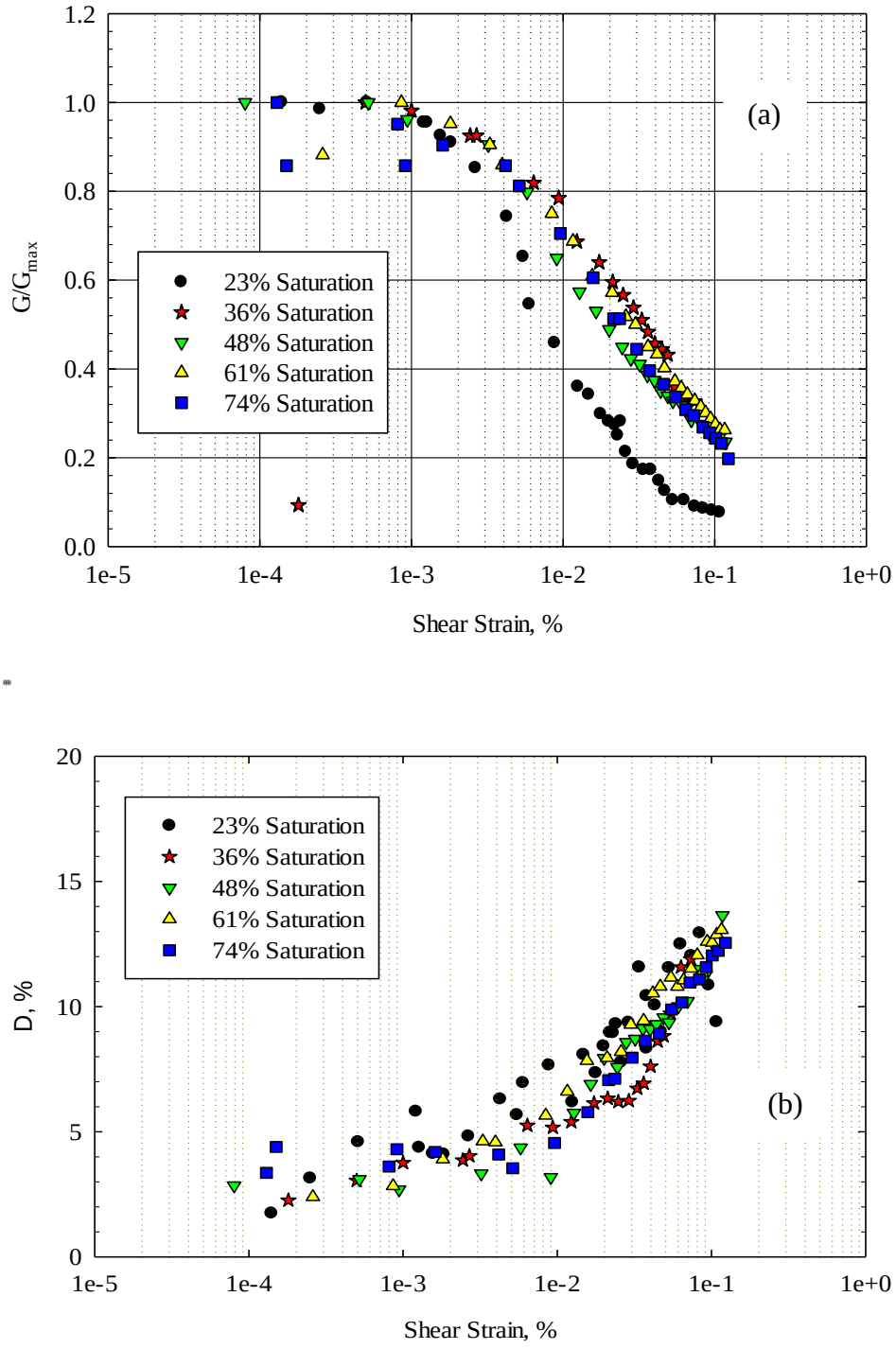


Figure 4.2: Effect of saturation on (a) shear modulus degradation and (b) damping of 0.87 void ratio specimen at 100 kPa confining stress

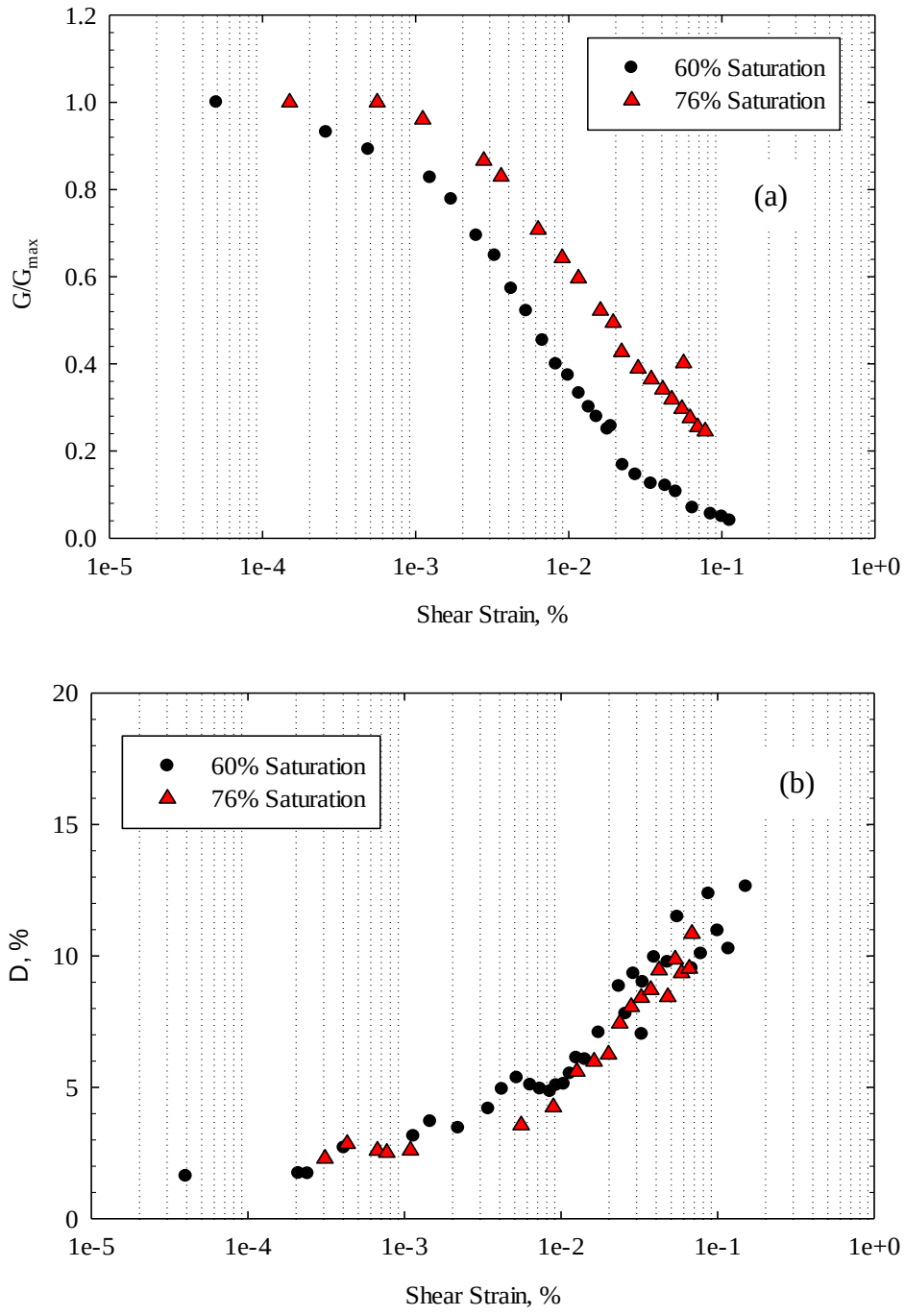


Figure 4.3: Effect of saturation on (a) shear modulus degradation and (b) damping of 0.7 void ratio specimen at 100 kPa confining stress

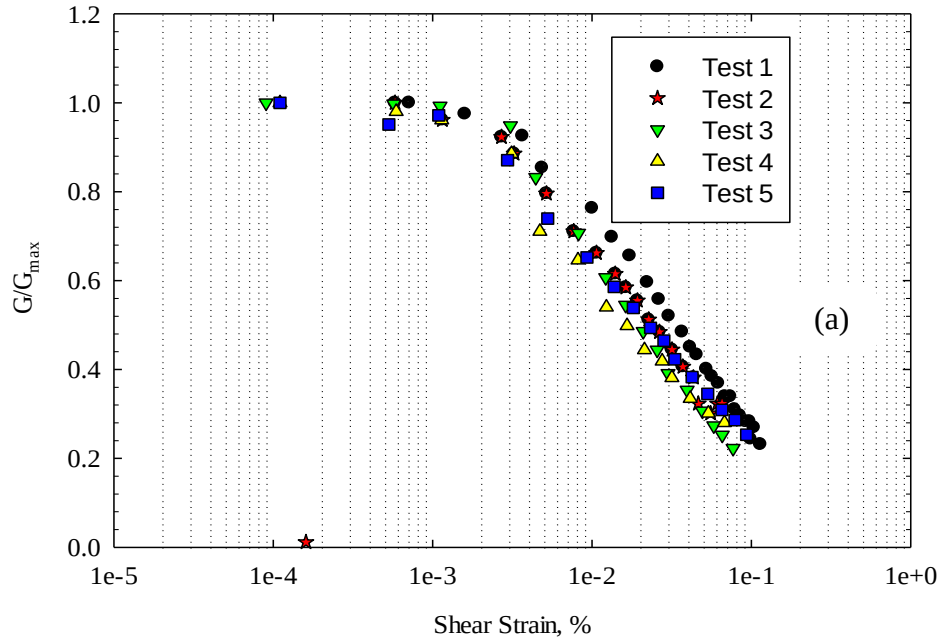


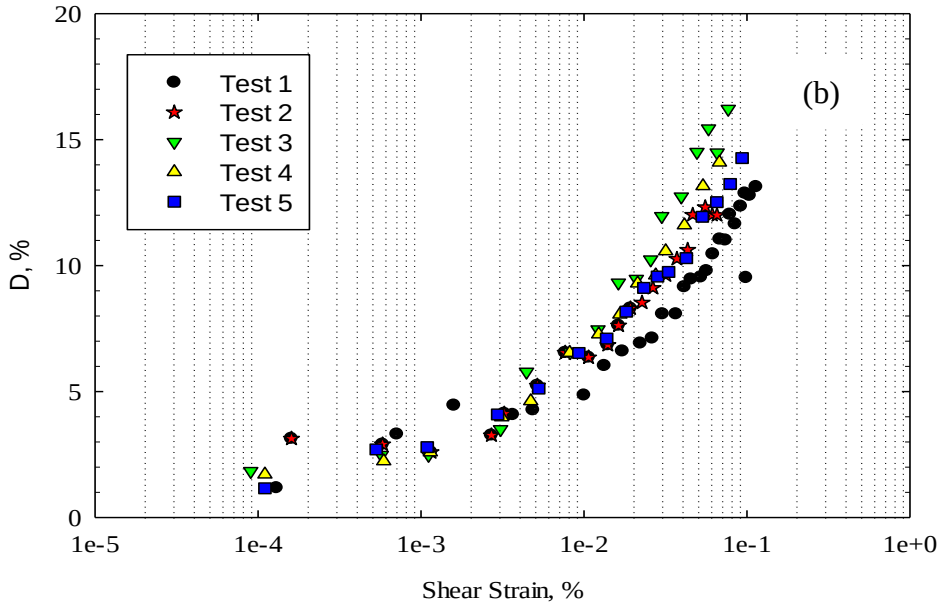


Figure 4.4: (a) shear modulus degradation and (b) damping of five specimens at 0.87 void ratio and 61% saturation, and tested at 25 kPa confining stress

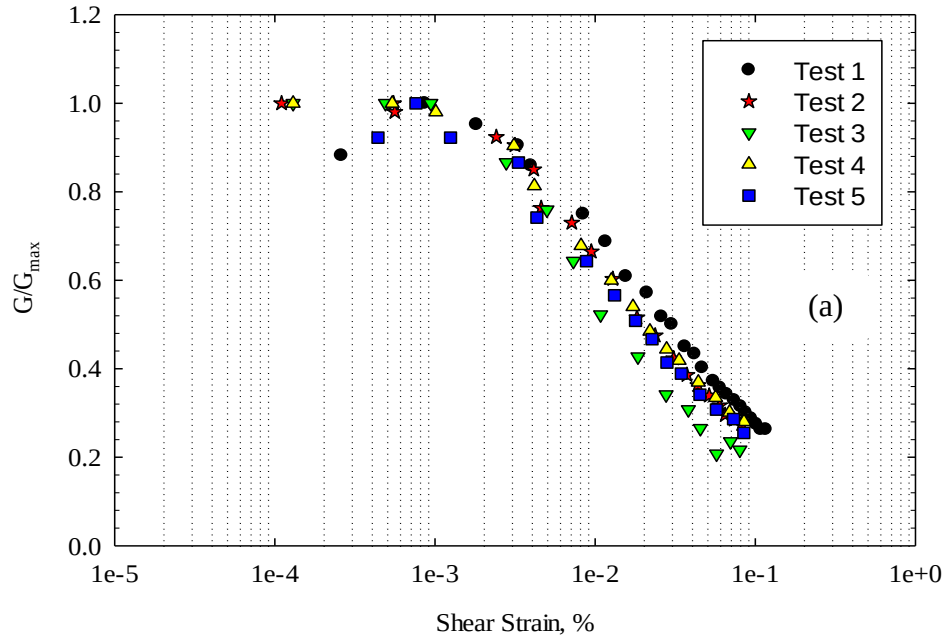


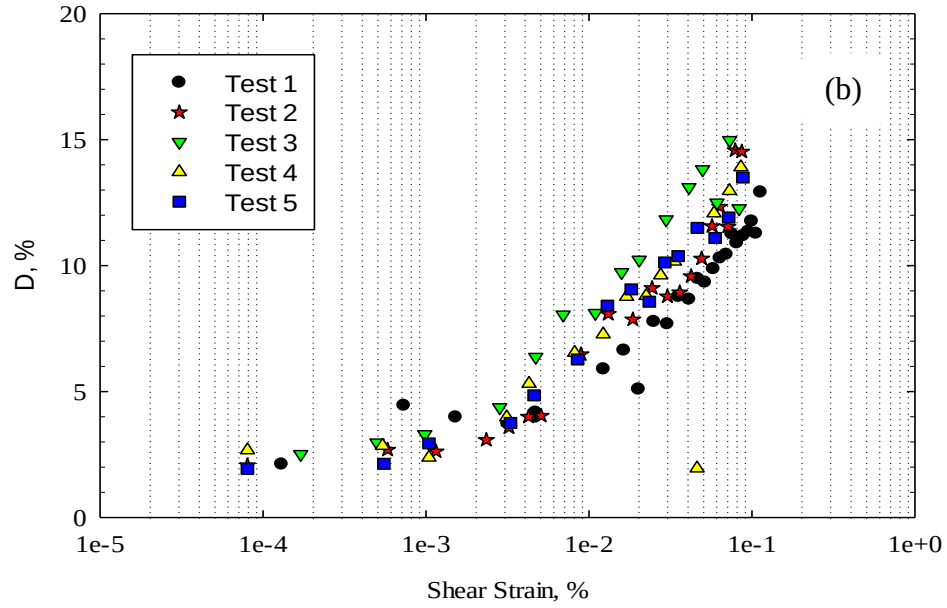


Figure 4.5: (a) shear modulus degradation and (b) damping of five specimens at 0.87 void ratio and 61% saturation, and tested at 100 kPa confining stress

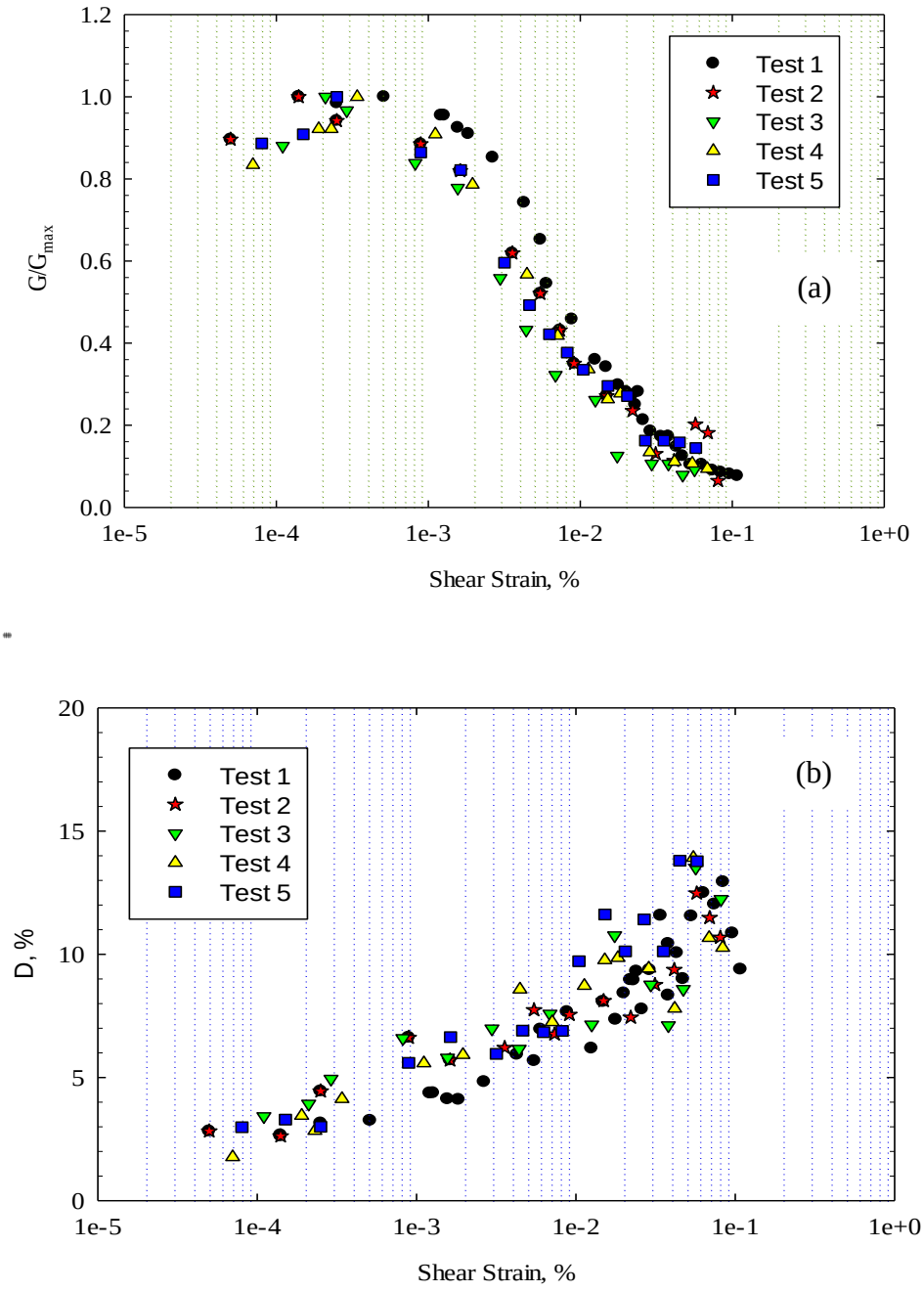


Figure 4.6: (a) shear modulus degradation and (b) damping of five specimens at 0.87 void ratio and 23% saturation, and tested at 100 kPa confining stress

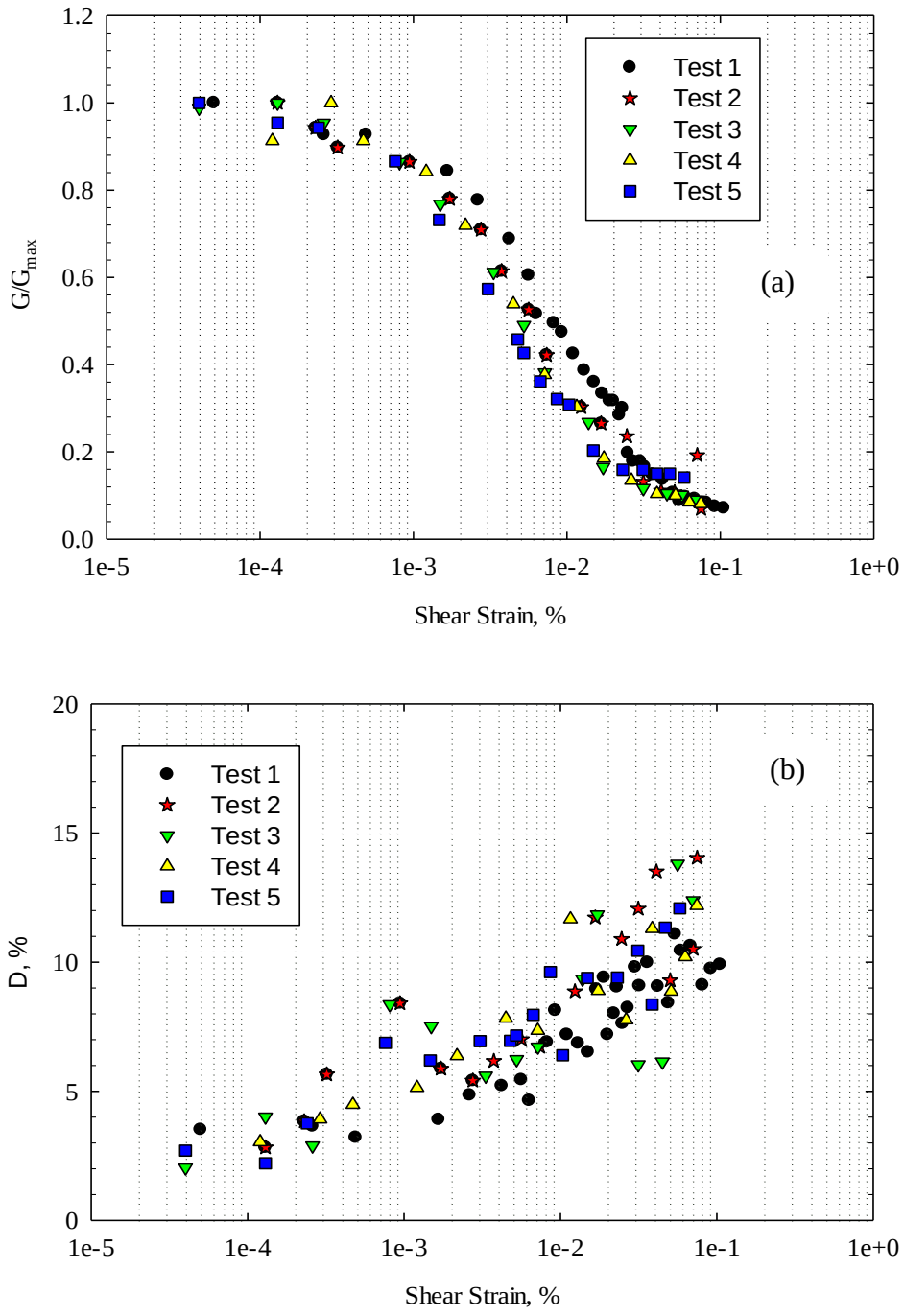


Figure 4.7: (a) shear modulus degradation and (b) damping of five specimens at 0.87 void ratio and 23% saturation, and tested at 200 kPa confining stress

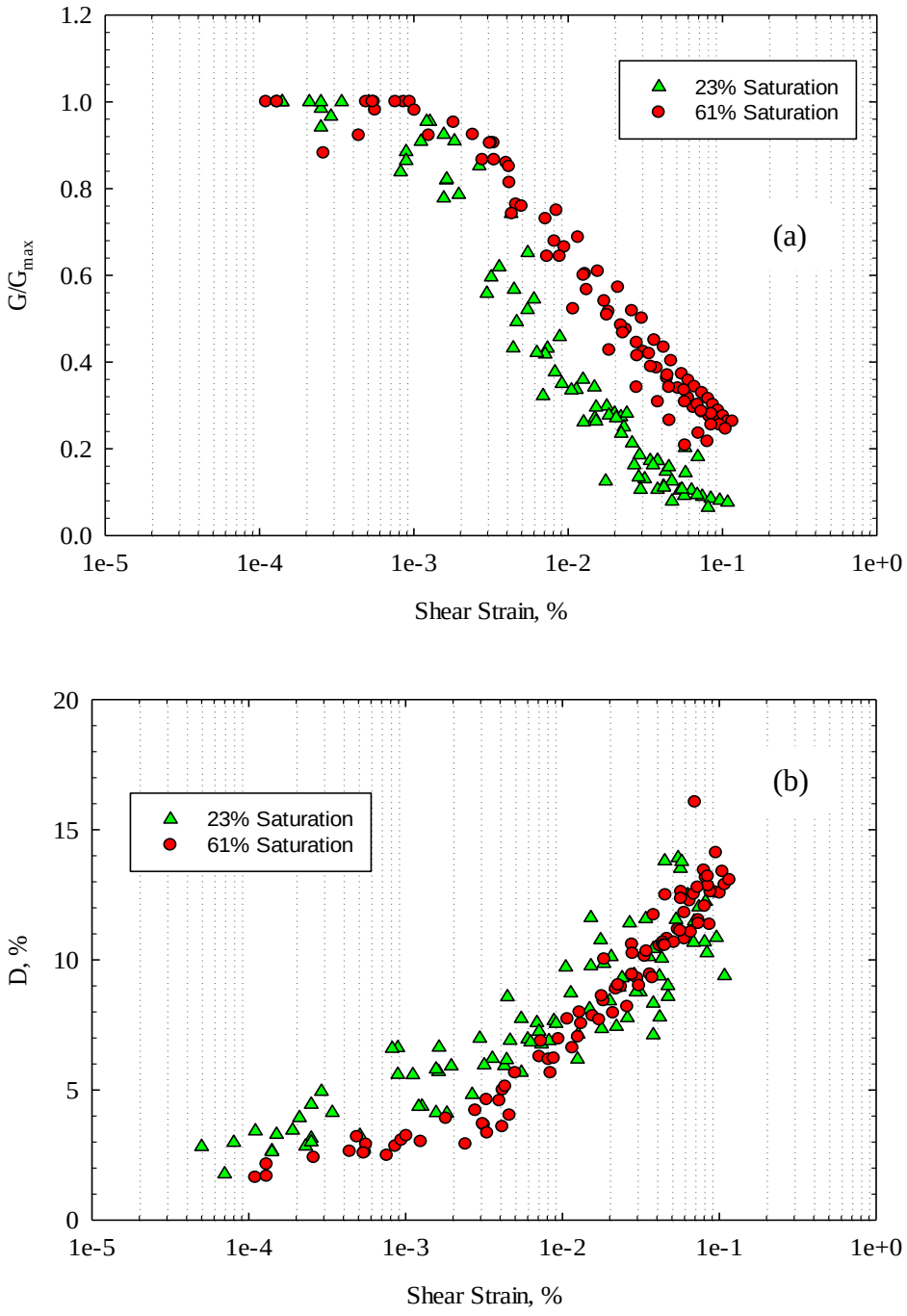


Figure 4.8: (a) shear modulus degradation and (b) damping of five specimens each at 0.87 void ratio and tested at 100 kPa confining stress

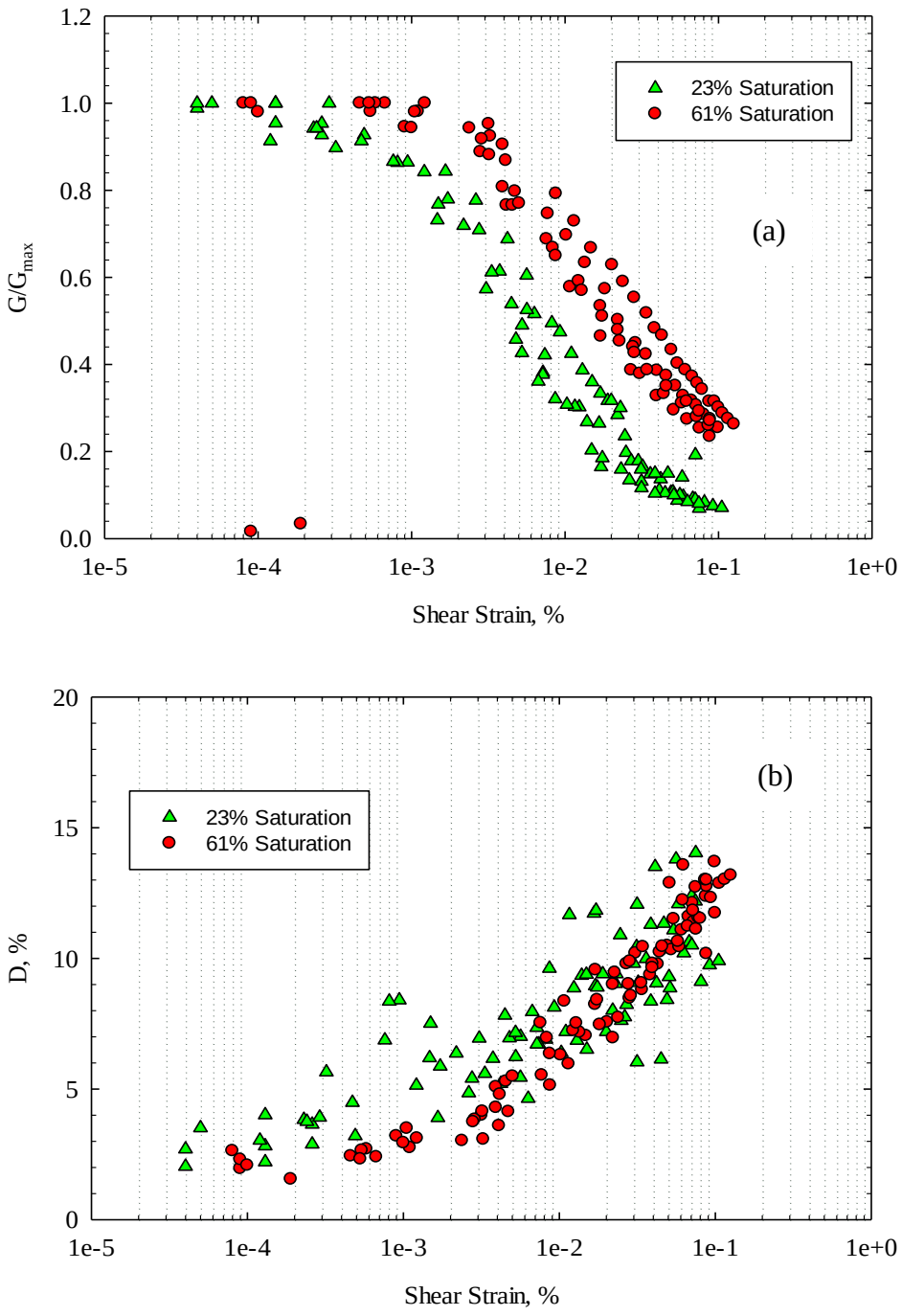


Figure 4.9: (a) shear modulus degradation and (b) damping of five specimens each at 0.87 void ratio and tested at 200 kPa confining stress

## 4.3 Effect of Confining Stress

As shown in the test matrix of Table 3.2, all of the specimens were tested at varying confining stresses of 25, 50, 100, 200, and 400 kPa to investigate the effect of confining stress on

dynamic properties of loess. Figure 4.10 shows the effect of confining stress on $G/G_{max}$ and D for a specimen prepared at 23% saturation and 0.87 void ratio. The effect of confining stress on $G/G_{max}$ and D for all other specimens are provided in Appendix B, in Figures B.7 through B.13. The shear modulus degradation, $G/G_{max}$, generally increased with an increase in confining stress as seen in Figure 4.10(a). However, the damping ratio decreased with an increase of confining stress, see Figure 4.10(b), though the effect is not clear due to the scatter in test results as explained in Section 4.2. In the previous section, the comparison of saturation was made using raw data. In this section, comparison of the test results at varying confining stress is found to be difficult because the scatter is large relative to the measured differences. Therefore, a comparison based on best-fit curves is used, even though comparison using raw data would be preferable.

Darendeli's modified hyperbolic model (Darendeli 2001), discussed in Section 2.3.3, is being utilized to model the test results due to its more accurate representation of the dynamic properties of soils as discussed in 2.3.3. The $G/G_{max}$ best-fit curve is determined using Equation 2.8 as

$$\frac{G}{G_{max}} = \frac{1}{1 + (\gamma/\gamma_r)^a} \tag{4.1}$$

The best-fit damping ratio, D, curve is determined using Equations 4.2 through 4.7

$$D_{Adjusted} = b * (\frac{G}{G_{max}})^{0.1} * D_{Masing} + D_{min} \tag{4.2}$$

where $D_{Adjusted}$ = scaled and capped material damping ratio (%),

$$D_{Masing} = c_1 D_{Masing,a=1.0} + c_2 D_{Masing,a=1.0}{}^2 + c_3 D_{Masing,a=1.0}{}^3 \ (\%) \tag{4.3}$$

$$D_{Masing,a=1.0} = \frac{100}{\pi}\left(4\frac{\gamma - \gamma_r \, ln\left(\frac{\gamma+\gamma_r}{\gamma_r}\right)}{\frac{\gamma^2}{\gamma+\gamma_r}} - 2\right) \ (\%) \tag{4.4}$$

$$c_1 = 1.1143a^2 + 1.8618a + 0.2523 \quad (4.5)$$

$$c_2 = 0.0805a^2 + 0.0710a + 0.0095 \quad (4.6)$$

$$c_3 = 0.0005a^2 + 0.0002a + 0.0003 \quad (4.7)$$

For $G/G_{max}$, Equation 4.1, the unknowns are the reference strain, $\gamma_r$, and coefficient, a. In damping ratio, Equations 4.2 through 4.7, the unknowns are reference strain, $\gamma_r$, and coefficients, a and b, and $D_{min}$. A computer program using R code is written to determine the unknowns by fitting to the test results. The R code employs nonlinear regression analysis using the non-linear least squares approach. The nonlinear regression (function nls in R) determines the best parameter values by approximating the non-linear function initially using a linear one and refining it by successive iterations (Baty et al. 2015). Appendix D provides the R code. An example of the best-fit curves for $G/G_{max}$ and D, including the 95% prediction interval, for a specimen prepared at 0.87 void ratio and 61% saturation and tested at 100 kPa confining stress, is presented in Figure 4.11(a) and (b).

Figures 4.12 through 4.16 provide the best-fit curves for specimens prepared at 0.87 void ratio and at saturation levels of 23, 36, 48, 61, and 74%, respectively, and Figures 4.17 through 4.18 include the best-fit curves for specimens prepared at 0.7 void ratio at saturation levels of 60 and 76%. Figure 4.19 provides the best-fit curves for the intact specimen at 1.21 void ratio and 61% saturation.

The results for all the specimens show that the $G/G_{max}$, generally, increases with an increase of confining stress. The 0.87 void ratio specimens show an increase $G/G_{max}$ with each increment of confining stress as illustrated in Figures 4.12 through 4.16 with the exception of specimens saturated at 23% and 36%, shown in Figure 4.12 and 4.13, respectively, in which the 200 kPa curve has a less $G/G_{max}$ than the 100 kPa curve up to shear strain of $10^{-2}$%. Similarly, in

the 0.7 void ratio specimens at 60% and 76% saturation, as shown in Figures 4.17 and 4.18, the $G/G_{max}$ increased with an increase of confining stress. However, the 60% saturated specimen at 50 kPa did not conform with the general trend in which it has lower $G/G_{max}$ than the 25 kPa as shown in Figure 4.17. The $G/G_{max}$ of the intact specimen increasees uniformly with the increase of confining stress as illustrated in Figure 4.19.

The average best-fit curves for the five specimens at 23% and 61% saturation have shown similar results as depicted in Figures 4.20 and 4.21. The $G/G_{max}$ generally increases with the increase of confining stress. However, the effect of confining stress on $G/G_{max}$ is found to be dependent on saturation level. At low saturation, 23%, the effect of confining stress is more pronounced than at high saturation, 61%, as shown in Figures 4.20 and 4.21, respectively. The reason can be due to the decrease of matric suction as saturation increases. According to Adrian (2012), matric suction of Fulton loess decreses with increase of saturation. Increase of pore pressure may also have played a role. But, since pore pressure transducer was not available for the RCTS device, pore pressure during testing was not monitored.

The resonant column is a nondestructive test, and same specimen was tested at all increments of confining stresses. Shear modulus degradation has to increase with increase of confining stress. However, the 36% and 76% saturated specimen show a different trend. Figure 4.13 shows that the $G/G_{max}$ for a void ratio of 0.87and 36% saturation at 400 kPa is much less than the other lower confining stresses. Also, the specimen at 0.7 void ratio and 76% saturation and tested at 200 and 400 kPa confining stress showed a similar behavior of decrease in $G/G_{max}$ as that of the specimen at 36% saturation and tested at 400 kPa stress as shown in Figure 4.18. This indicates a decrease of strength. Each specimen was checked visually after the end of the test for failure such as cracks and slippage between layers. However, there was no visual

indication of failure. Therefore, the degradation of strength at higher confining stress can be due to partial failure within the specimen, which is not visible, caused by the accumulation of cyclic strain contrary to the test being a nondestructive test. Hence these test results have been ignored in the comparison of the effect of confining stress.

The damping ratio, D, also decreases with an increase of confining stress. All the specimens have shown a decrease of D at shear strains larger than $10^{-2}$% with each increment of confining stress as illustrated in Figures 4.12(b) through 4.21(b) with some exceptions discussed here. For the 0.87 void ratio specimen at 36% saturation, shown in Figure 4.13, the 25 kPa results show a lower D than the 50 and 100 kPa results. The D of the intact specimen has decreased uniformly with an increase of confining stress as illustrated in Figure 4.19. Similarly, the average best-fit damping ratio curves for the five specimens at 23% and 61% saturation, depicted in Figures 4.20 and 4.21, generally increase with an increase of confining stress. Nonetheless, the effect of confining stress on D is found to be more pronounced at low saturation, 23%, than at high saturation, 61%, as shown in Figures 4.20 and 4.21, respectively. This may be due to, similar to $G/G_{max}$, the decrease of matric suction and increase of pore pressure with the increase of saturation.

In summary, $G/G_{max}$ increases, and D decreases with an increase of confining stress. But, the effect of confining stress was more pronounced at low saturation than at high saturation. This may be due to the decrease of matric suction and increase of pore pressure as saturation increases. Therefore, the dynamic properties of loess soil varies with confining stress and is dependent on the saturation level of the soil.

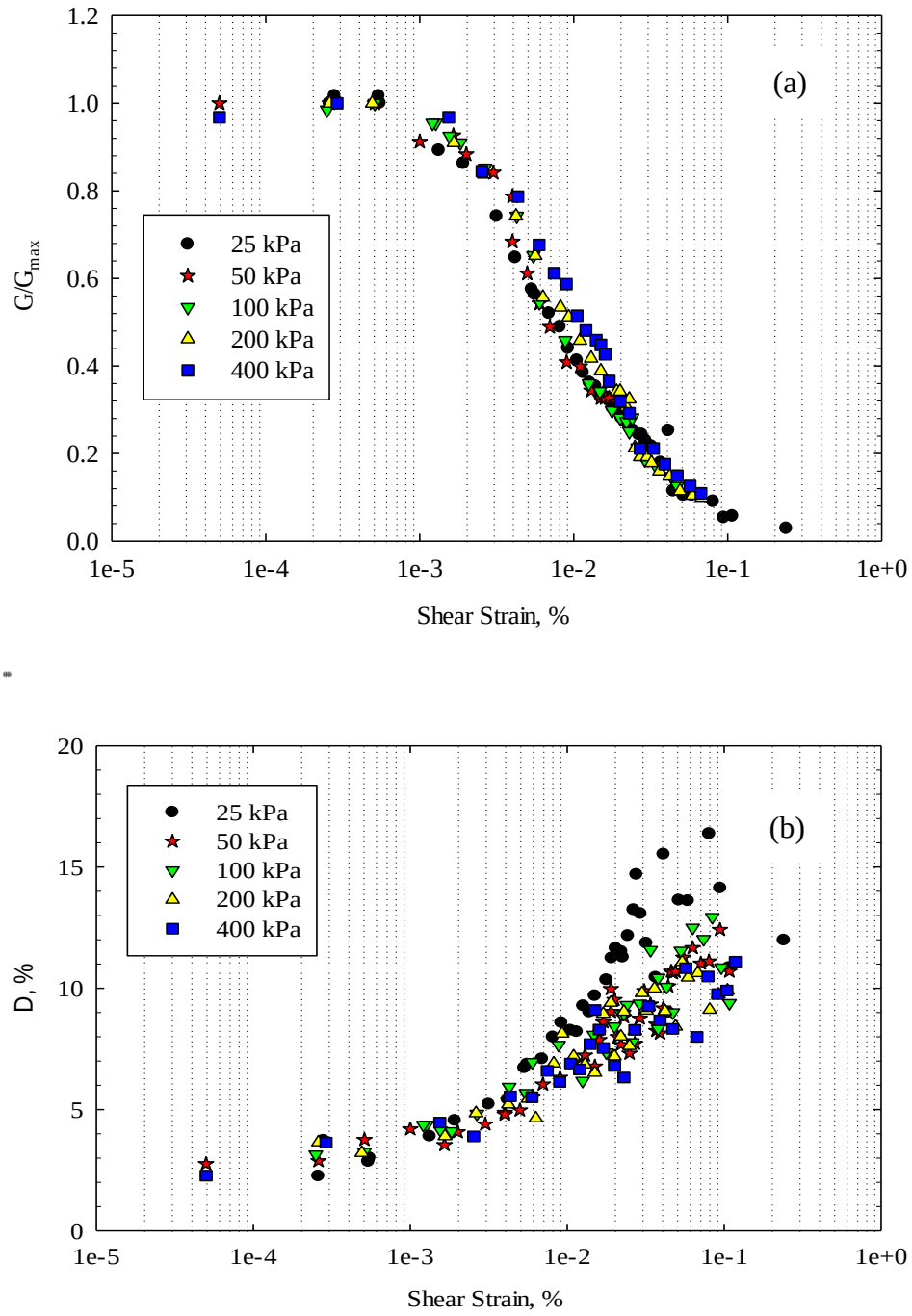


Figure 4.10: Effect of confining stress on (a) shear modulus degradation and (b) damping ratio for a specimen prepared at 0.87 void ratio and 23% saturation

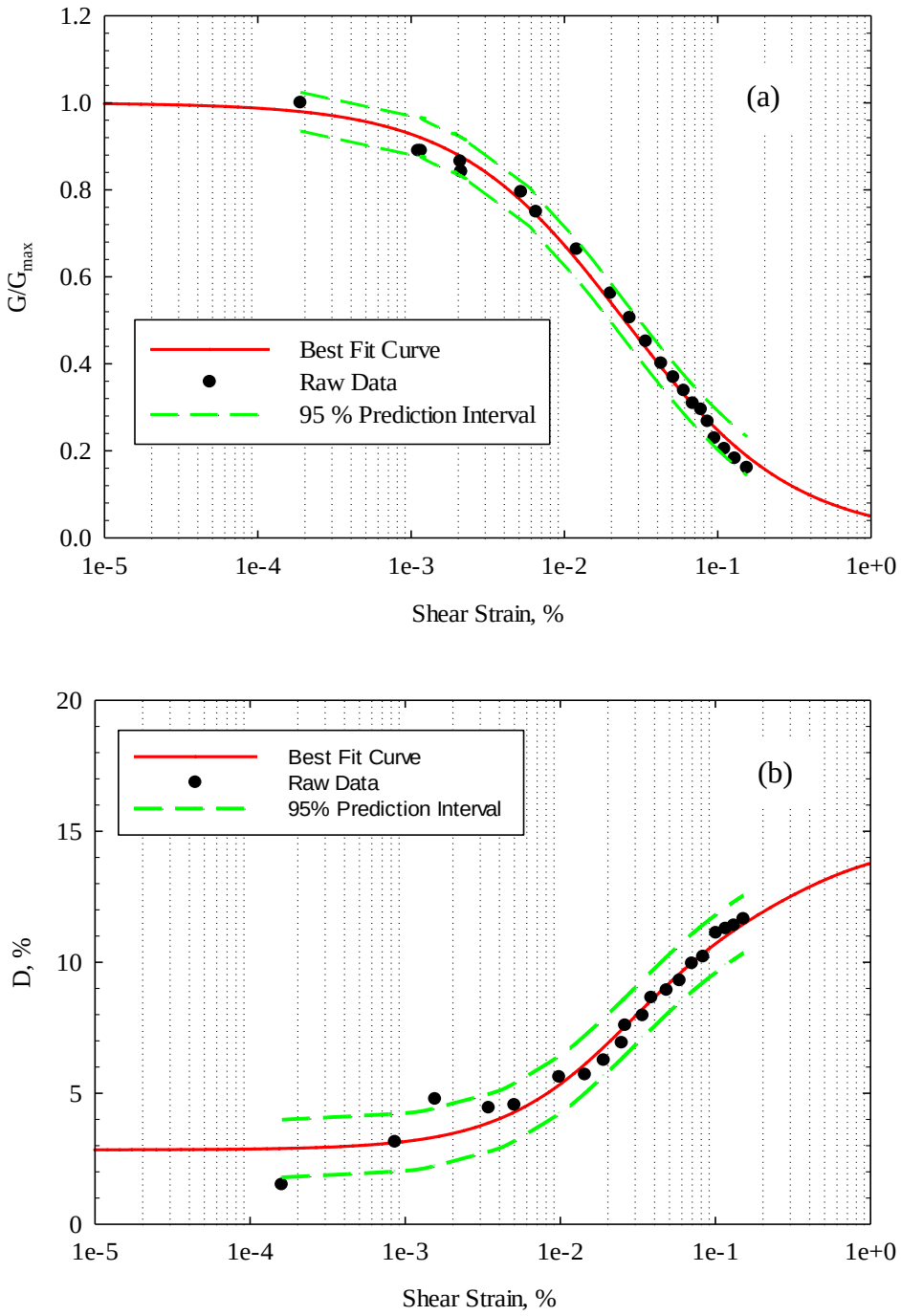


Figure 4.11: Best fit curve with 95% prediction level for (a) shear modulus degradation and (b) damping ratio using Darendeli's model for 61% saturation specimen and tested at 100kPa confining stress

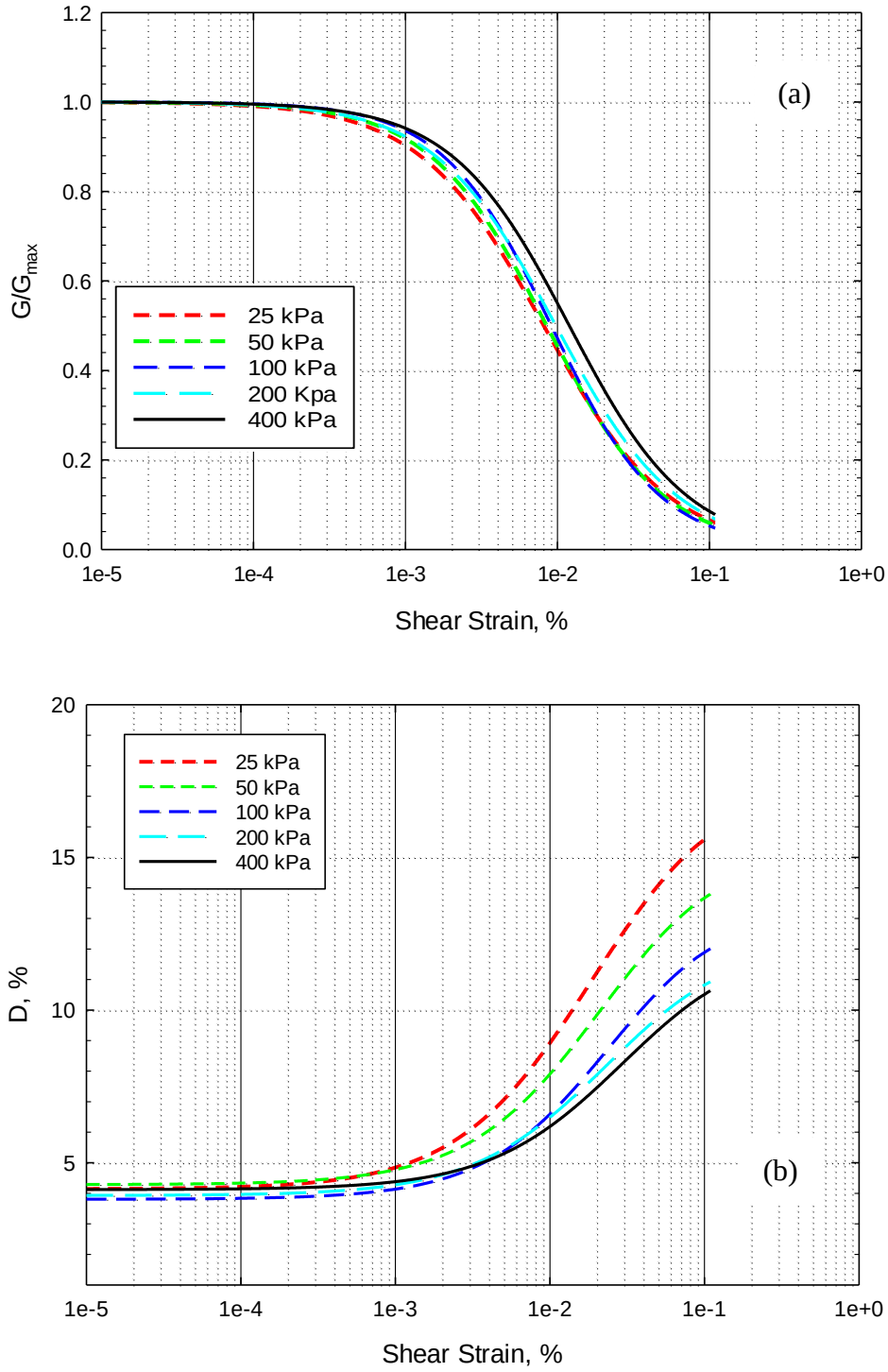


Figure 4.12: Effect of confining stress on (a) shear modulus degradation and (b) damping ratio for a specimen prepared at 0.87 void ratio and 23% saturation

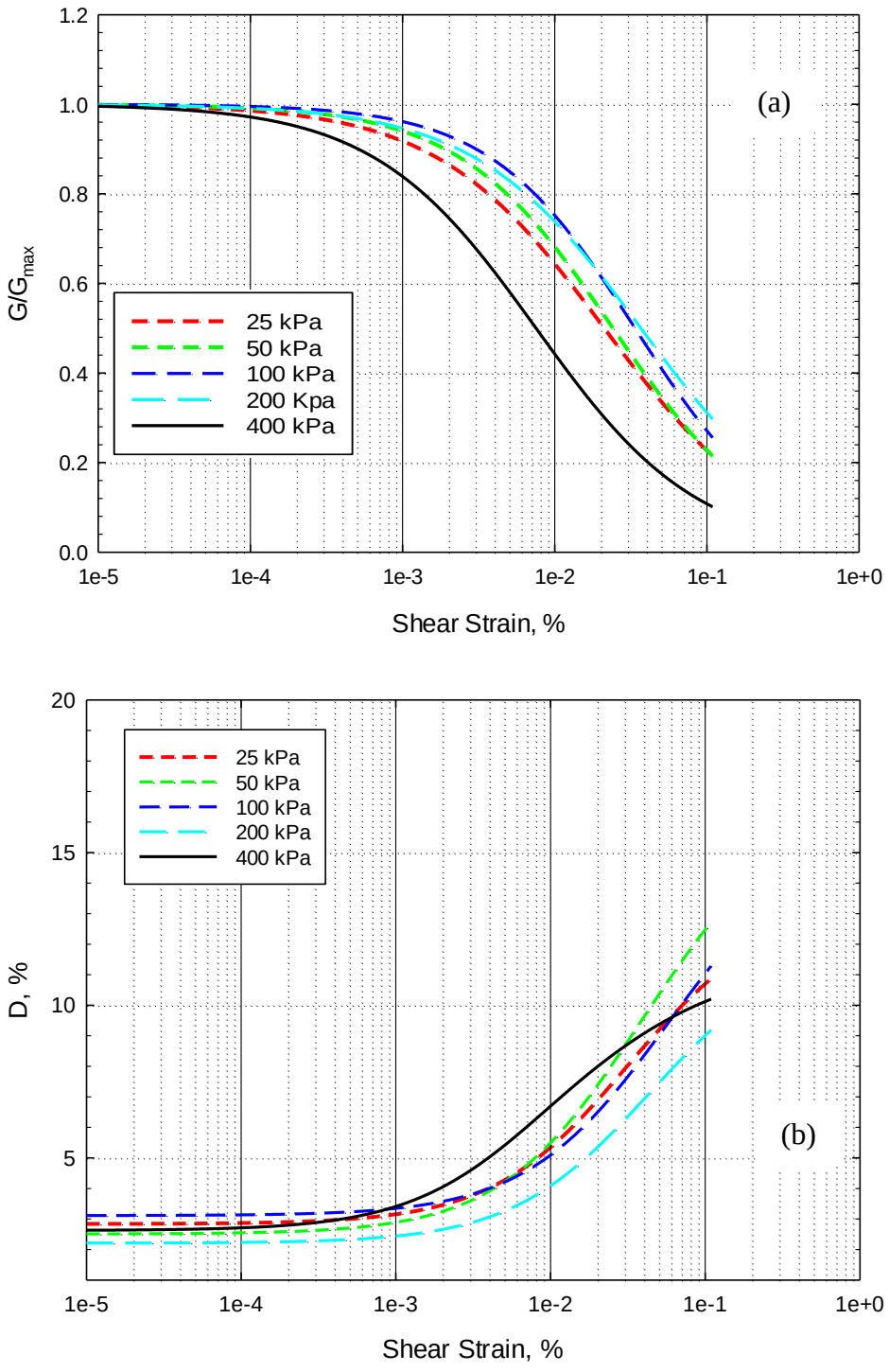


Figure 4.13: Effect of confining stress on (a) shear modulus degradation and (b) damping ratio for a specimen prepared at 0.87 void ratio and 36% saturation

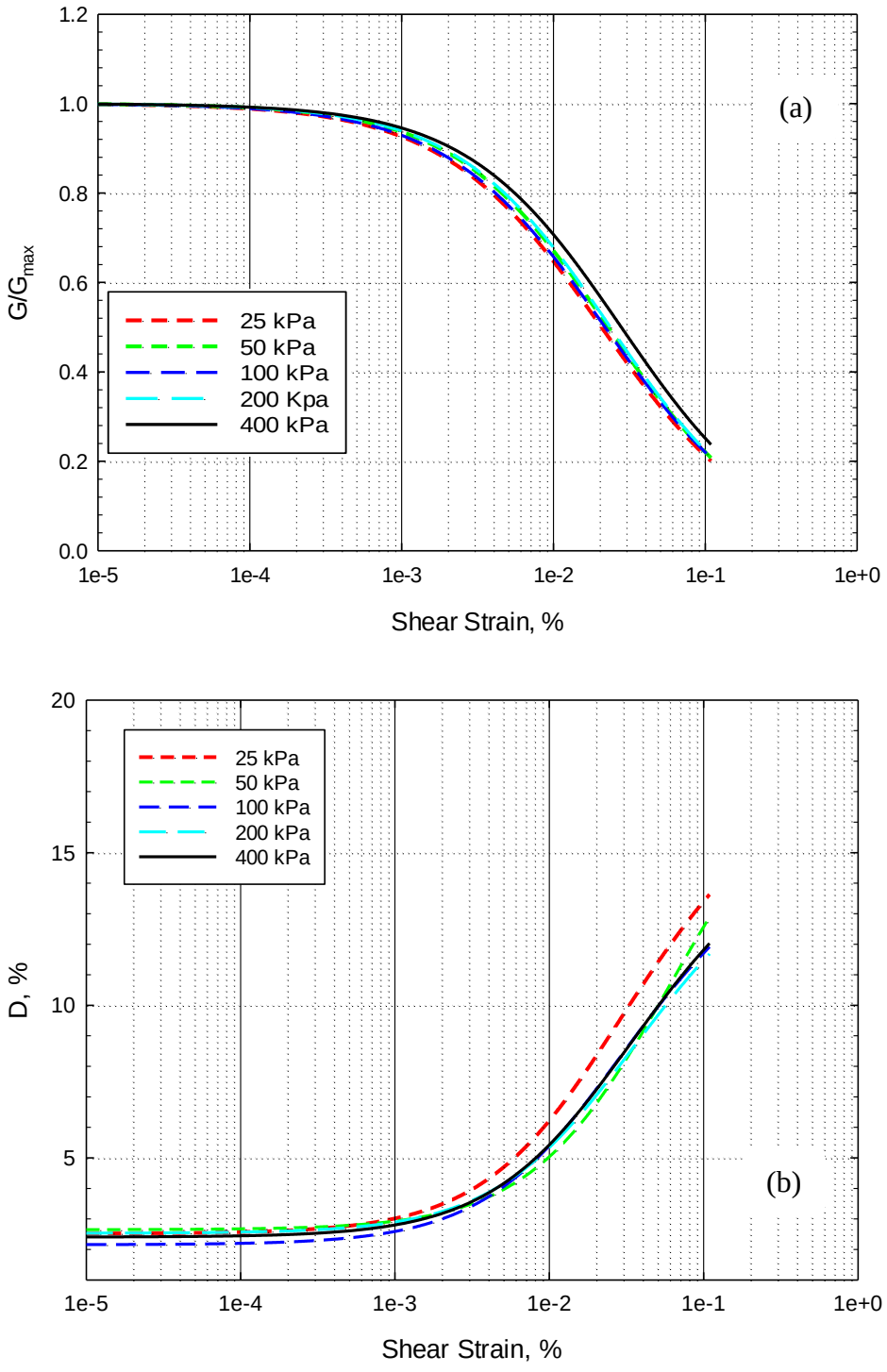


Figure 4.14: Effect of confining stress on (a) shear modulus degradation and (b) damping ratio for a specimen prepared at 0.87 void ratio and 48% saturation

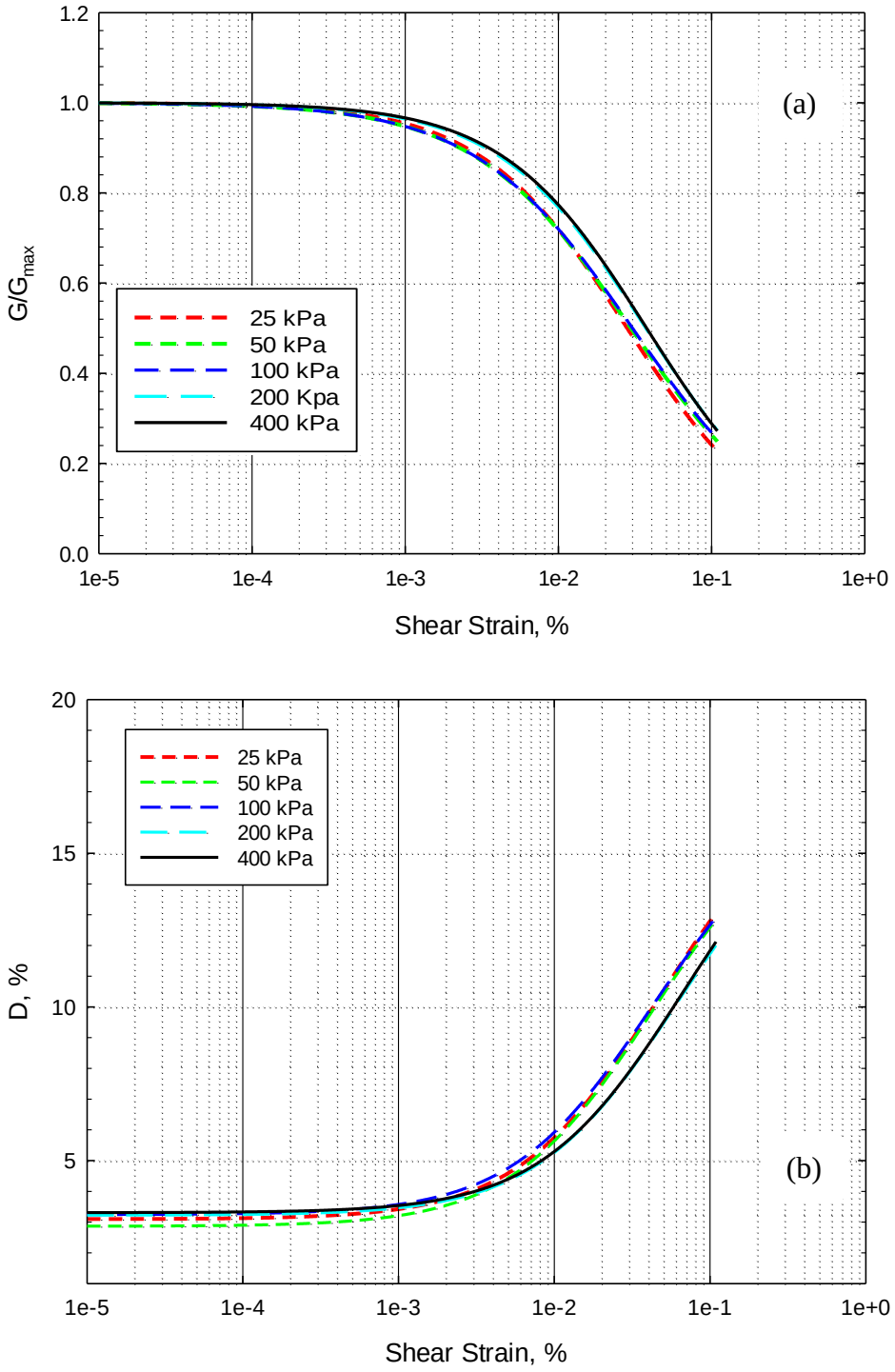


Figure 4.15: Effect of confining stress on (a) shear modulus degradation and (b) damping ratio for a specimen prepared at 0.87 void ratio and 61% saturation

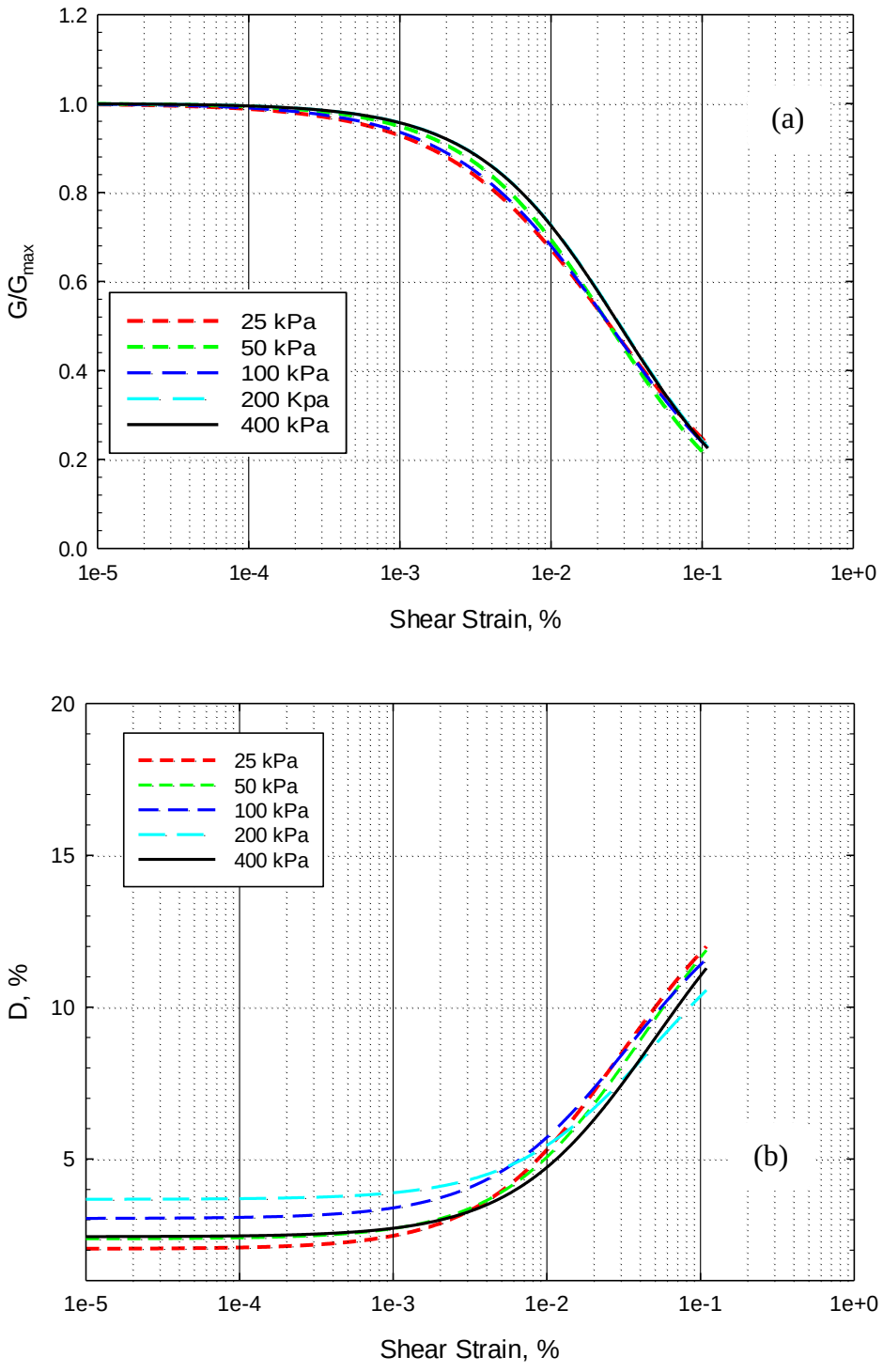


Figure 4.16: Effect of confining stress on (a) shear modulus degradation and (b) damping ratio for a specimen prepared at 0.87 void ratio and 74% saturation

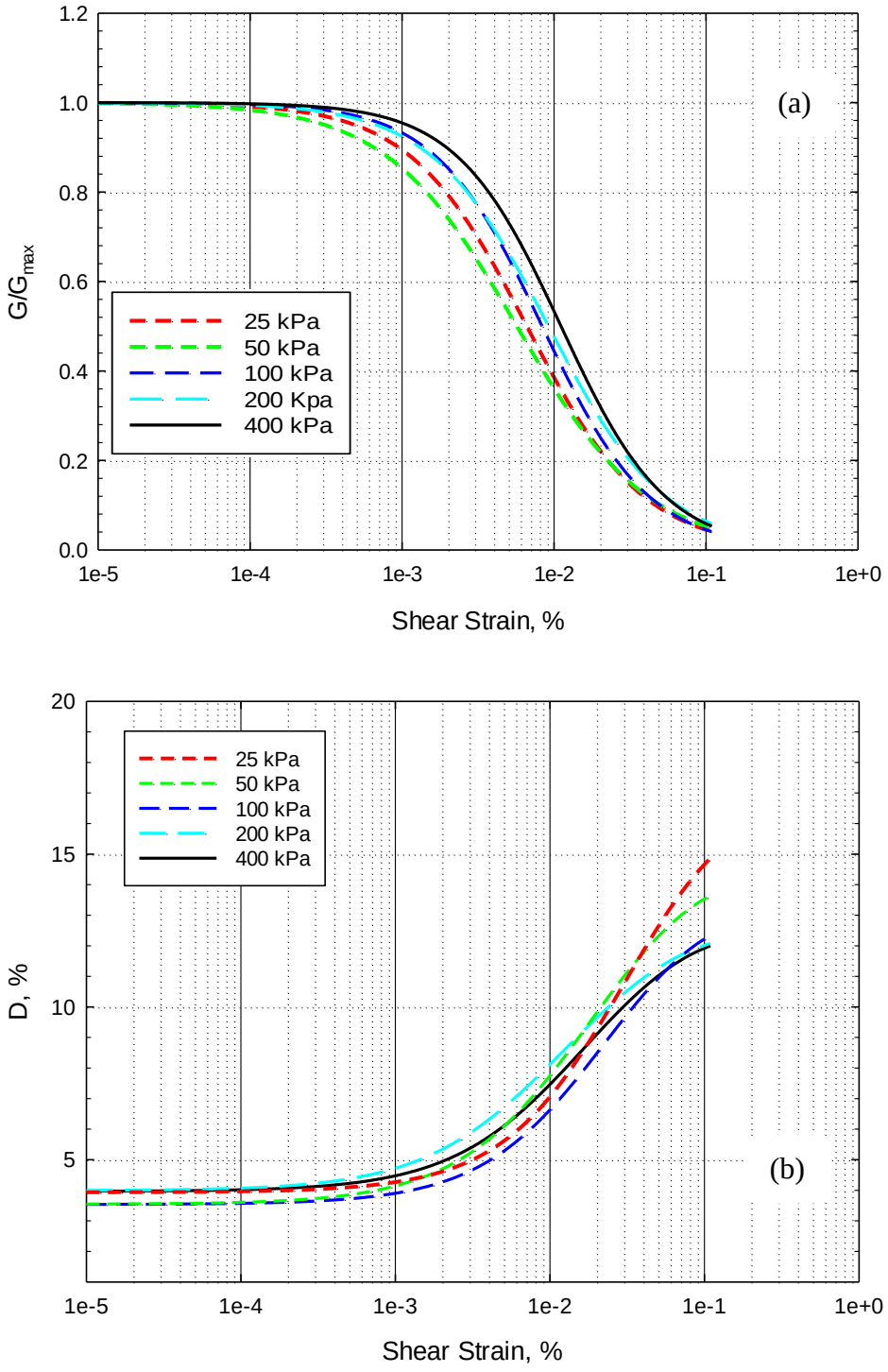


Figure 4.17: Effect of confining stress on (a) shear modulus degradation and (b) damping ratio for a specimen prepared at 0.7 void ratio and 60% saturation

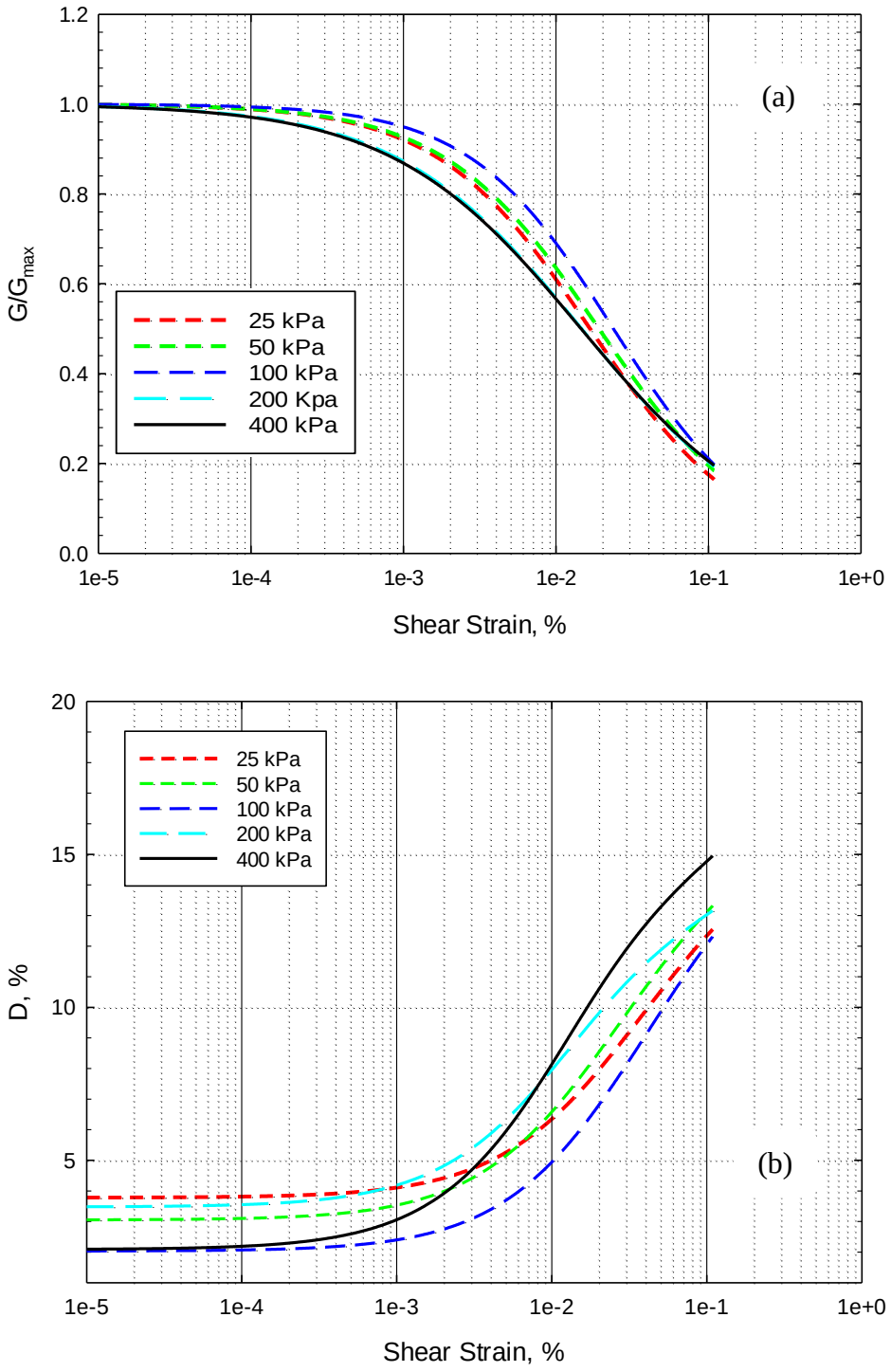


Figure 4.18: Effect of confining stress on (a) shear modulus degradation and (b) damping ratio for a specimen prepared at 0.7 void ratio and 76% saturation

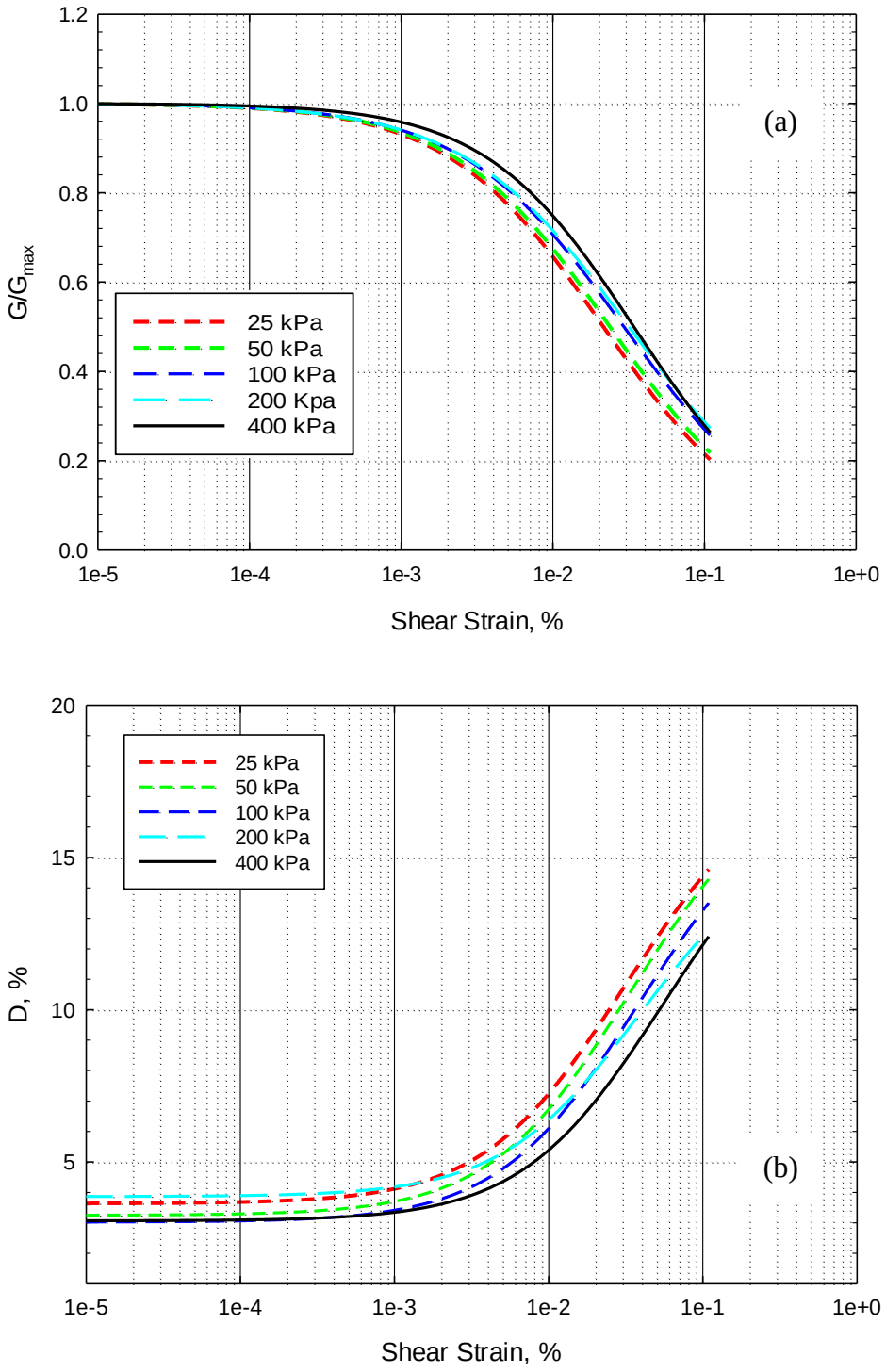


Figure 4.19: Effect of confining stress on (a) shear modulus degradation and (b) damping ratio for an intact specimen at 1.21 void ratio and 61% saturation

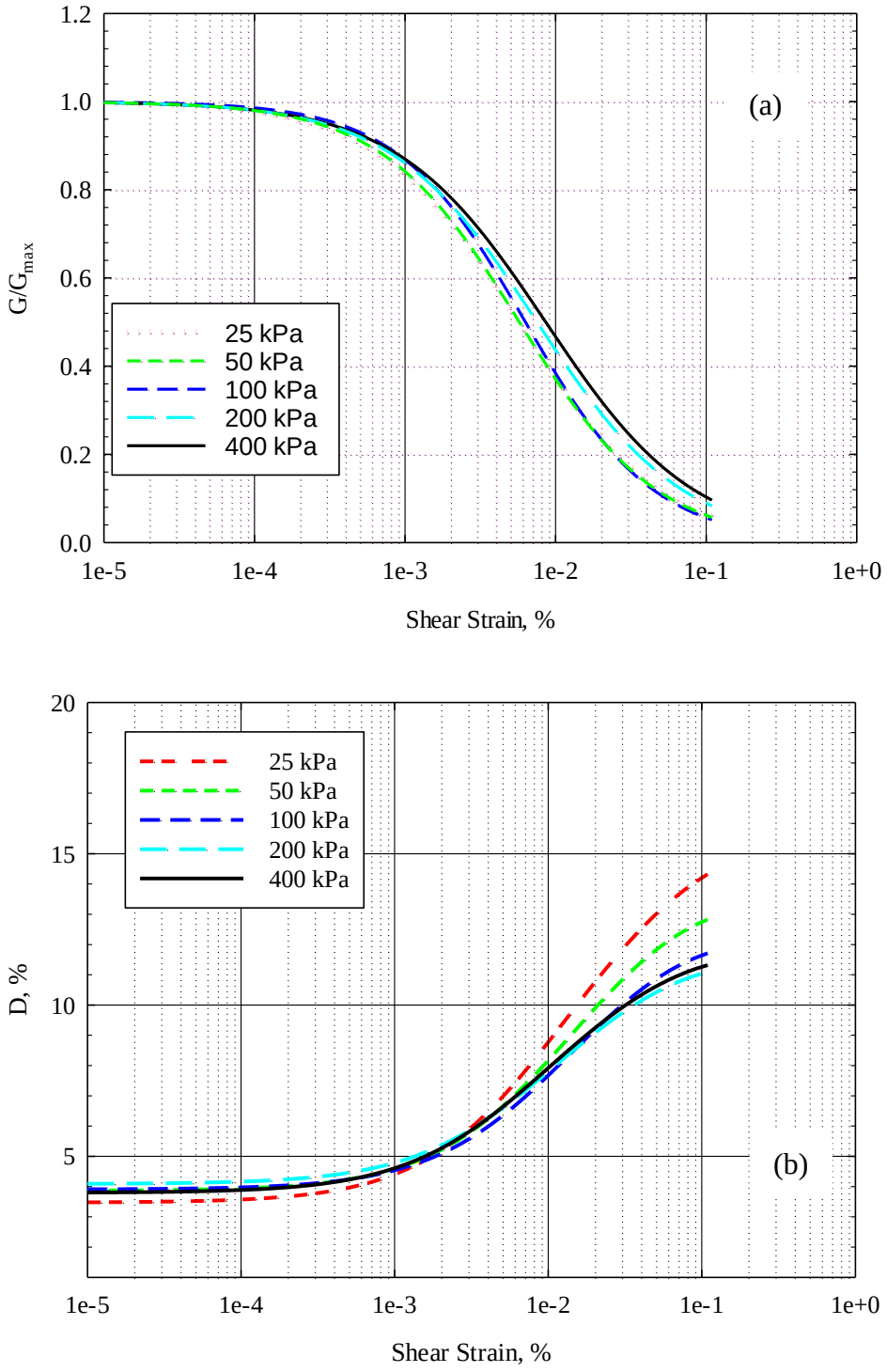


Figure 4.20: Effect of confining stress on (a) shear modulus degradation and (b) damping ratio for the five specimen prepared at 0.87 void ratio and 23% saturation

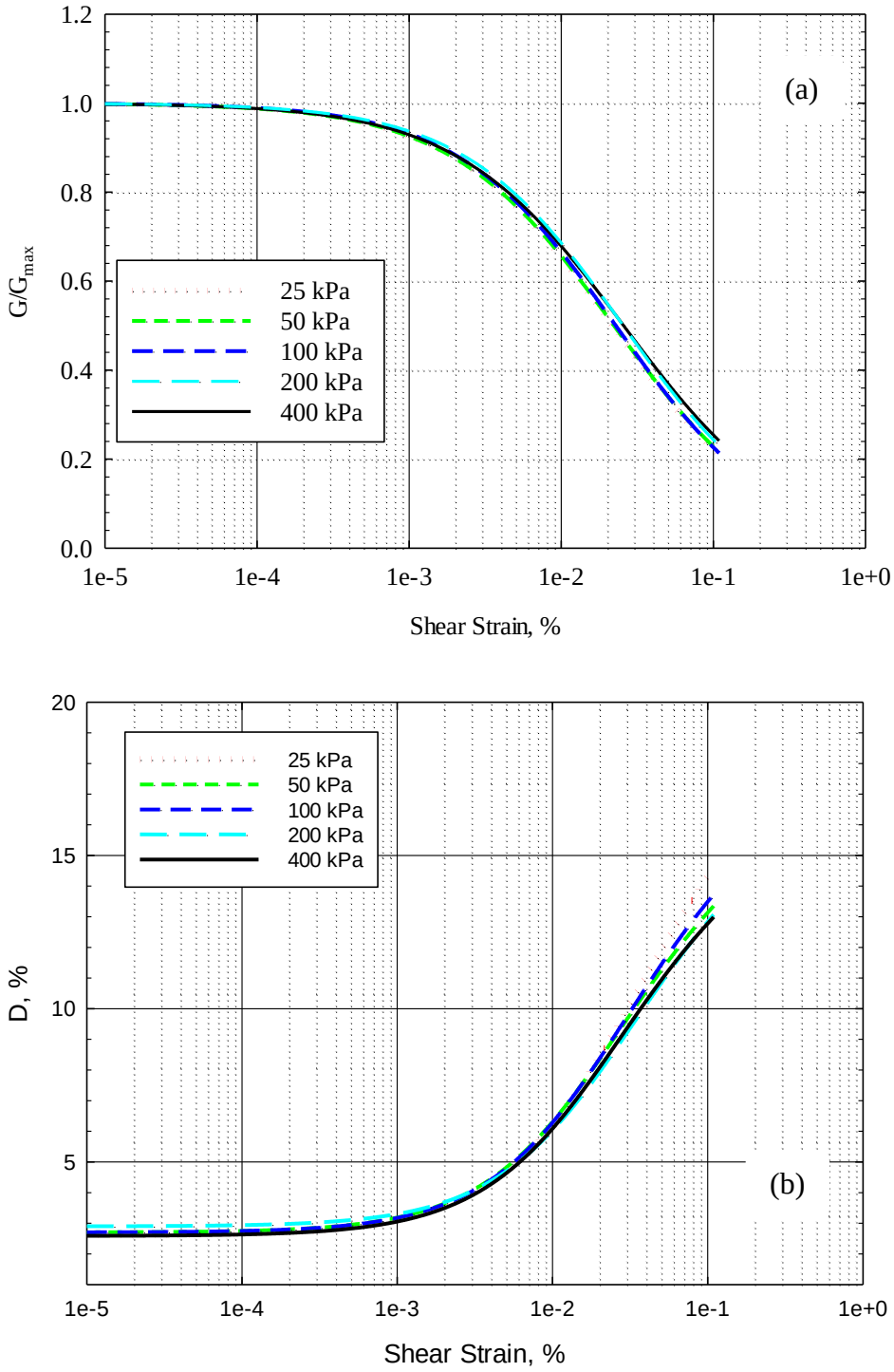


Figure 4.21: Effect of confining stress on (a) shear modulus degradation and (b) damping ratio for the five specimens prepared at 0.87 void ratio and 61% saturation

## 4.4 Effect of Void Ratio

As discussed in Chapter 2, Darendeli (2001) revealed that void ratio has only slight effect on $G/G_{max}$ and damping ratio contrary to Hardin and Drnevich (1972). Meanwhile, both Darendeli (2001) and Hardin and Drnevich (1972) confirmed that it affects significantly the maximum shear modulus of soil. The effect of void ratio on Memphis loess soil is investigated in this study. Specimens were prepared at 0.87 and 0.70 void ratios. To examine if the effect of void ratio varies with degrees of saturation, specimens prepared at 61% and 74% saturation were compared. Specimens at 23%, 36%, and 48% saturation could not be prepared at a void ratio of 0.7 because the load required to compact the specimens was greater than the load capacity of the triaxial loading system. Figures 4.22 through 4.24 provide the shear modulus degradation and damping best-fit curves and presents the effect of void ratio on specimens prepared at saturation levels of 61% and 74%. In the figures, σ represent the confining stress and e represent void ratio.

Figure 4.22 illustrates the effect of void ratio on shear modulus degradation and damping curves for 61% saturated remolded specimens tested at confining stresses of 25, 50, 100, 200, and 400 kPa in which the solid and broken lines represent the test results for 0.87 and 0.7 void ratio, respectively. The result shows that the higher void ratio has a higher $G/G_{max}$ and lower D.

However, Figures 4.23 and 4.24 do not show significant differences in $G/G_{max}$ and D. Figure 4.23 presents the comparison of remolded and intact specimen with void ratios of 0.87 and 1.21, respectively. The differences in the $G/G_{max}$ and D results are insignificant despite the difference in soil structure between disturbed and undisturbed specimens. The result also reveals that remolded and intact specimens may have comparable dynamic properties, although more test data are required to confirm this. Figure 4.24 also compares 0.7 and 0.87 void ratio of remolded specimens tested at 25, 50, and 100 kPa confining stress. The tests at 200 and 400 kPa

have been excluded from the comparison as the 0.70 void ratio specimen at these confining stresses has shown excessive degradation of strength as discussed in Section 4.3. The results show that the void ratio has only slight effect on G/Gmax and D.

Taking in to consideration the error with inherent physical differences between specimens discussed in section 4.2, void ratio does not have significant influence on shear modulus degradation and damping curves with the exception of Figure 4.22. This observation agrees with Darendeli (2001). In summary, the data suggest that void ratio may have insignificant impact on the dynamic properties of loess soil but more test data are required to validate this observation.

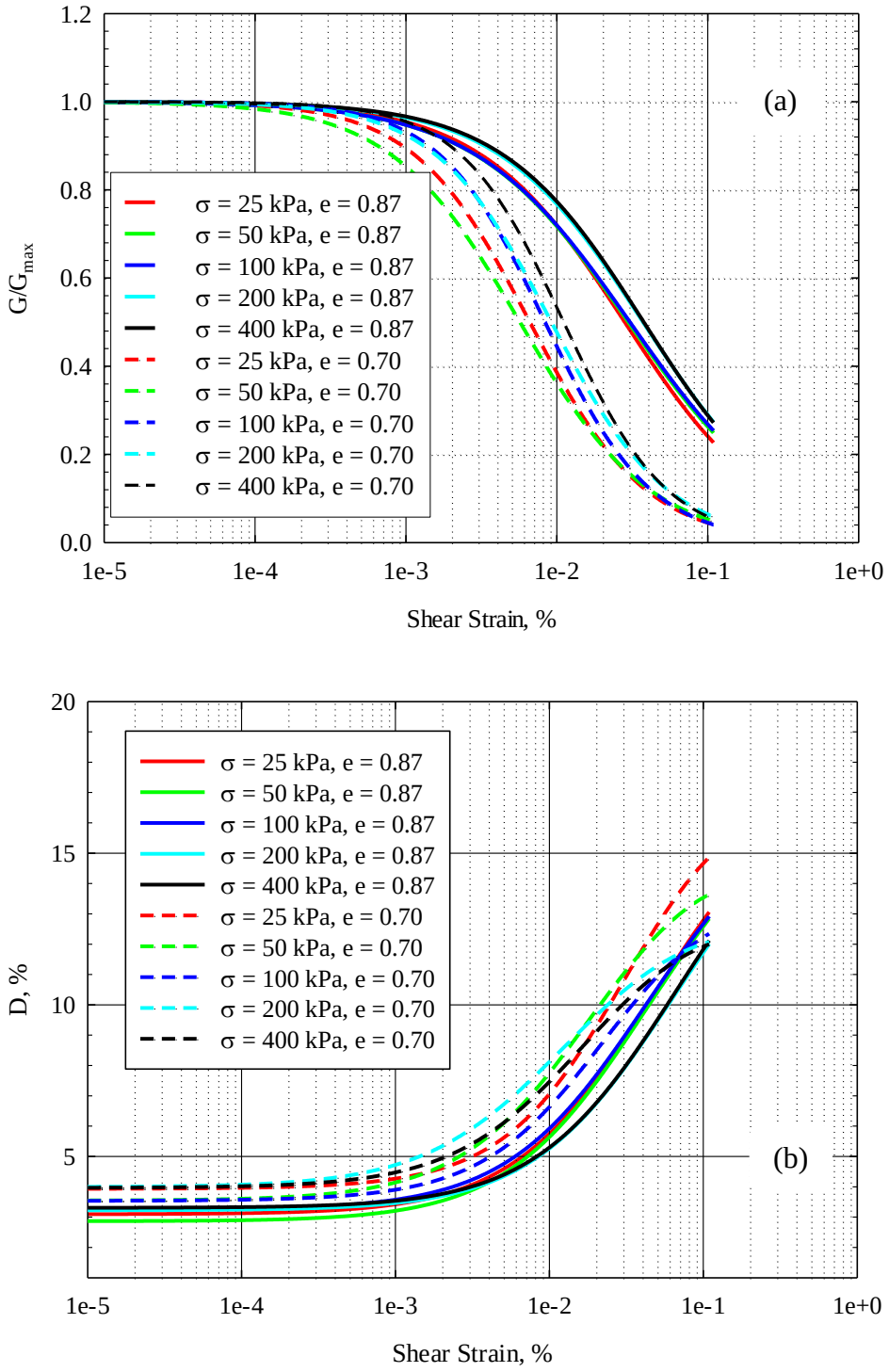


Figure 4.22: Effect of void ratio on (a) shear modulus degradation and (b) damping ratio for specimens at 61% saturation

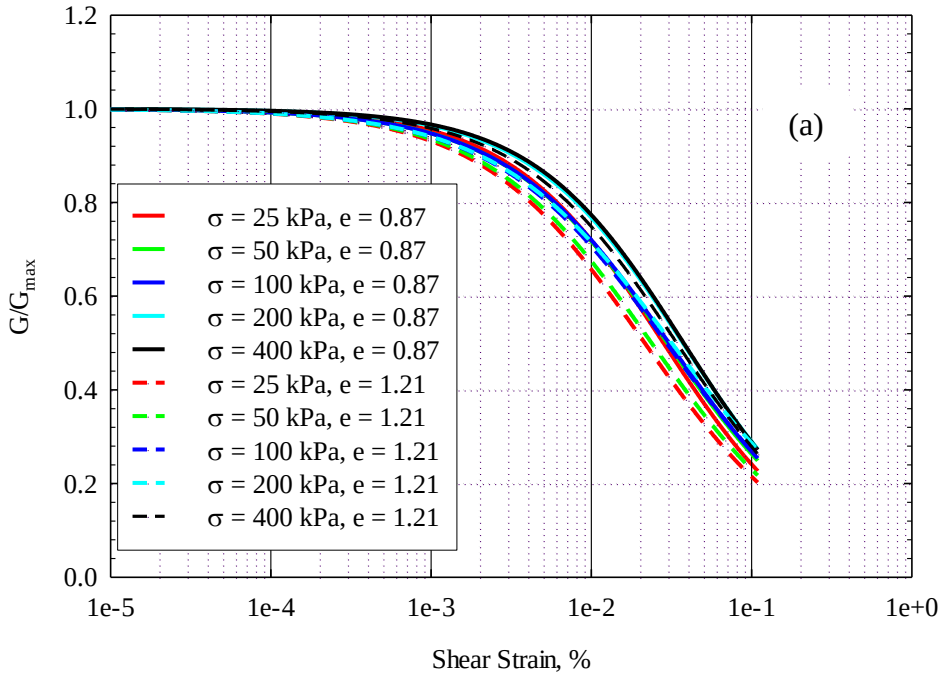


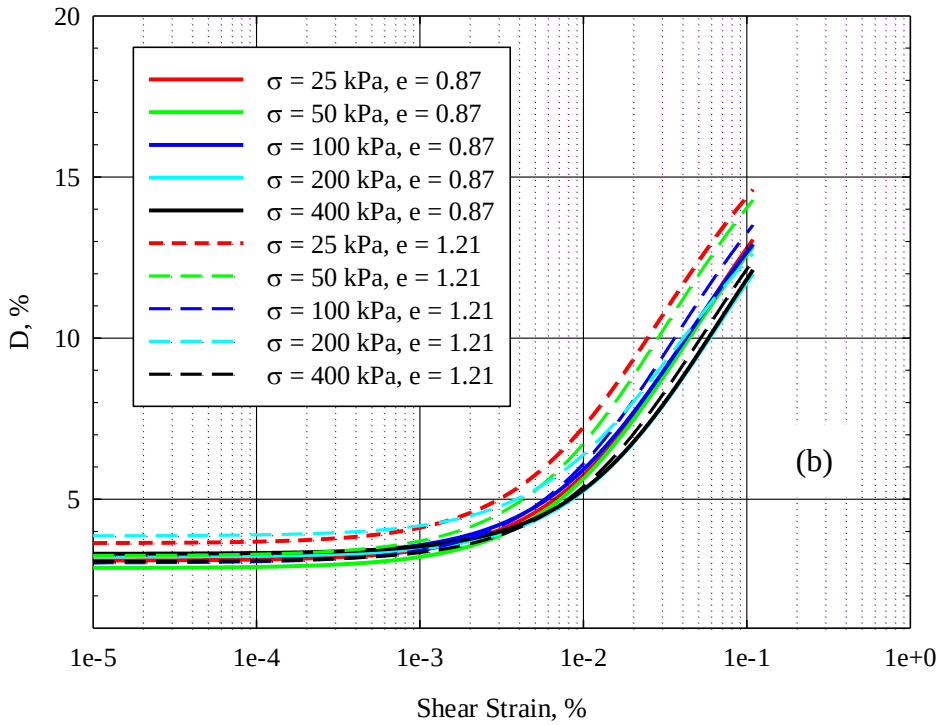


Figure 4.23: Effect of void ratio on (a) shear modulus degradation and (b) damping ratio for 61% saturated remolded (0.87 void ratio) and intact specimens (1.21 void ratio)

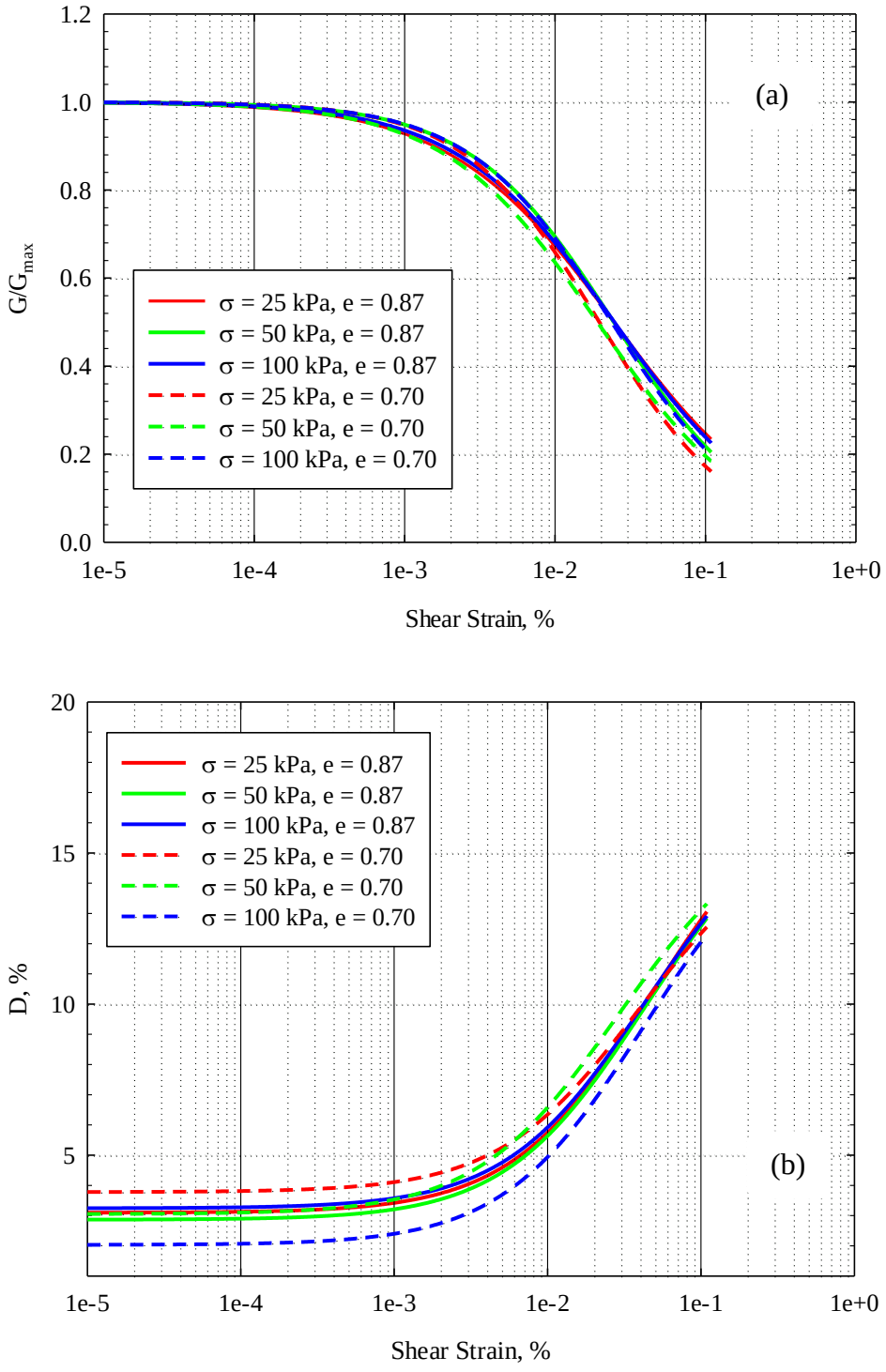


Figure 4.24: Effect of void ratio on (a) shear modulus degradation and (b) damping ratio for specimens prepared at 74% saturation

## 4.5 Effect of Coefficient of Lateral Earth Pressure, K

The coefficient of at-rest lateral earth pressure, K, is defined as the ratio of the horizontal stress to the vertical stress. The effect of K is tested by applying an isotropic all-around confining stress and additional vertical deviator stress to the specimen. However, it was observed that specimens tested at K less than 0.8 were developing stress cracks. Therefore, tests were only performed for a K of 0.8, in addition to those tests discussed at a K of 1.

To investigate the impact of lateral earth pressure, K, the 48%, 61%, and 74% saturated specimens with 0.87 void ratio as well as 76% saturated specimen with 0.70 void ratio was tested for a K of 0.8. The 0.87 void ratio specimen saturated at 36% as well as the 0.7 void ratio specimen saturated at 76% showed degradation of strength as discussed in Section 4.3 and have been excluded from the comparison. Therefore, comparisons are made only on three specimens with 0.87 void ratio saturated at 48%, 61%, and 74%.

Figures 4.25 through 4.27 present comparison of K at 1.0 and 0.8 for specimens prepared at 48%, 61%, 74% saturation, respectively. The coefficient of lateral earth pressure, K, is defined as the ratio of the horizontal stress to the vertical stress. As discussed in Section 3.3.2, for K of 1.0 the specimen was tested at an isotropic confining stress of 100 kPa, but for K of 0.8 the same specimen was tested by applying an additional vertical stress of 25 kPa to make a total of 125 kPa vertical stress. Therefore, the same specimen was tested at K of 1.0 (25, 50, 100, 200, 400 kPa confining stress) and K of 0.8 (100 kPa horizontal stress and 125 kPa vertical stress. As shown in Figures 4.25(a) and 4.27(a) for 48% and 74% saturated specimens, the results of $G/G_{max}$ tested at 0.8 and 1.0 K has displayed a variation. The $G/G_{max}$ is higher at 0.8 K than 1.0. This variation indicates that the specimens have degraded faster at a K of 1.0 than at 0.8.

However, the specimen prepared at 61% saturation, presented in Figure 4.26(a) has shown similar results of $G/G_{max}$ at 0.8 and 1.0 K.

Results for damping ratio are illustrated in Figures 4.23(b), 4.24(b), and 4.25(b). Contradictory to the findings of $G/G_{max}$, the damping ratio results are more in agreement at 0.8 and 1.0 K. Therefore, damping ratio is independent of the change of K.

In summary, the $G/G_{max}$ of loess soil may vary, but D remains constant with a change in the coefficient of lateral earth pressure. However, more data are required to validate this observation.

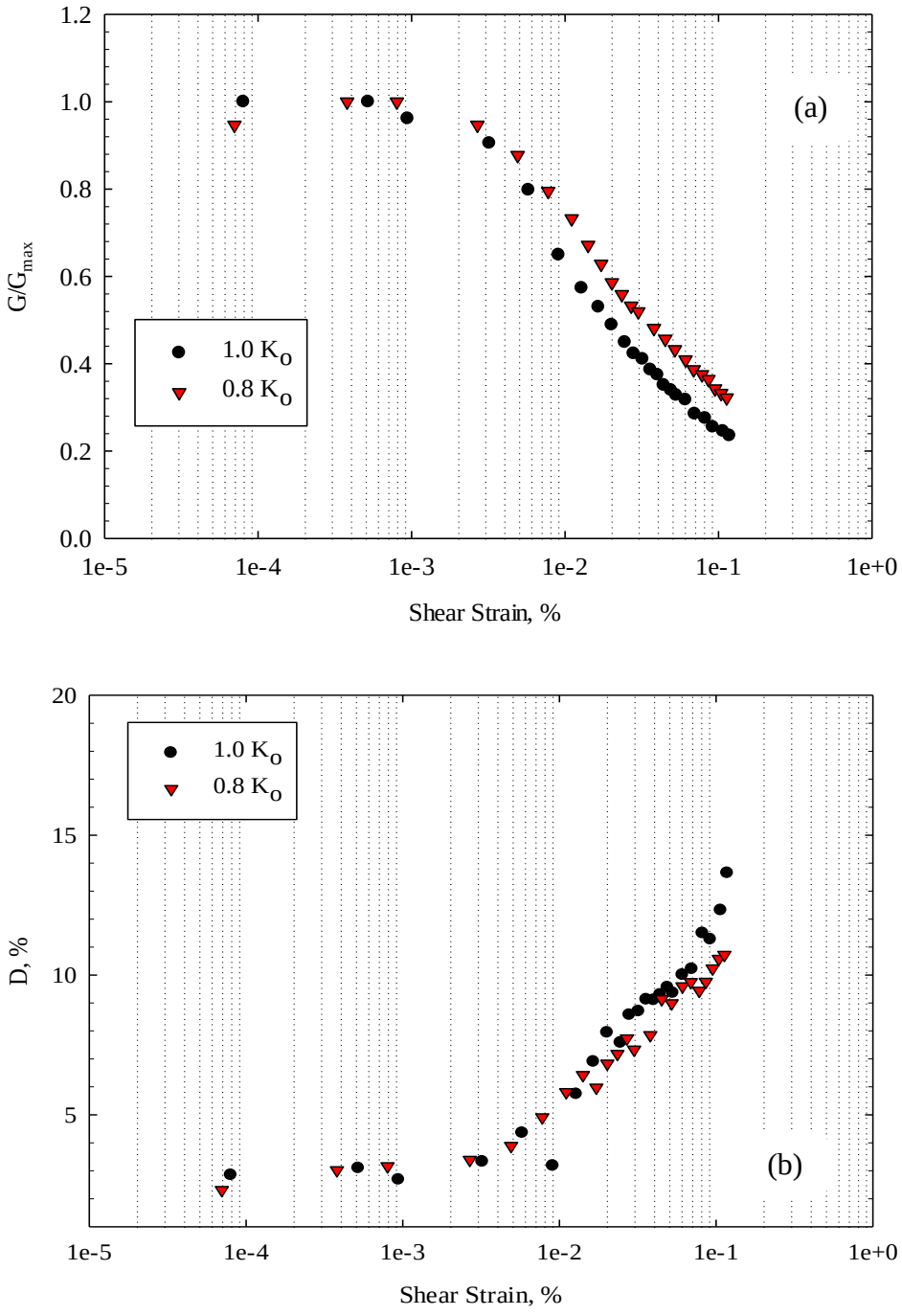


Figure 4.25: Effect of K on (a) shear modulus degradation and (b) damping ratio for specimens prepared at 48% saturation and 0.87 void ratio

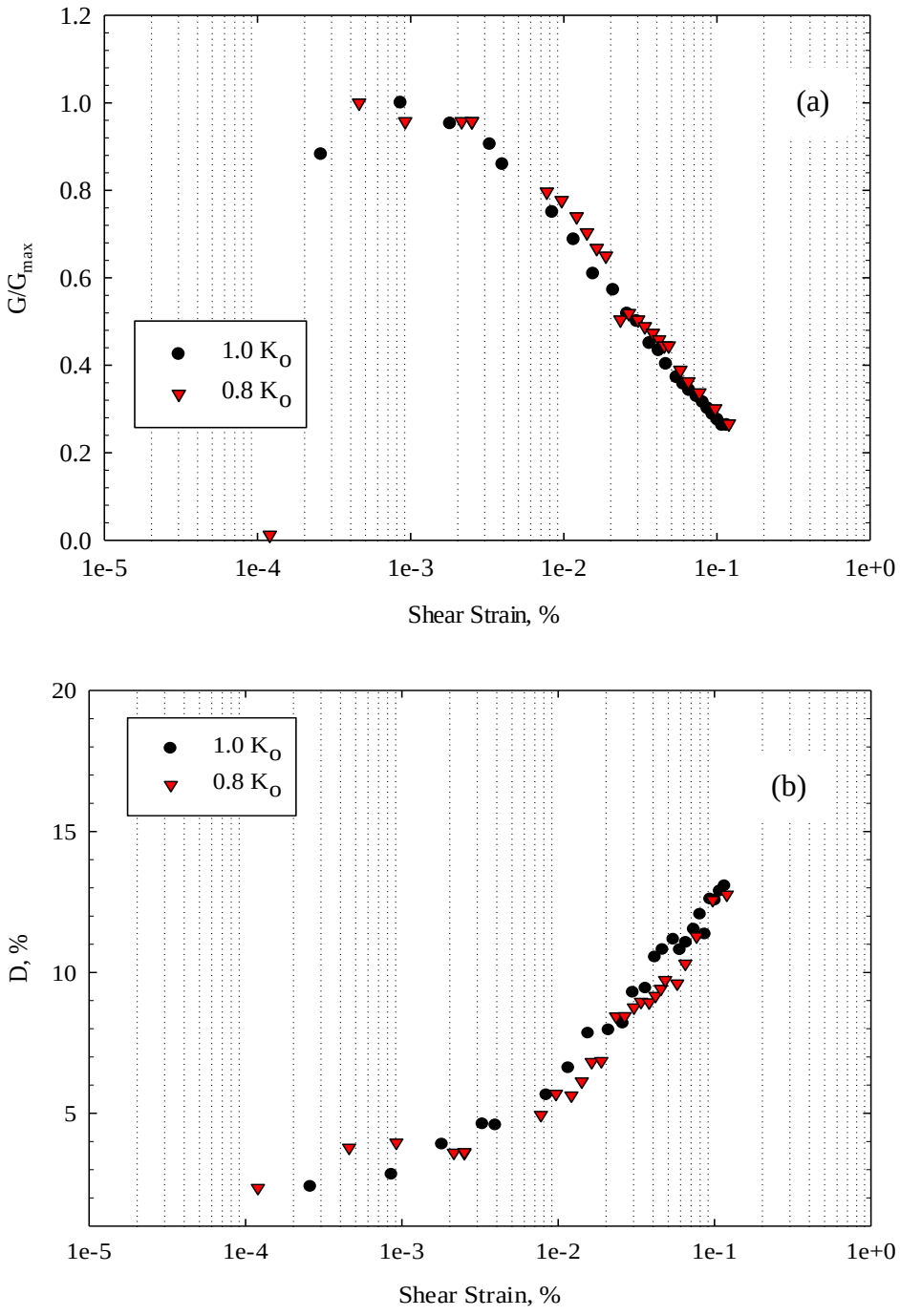


Figure 4.26: Effect of K on (a) shear modulus degradation and (b) damping ratio for specimens prepared at 61% saturation and 0.87 void ratio

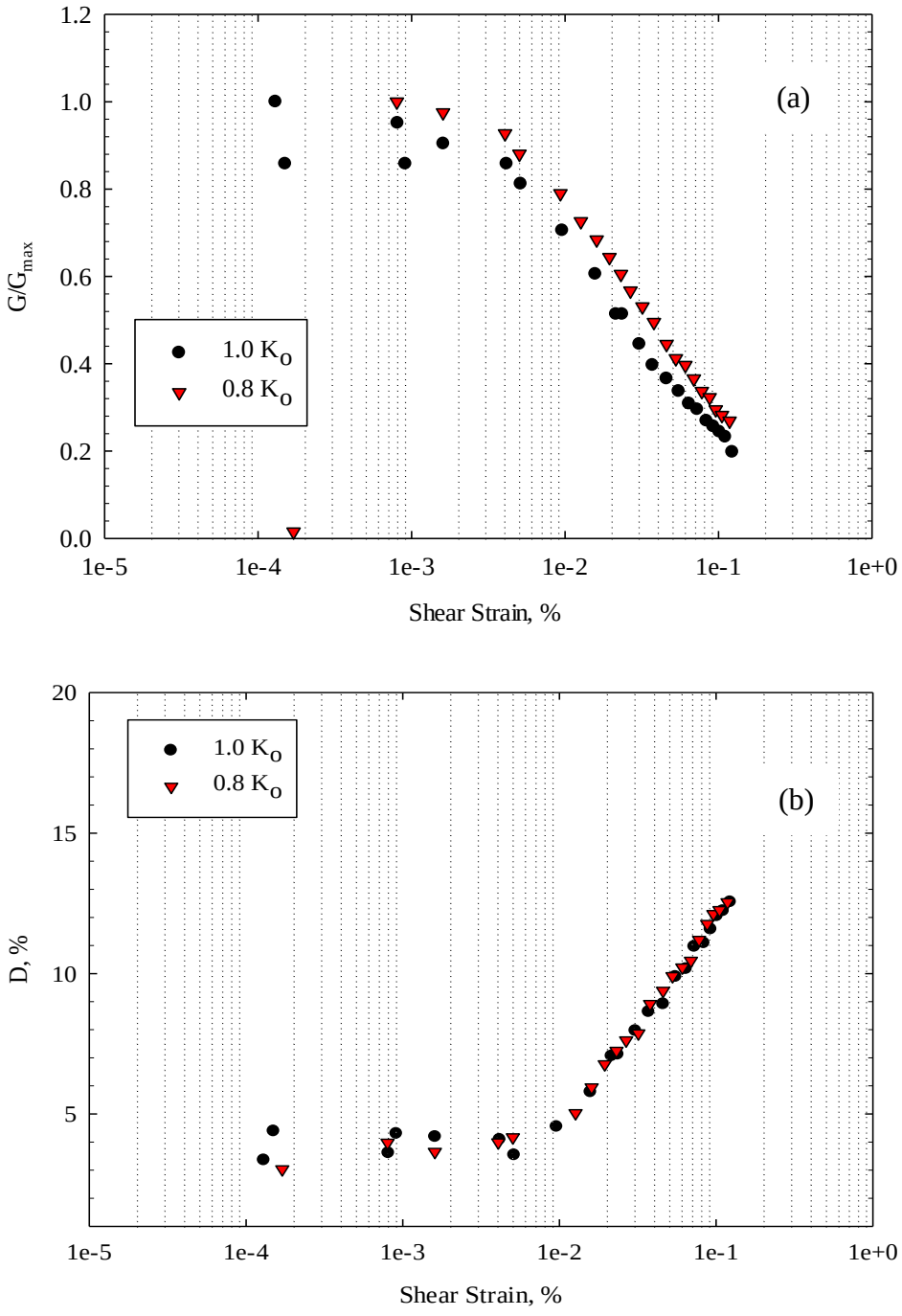


Figure 4.27: Effect of K on (a) shear modulus degradation and (b) damping ratio for specimens prepared at 74% saturation and 0.87 void ratio

## 4.6 Summary

This chapter has presented the experimental results obtained from resonant column tests on loess soil. The trends observed with varying saturation level, confining stress, void ratio, and

coefficient of lateral earth pressure on shear modulus degradation and damping has been discussed.

The test results indicate that the dynamic property of loess vary with saturation. At low saturation, 23%, the dynamic properties of loess are found to be different. However, the test results reveal that the dynamic properties of loess are independent of saturation from 36% to 74% saturation. This trend agrees with Jennings et al. (1997). Therefore, it can be concluded that the dynamic properties of loess soil vary at low saturation and remain the same from medium to high saturation levels. The test results also reveal that G/Gmax increases and D decreases with an increase of confining stress. But, the effect of confining stress is found to be more pronounced at low saturation than at high saturation. This can be due to the decrease of matric suction as saturation increases. Hence, though the dynamic properties of loess soil vary with confining stress, it is also dependent on the saturation level of the soil.

The effect of void ratio on the dynamic properties of remolded loess soil is found to differ at 61% and 74% saturation. At 61% saturation as the void ratio decreases, the $G/G_{max}$ decreases but D increases. However, at 74% saturation, the void ratio does not show significant impact on the dynamic properties of loess soil. Similarly, at 61% saturation, the remolded and intact specimens showed comparable results. Thus, the data suggest that void ratio may not impact the dynamic properties of loess which agrees with Darendeli (2001) results but more test data are required to validate this observation. This chapter also presents the effect of coefficient of lateral earth pressure, K, on the dynamic properties of loess soil. The test results reveal that the $G/G_{max}$ of loess soil varies, but D remains constant with the change in K.

# 5 ANALYSIS OF TEST RESULTS

## 5.1 Introduction

Numerous researchers have conducted investigations related to the dynamic properties of soils (Seed and Idriss 1970; Hardin and Drnevich 1972; Vucetic and Dobry 1991; Darendeli 2001; and EPRI 1993). In practice, the Darendeli (2001) and EPRI (1993) shear modulus degradation and damping ratio curves are most widely used for geotechnical seismic analysis. This chapter compares the test results of this study with these two widely used sets of curves. As discussed in Section 2.4, the only study carried out on Memphis loess is by Chang (1992). Hence, his results are also compared in this chapter. This chapter also provides the results of an example seismic site response analysis that was performed as part of this study to determine the influence of the shear modulus degradation and damping ratio curves measured for Memphis area loess in this study.

## 5.2 Comparison of Test Results

The shear modulus degradation and damping ratio curves of this study are compared with the Darendeli (2001), EPRI (1993), and Chang (1992) curves. As discussed in Section 2.3.3, Darendeli developed curves for various soils as a function of the PI of the soil as shown in Figure 2.6. The loess soil in this study has a PI of 1. Therefore, the comparison is made only with Darendeli's shear modulus degradation and damping ratio curves of PI=0. As discussed in the previous chapter, the dynamic properties of loess are found to differ at 23% saturation compared to medium and higher saturation levels tested. But, from 36% to 74% saturation the dynamic properties of loess are independent of saturation level. Hence, the specimens with 23% and 61% saturation, at 0.87 void ratio, have been selected to represent the low and high saturation levels, respectively, for this comparison.

Figure 5.1(a) presents the comparison of $G/G_{max}$ curves at 61% saturation and 0.87 void ratio obtained in this study with the Darendeli (2001) curves. In the figure, each of the three broken lines represents the best-fit curves obtained at confining stresses of 25, 100, and 400 kPa, respectively, with each curve based on the results of five specimens with 61% saturation, which represent the medium to high saturation range, as discussed in Section 4.2. The Darendeli curves are developed for 0.25, 1.0, and 4.0 atm confining stress, which is equivalent to 25, 101, and 404 kPa, respectively. As shown in Figure 5.1(a), the $G/G_{max}$ curve at 25 kPa obtained in this study agrees with Darendeli's at 25 kPa confining stress. However, Darendeli's curves are higher at 100 and 400 kPa confining stresses. These differences may be due to the suction difference between the specimens at 61% saturation in this study and the Darendeli (2001) specimens which were tested at various degrees of saturation. Comparison of $G/G_{max}$ curves at 23% saturation and 0.87 void ratio with Darendeli's curves are also shown in Figure 5.2(a). The figure suggests that low saturation Memphis area loess has a lower G/Gmax than Darendeli (2001).

Figure 5.1(b) and 5.2(b) also presents the comparison of damping ratio between the Darendeli curves and the best-fit curves of 61% and 23% saturated specimens. The damping ratio results of this study are higher than Darendeli at the low-to-medium strain range. These results suggest that Darendeli's values of $D_{min}$ are less than the results obtained in this study. Darendeli's curves also have a steeper slope in the middle to high strain levels and have higher damping ratio values at high strain in comparison with the loess soil results.

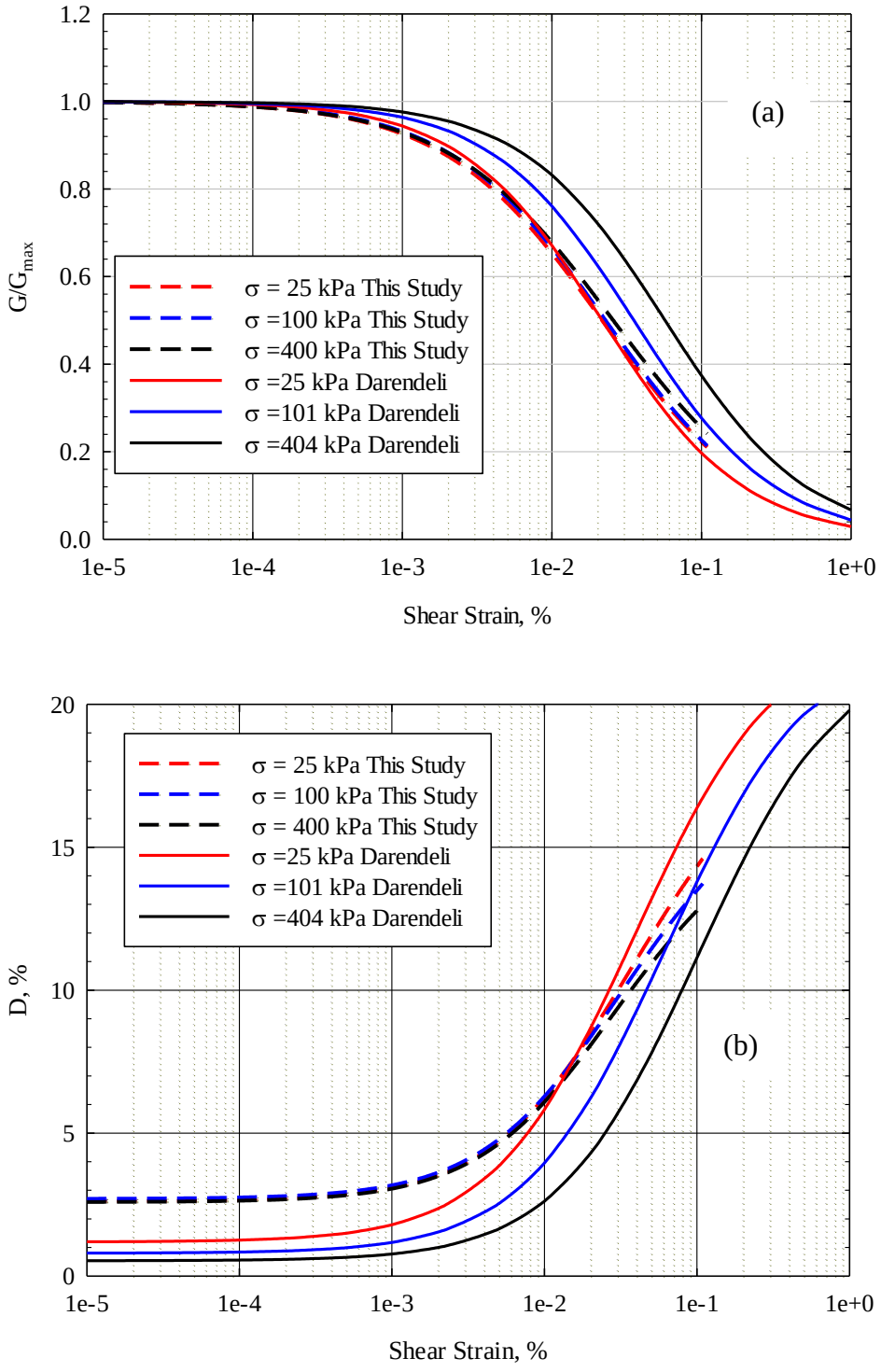


Figure 5.1: Comparison of (a) shear modulus degradation curves and (b) damping curves at 61% saturated specimens with curves of Darendeli (2001)

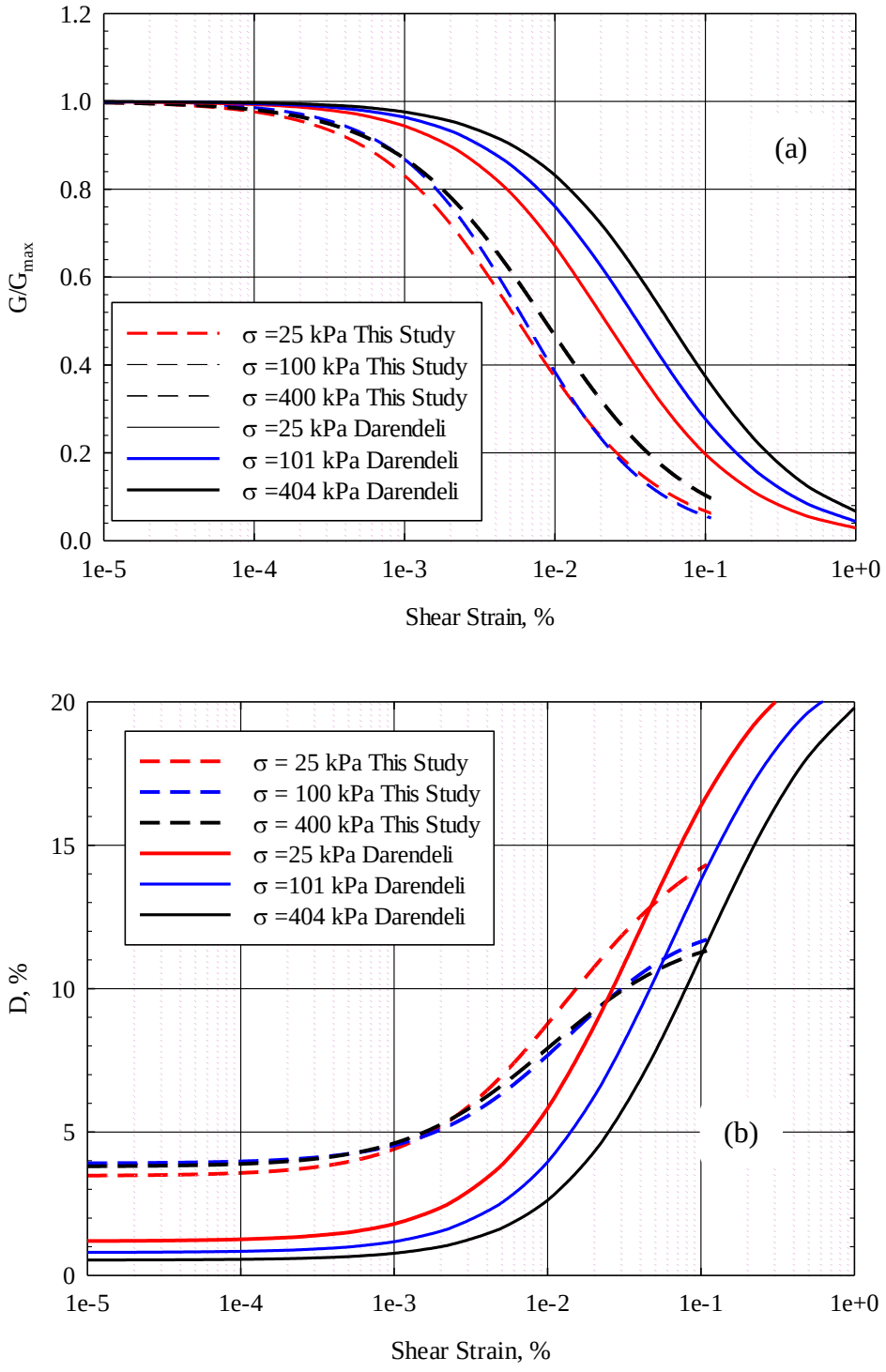


Figure 5.2: Comparison of (a) shear modulus degradation curves and (b) damping curves at 23% saturated specimens with curves of Darendeli (2001)

Another comparison is also made with the EPRI (1993) generic curves. The EPRI curves are established by testing undisturbed specimens and are based on specimen depth as discussed in Section 2.3.3. Figures 5.3 and 5.4 present comparisons of best-fit curves at 25, 100, and 200 kPa confining stresses with EPRI 0-20 ft, 20-50 ft, and 50-120 ft curves, which are equivalent to 0-6, 6-15, and 15-37 m curves, respectively. As shown in Figure 5.3(a), the $G/G_{max}$ results for 61% saturation in this study are found to be lower than EPRI's generic curves. The $G/G_{max}$ result for 23% saturation in this study is significantly lower than EPRI's generic curves as depicted in Figure 5.4(a).

Figures 5.3(b) and 5.4(b) also show the comparison of damping ratio test results from this study with EPRI. The damping ratio results obtained in this research are higher than EPRI's at the low and medium strain levels. At high strain, EPRI's damping curves are higher with steeper orientation than the results of this study.

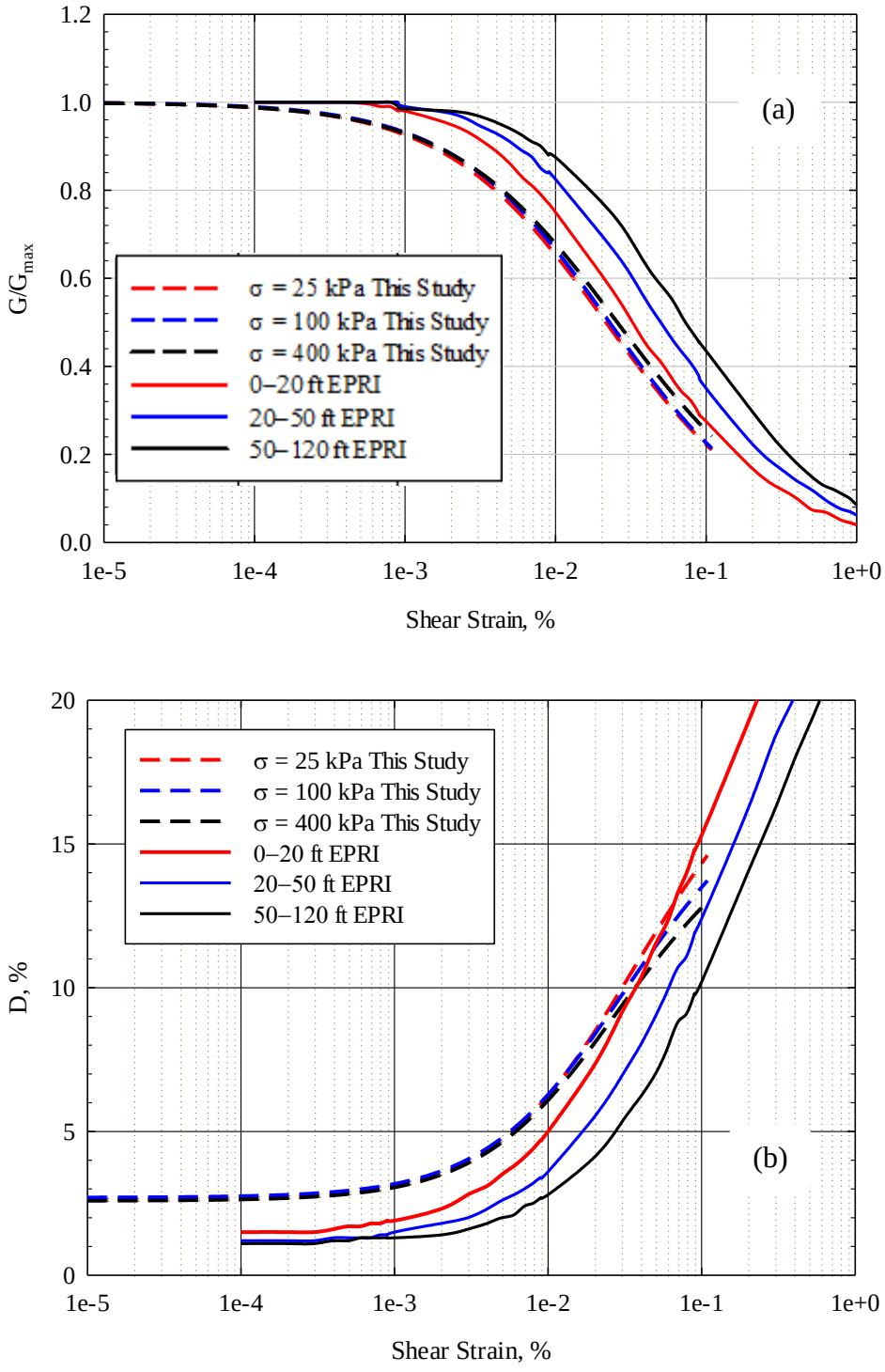


Figure 5.3: Comparison of (a) shear modulus degradation curves and (b) damping curves of 61% saturated specimens with curves of EPRI (1993)

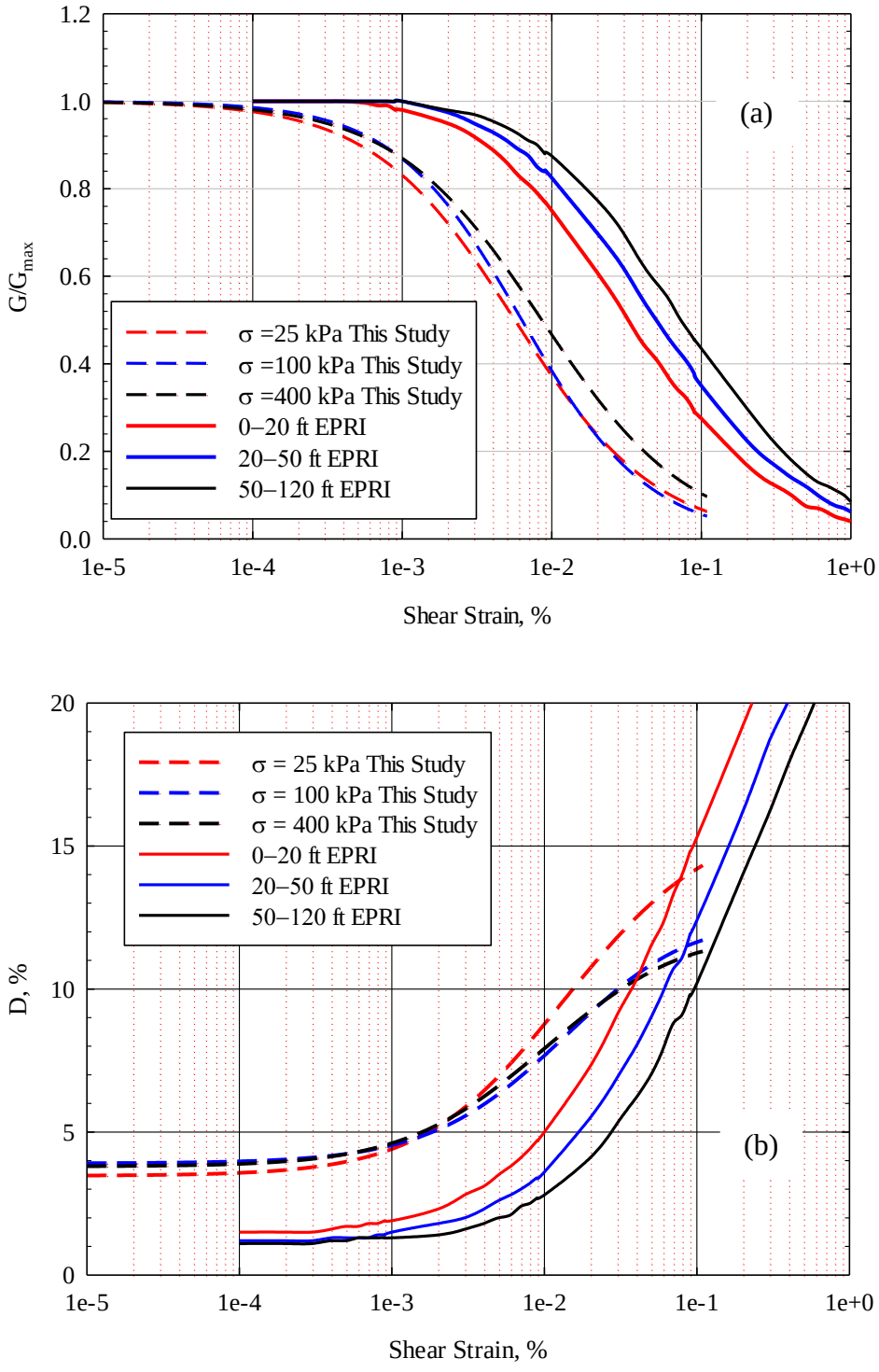


Figure 5.4: Comparison of (a) shear modulus degradation curves and (b) damping curves of 23% saturated specimens with curves of EPRI (1993)

The final comparison is made with the previous study done on Memphis soils by Chang (1992). Chang (1992) performed resonant column tests on two undisturbed Memphis soils: clayey loess (CL-ML with 25% clay and 75% silt) and sand (SP). The soils had 15 to 30% moisture content. As illustrated in Figure 5.5(a), the $G/G_{max}$ test results of this study at 61% saturated are comparable with Chang (1992) for the clayey loess. These can be due to testing similar soil and moisture content. But, the 23% saturated specimens have lower $G/G_{max}$ than Chang (1992) as shown Figure 5.6(a) due to the difference in moisture content. Moreover, Chang (1992) sand soil has higher $G/G_{max}$ than this study test results which is expected given the difference in soil types. The results also reveal that remolded specimens can have similar $G/G_{max}$ with remolded specimens confirming the observation made on section 4.4, though it requires more tests to conclude.

The damping ratio results of this study for the 61% saturation are lower in the small strain range and higher for strain >1-2% than Chang (1992) for clayey silt soil as shown in Figure 5.5(b). The results show that Chang's values of $D_{min}$ are higher than the results obtained in this studyfor 61% saturation speciemns. But the 23% saturation speciemns have similar damping up to strain less than 1-3% with Chang (1992) for clayey silt soil as shown in Figure 5.6(b) revealing comparable $D_{min}$. Chang's D curves are also also found to be more linear up to medium strain and very steep at high strain. These can be due the difference in the resonant column devices and fitting models employed in both studies.

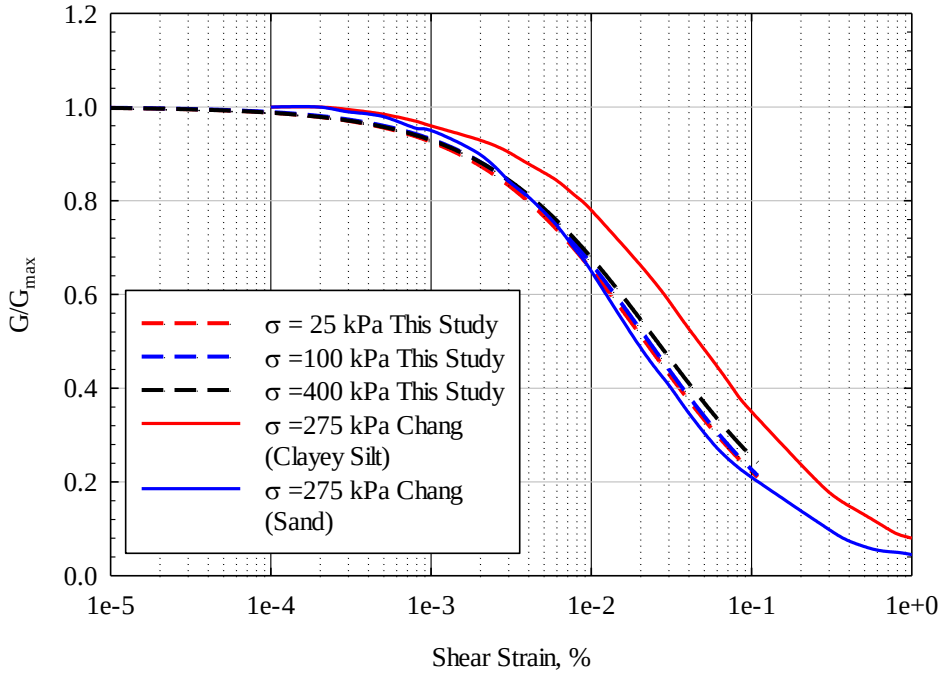


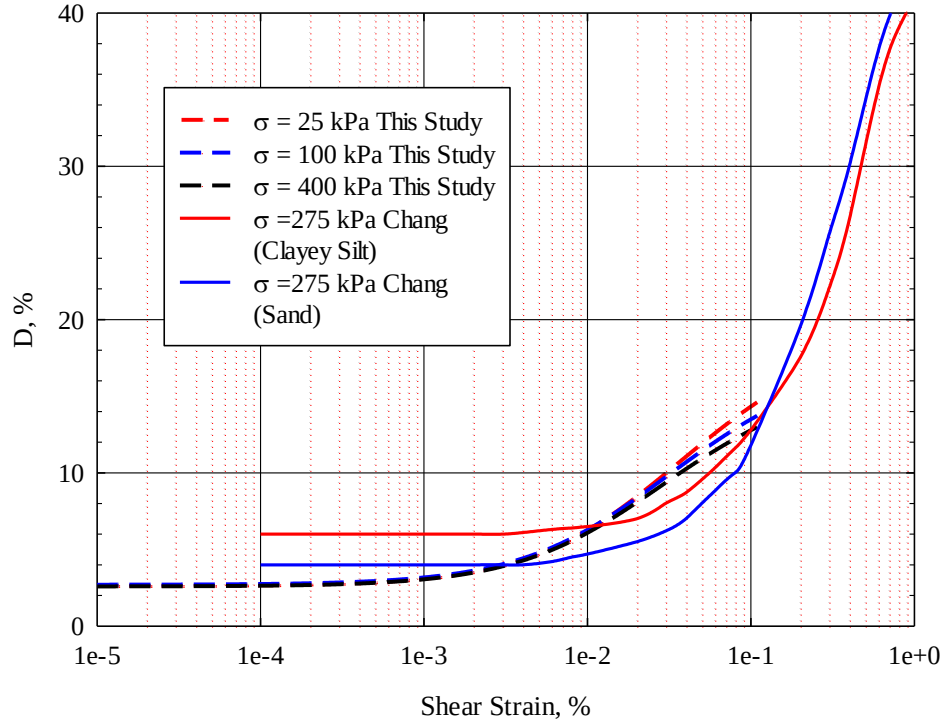


Figure 5.5: Comparison of (a) shear modulus degradation curves and (b) damping curves of 61% saturated specimens with curves of Chang (1992)

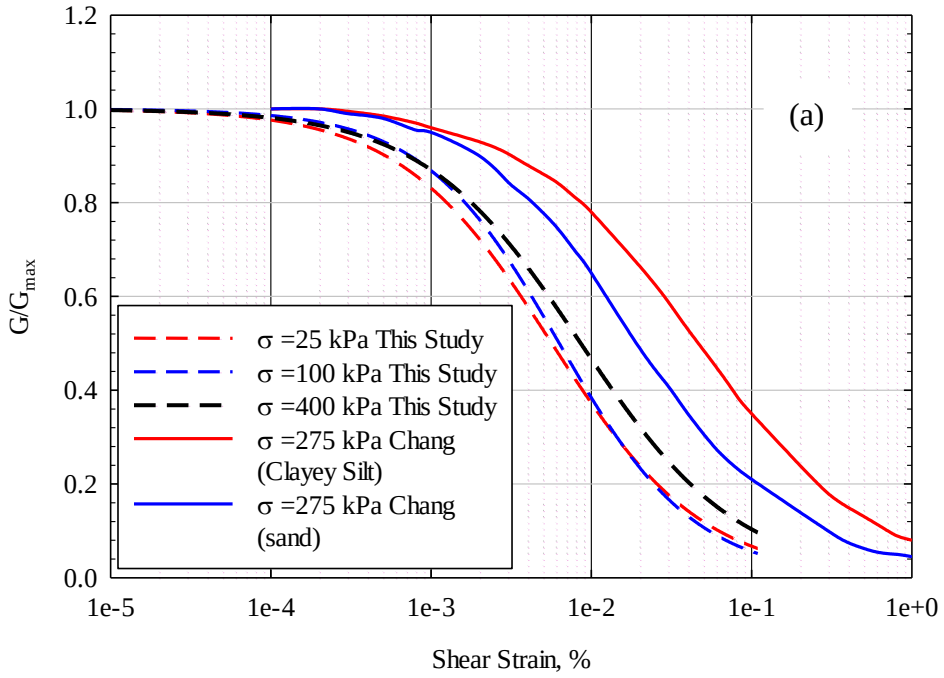


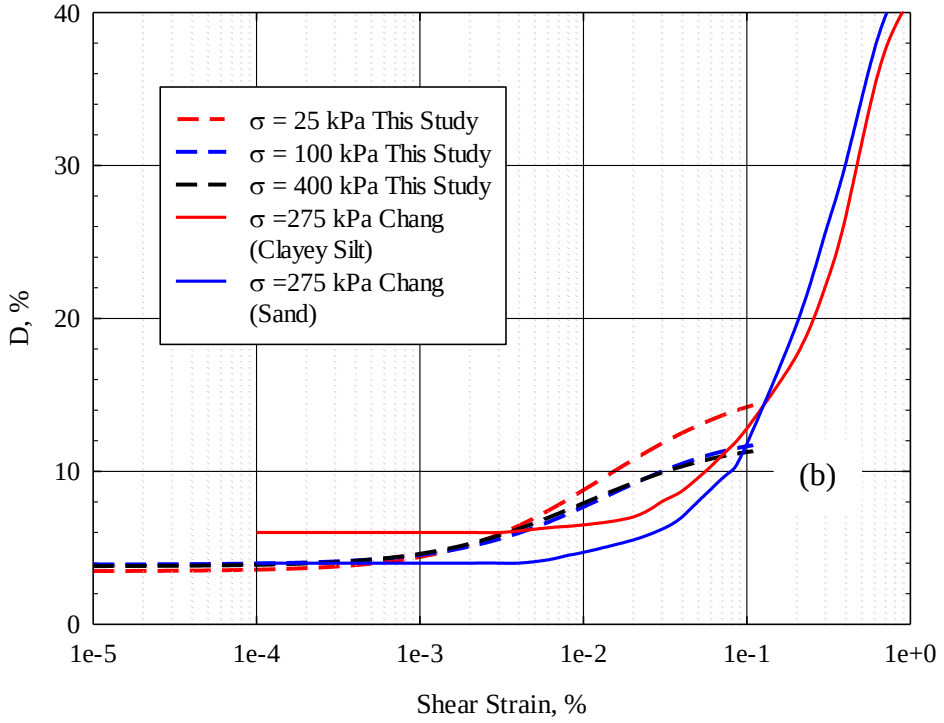


Figure 5.6: Comparison of (a) shear modulus degradation curves and (b) damping curves of 23% saturated specimens with curves of Chang (1992)

## 5.3 Influence of Test Results on Seismic Site Response Analysis

The influence of local site effects on ground shaking during an earthquake are quantified via site response analysis. The impact of test results on seismic site response analysis was investigated on Memphis and Washington state sites. Site response analysis requires information about the shear modulus reduction and damping curves as well as the shear-wave velocity profile. The dynamic curves from this study were compared with Darendeli (2001) and EPRI (1993) shown in Figures 5.1 through 5.4.

The Memphis site has a very deep soil deposit reaching up to 1000 m. The assumed shear wave velocity for the Memphis site is shown in Figure 5.7. The shear wave velocity profile up to a depth of 60 m was adopted from a TDOT subsurface exploration in Covington, Tennessee, which was found to be the nearest exploration from the specimen retrieval site. Below 60 m, the shear wave velocity is adopted from Romero and Rix (2001) for lowland zones. The 1000 m soil deposit was subdivided into 27 sublayers for site response analysis.

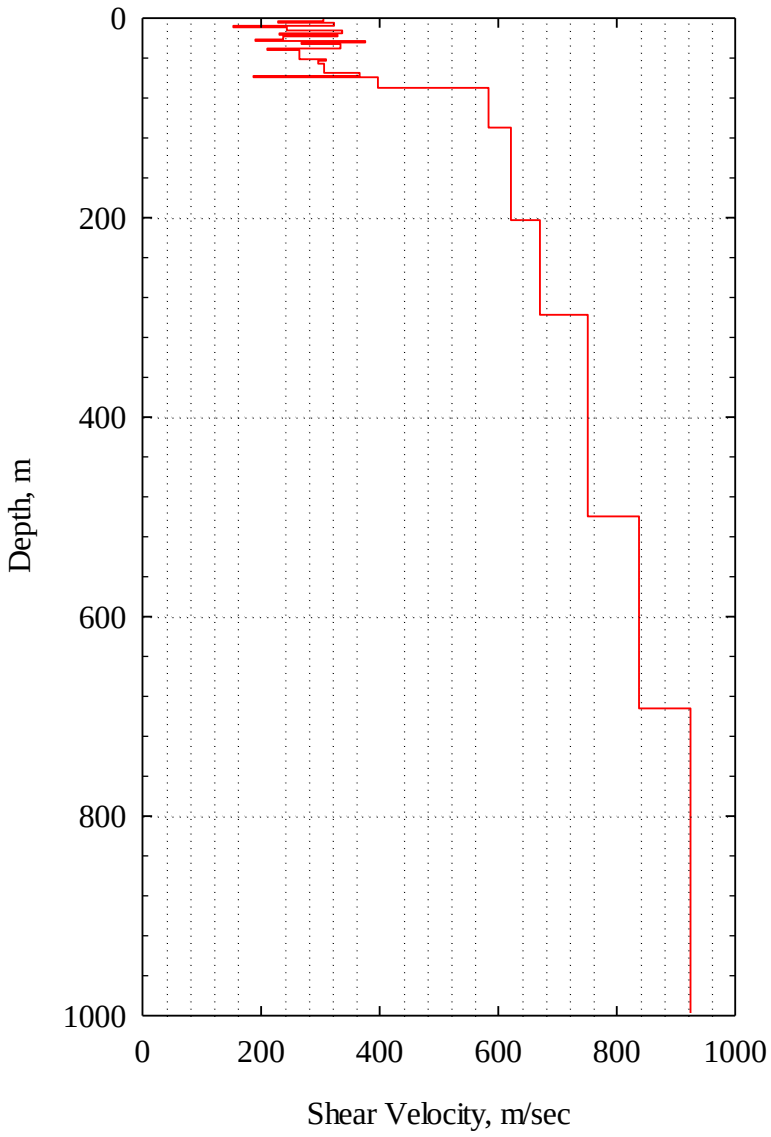


Figure 5.7: Average Shear Wave Velocity Profile Assumed for Memphis Site

The rock input motion was selected using the USGS seismic deaggregation data and PEER strong motion database. First, the earthquake moment magnitude, $M_W$, and the site-to-source distance, R, for the site were obtained from the USGS national seismic hazard website (USGS 2016) for an exceedance probability of 2% in 50 years. The site is assumed to be located where the loess soil samples ware obtained at 35.634$^o$N and 89.822$^o$W. The magnitude-distance deaggregation provides a representative magnitude and distance to a design earthquake ground motion for a given hazard level. Then, based on the magnitude-distance results, recorded strong

motions are selected from the PEER strong motion database (https://ngawest2.berkeley.edu/) and used as an outcrop motion on hard rock. Figure 5.8 illustrates the assumed ground motion for the Memphis site obtained from the PEER database from station LA - Chalon Rd (earthquake "Northridge-01",1994 with magnitude 6.69).

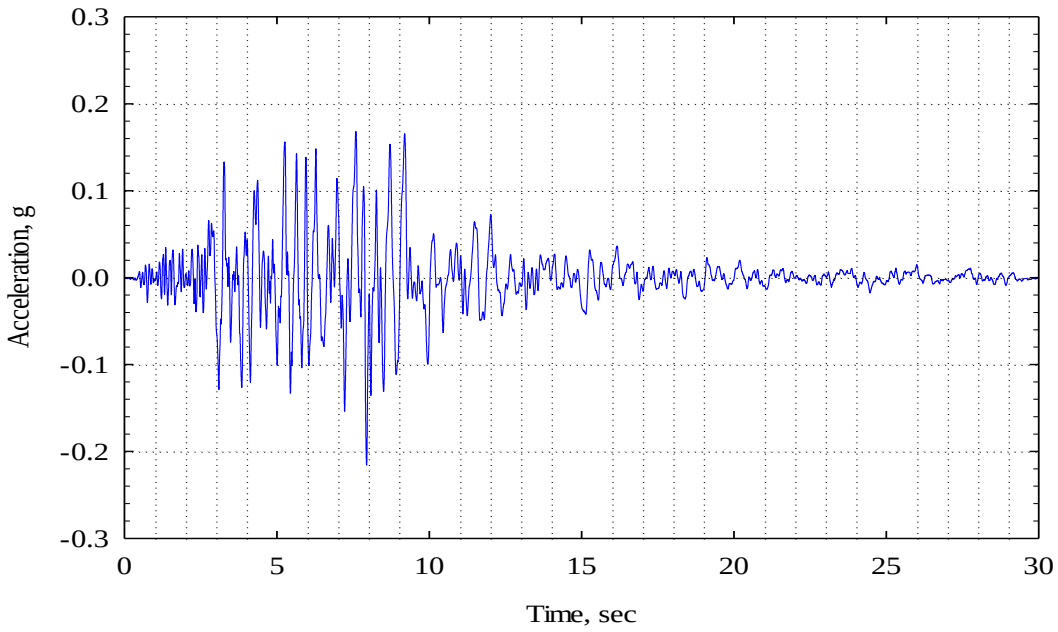


Figure 5.8: Time history of acceleration for the Memphis Site

One-dimensional equivalent linear site response analyses were performed using SHAKE91, a computer program initially written by Schnabel et al. (1972) and later modified by Idriss & Sun (1992). This is a widely used program because of its ease of application (Hartzell et al. 2004). The program assumes a homogenous and semi-infinite horizontally layered soil deposit overlying a uniform half-space subjected to vertically propagating shear waves. The analysis is conducted by assigning shear modulus, damping, and unit weight to each layer and selecting an input ground motion.

Figure 5.9 illustrates a comparison of spectral acceleration using curves from this study, for 23% and 61% saturated specimens, Darendeli (2001), and EPRI (1993). The result shows that

the 61% saturated loess curves produced a similar spectral acceleration as the EPRI (1993) and Darendeli (2001) curves. However, 23% saturated loess curves have a slightly higher spectral acceleration contrary to the significant difference in shear modulus degradation and damping ratio curves from EPRI (1993) and Darendeli (2001) curves as discussed in Section 5.2. The slight difference in spectral acceleration can be due to the presence of very shallow loess, about 17 m in this example, being insignificant compared to the overall thickness the soil deposits, reaching up to 1000 m. To investigate the effect of bedrock depth difference, a site response analysis in Washington State with a shallow bedrock was also performed.

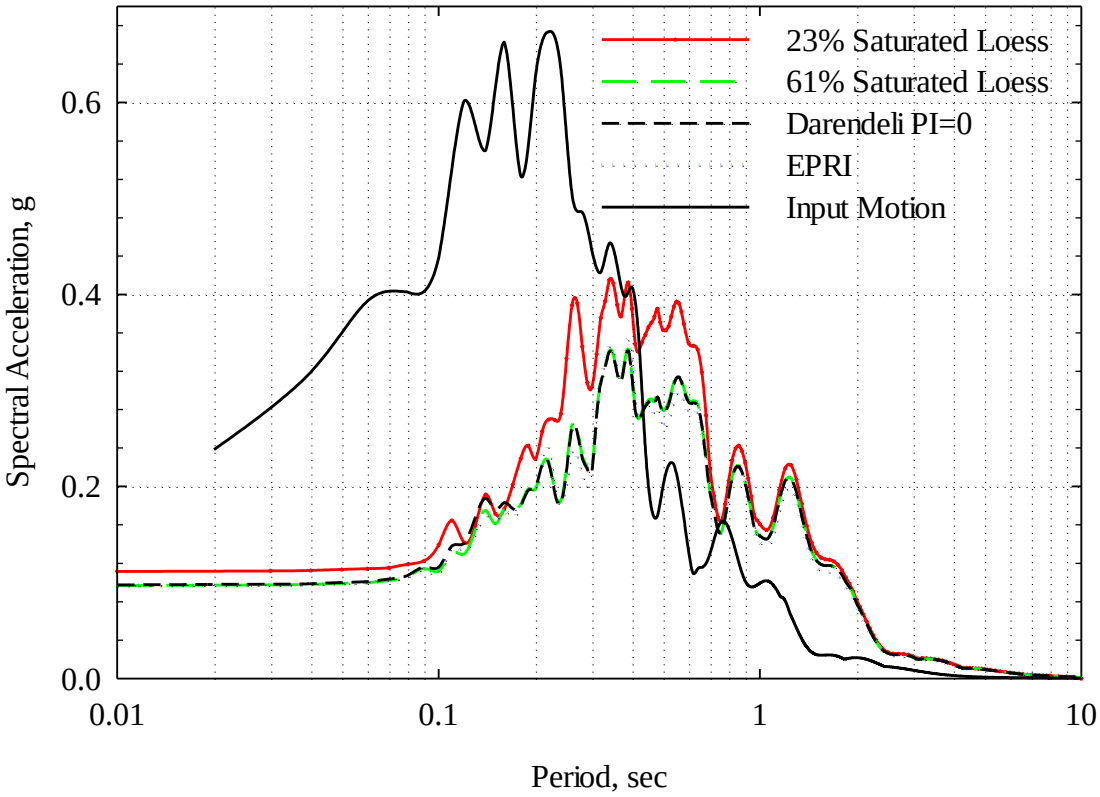


Figure 5.9: Comparison of Spectral Acceleration results using SHAKE91 for Memphis site

Washington State has loess deposits in the southeastern part called the Palouse Region. The loess soil has a depth of over 200 feet (60 m) in some places according to USRA (2010). The bedrock depth considered in the site response analysis was about 50 m and the loess deposit

was about 15 m. The site was considered to have the same soil deposit as Memphis site from 15 to 50 m depth. Figure 5.10 shows the assumed input motion used for the site response analysis obtained from the PEER database from station Gilroy - Gavilan Col (earthquake "Morgan Hill," 1984 with magnitude 6.19).

Figure 5.11 shows site response results for the Washington site. The figure shows that the 61% saturated loess curve has comparable spectral acceleration results as the EPRI (1993) and Darendeli (2001) curves. However, the 23% saturated loess curves have a much lower spectral acceleration when compared with the other curves. Results from this study show more influence of spectral acceleration on a shallower bedrock site like Washington than the deep deposits in the Mississippi Embayment.

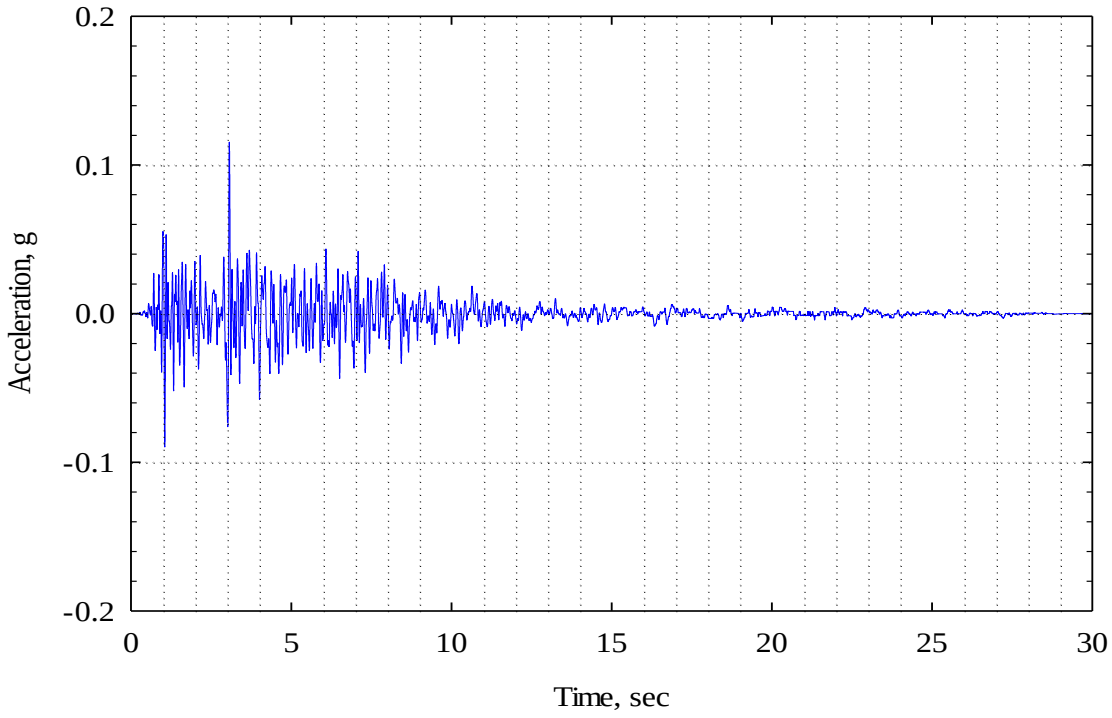


Figure 5.10: Time history of acceleration for the Washington Site

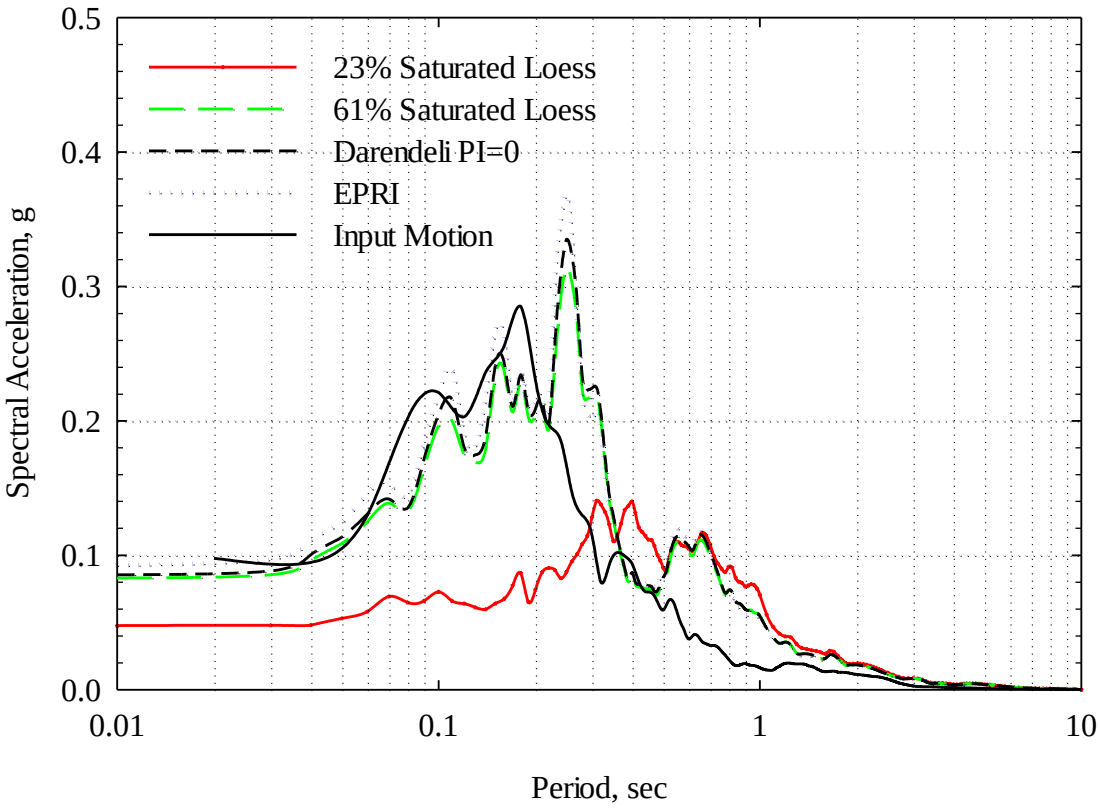


Figure 5.61: Comparison of Spectral Acceleration results using SHAKE91 for Washington site

To investigate the impact of this study on design, a design example of a retaining wall under earthquake load was conducted. A sample calculation using the PGA of 23% saturated loess is provided in Appendix C. The seismic pressure was determined using the Mononobe-Okobe method. Then, the factor of safety against sliding, overturning, and bearing capacity were computed using the PGA results from the site response analysis performed. Table 5.1 presents the factor of safety results using curves from the 23% saturated specimens, 61% saturated specimens, Darendeli (2001), and EPRI (1993). The table shows that the factor of safety results against sliding are comparable. However, the factor of safety results against overturning and bearing capacity have a 0.2 difference using curves from the 23% saturated specimens and Darendeli (2001). These differences in the factor of safety indicate that the study results can have a considerable effect on the safety and design economy of the structures.

Table 5.1: Influence of dynamic curves on the factor of safety of a retaining wall for Memphis site

| Dynamic curve used in site response | PGA | Factor of safety against sliding | Factor of safety against overturning | Factor of safety against bearing |
|---|---|---|---|---|
| This study (23% saturated specimens) | 0.416 | 0.40 | 1.81 | 2.43 |
| This study (61% saturated specimens) | 0.344 | 0.43 | 2.00 | 2.62 |
| Darendeli (2001) | 0.342 | 0.43 | 2.00 | 2.63 |
| EPRI (1993) | 0.355 | 0.42 | 1.97 | 2.59 |

## 5.4 Summary

In this chapter, the results of this study are compared with Darendeli (2001), EPRI (1993), and Chang (1992). At 61% saturation, the shear modulus degradation result is found to be comparable at low confining stress and lower at high confining stress than Darendeli (2001). It is also found to be lower than EPRI (1993). However, at 23% saturation, the shear modulus degradation curves in this study are significantly lower than Darendeli (2001) and EPRI (1993). The observed trend in the damping ratio of 23% and 61% saturation specimens are higher than Darendeli (2001) and EPRI (1993) at low-to-medium strain levels. Meanwhile, at high strain the Darendeli (2001) and EPRI (1993) damping curves are higher, with steeper orientation, than the results of this study. Regarding the comparison with previous studies on shear modulus degradation of local loess, the the shear modulus degradation results of this study for the 61% saturated specimens are quite similar with Chang (1992) clayey loess soil test results, but the 23% saturated specimens are significantly lower. The damping ratio for the 61% saturated specimens are found to be much lower at small strain and higher at medium strain ($1^{-2}$%) than Chang (1992). Chang's D curves are also found to be more linear up to medium strain and very

steep at high strain. The comparison also suggest that remolded and intact specimens with similar saturation have comparable shear modulus degradation results.

This chapter also discusses the site response analysis performed on Memphis as well as Washington State sites. Specimens with 61% saturation have shown comparable site response results with Darendeli (2001) and EPRI (1993). However, 23% saturated specimens have shown a considerable difference in site response results in comparison with Darendeli (2001) and EPRI (1993).

# 6 CONCLUSIONS AND RECOMMENDATIONS

The main findings drawn from this thesis are summarized in this chapter. Recommendations for future research are also presented.

## 6.1 Conclusions

- The dynamic properties of loess soil varies at low saturation, 23%, and remains the same from medium to high saturation levels, 36% to 74%.
- Shear modulus degradation increases and damping ratio decreases with an increase of confining stress. However, the effect of confining stress is found to be more pronounced at low saturation than at high saturation.
- The effect of void ratio on the dynamic property of loess soil is found to be insignificant.
- The coefficient of lateral earth pressure, K, influences the dynamic properties of loess soil. Shear modulus degradation of loess soil increases slightly but D remains constant with a decrease of K.
- At 61% saturation, the shear modulus degradation results are comparable at low confining stress and lower at high confining stress than Darendeli (2001) but lower than EPRI (1993) at all confining stresses. Meanwhile, the damping ratio results are higher than Darendeli (2001) and EPRI (1993) at low-to-medium strain levels.
- At 23% saturation, the shear modulus degradation results are much lower than Darendeli (2001) and EPRI (1993). Similarly, the damping ratio results are higher than Darendeli (2001) and EPRI (1993) at low-to-medium strain levels.
- The shear modulus degradation results of this study at 61% saturated specimens are found to be similar with Chang (1992) clayey loess soil test results, but the 23% saturated

specimens are significantly lower. The damping ratio are much lower at small strain and higher at medium strain ($1^{-2}$%) than Chang (1992).

- Remolded and intact loess specimens with comparable saturation have similar shear modulus degradation curves.

## 6.2 Recommendations

The following recommendation can be drawn from this study:

- The analysis method in use determining the damping in the CATS software contributes to the scatter in damping. Introducing an option to ignore cycles in the middle or manual manipulation of the average slope can reduce the inaccuracy of damping ratio results.
- Testing each specimen at successive confining stresses may degrade the strength of the specimen and may hinder achieving the accurate effect of confining pressure.
- More test data at low saturation are required to validate the effect of void ratio and coefficient of lateral earth pressure on the dynamic property of loess soil.
- More tests on remolded and intact loess specimens are required to evaluate the difference or similarity in dynamic properties in order to use remolded specimens for future research.
- A pore water pressure transducer for measuring the pore water pressure was not available for the RCTS device. Its availability would help determine the effective confining stress of the test.

## REFERENCES


Adrian, D. B. (2012). "The Collapse Behavior of Compacted West Tennessee Loess." Master's thesis, The University of Memphis.

ASTM D4015-15, (2016). "Standard Test Methods for Modulus and Damping of Soils by Fixed-Base Resonant Column Devices," (November 2015), 1–22.

Alonso, E. E., Pinyol, N. M., and Gens, A. (2013). "Compacted soil behaviour: initial state, structure and constitutive modelling." Géotechnique, 63(6), 463–478.

Baty, F., Ritz, C., Charles, S., Brutsche, M., Flandrois, J.-P., and Delignette-Muller, M.-L. (2015). "A Toolbox for Nonlinear Regression in R : The Package nlstools." Journal of Statistical Software, 66(5), 1–21.

Çabalar, A. F. (2009). "Dynamic Properties of Various Plasticity Clays." Electronic Journal of Geotechnical Engineering, 14, 14.

Cetin, H. Fener, M. Söylemez, M. and Günaydin, O. (2007). Soil structure changes during compaction of a cohesive soil. Engineering Geology, 92(1-2), 38–48.

Chang, T.-S. (1992). "Dynamic properties of typical Memphis soils." Journal of the Tennessee Academy of Science, (2), 39–45.

Chen, A.T.F., and Stokoe, K.H., (1979), "Interpretation of Strain-Dependent Modulus and Damping from Torsional Soil Tests," Report No. USGS-GD-79-002, NTIS No. PB-298479, U.S. Geological Survey, Menlo Park, CA 94025.

Darendeli, M. B. (2001). "Development of a new family of normalized modulus reduction and material damping curves." PhD Dissertation, The University of Texas at Austin.

Dobry, R., and Vucetic, M. (1987). "Dynamic properties and seismic response of soft clay deposits." https://www.researchgate.net/publication/245984103

D'Onofrio, A. and Penna, A (2003). "Influence of compaction variables on the small strain behaviour of a clayey silt." In "Deformation Characteristics of Geomaterials, Di Benedetto et al. (eds), Swets & Zeitlinger, Lisse,"

Drnevich, V. P. (1978). "Resonant Column Test: Final Report", submitted to U. S. Army Engineer Waterways Experiment Station, July 1978

EPRI, Electric Power Research Institute. (1993a). "Guidelines for Determining Design Basis Ground Motions - Volume 2 : Appendices for Ground Motion Estimation." Palo Alto, Calif: Electric Power Research Institute, vol. 1-5, EPRI TR-102293.

EPRI, Electric Power Research Institute. (1993b). "Guidelines for Determining Design Basis

Ground Motions, Volume 1: Method and Guidelines for Estimating Earthquake Ground Motion in Eastern North America." Palo Alto, Calif: Electric Power Research Institute, vol. 1-5, EPRI TR-102293.

GCTS Testing Systems (2007). CATS Resonant Column & Torsional Shear Test, Mode 1.85. User's Guide & Reference Manual.

Fleureau, J. M., Dufour-Laridan, E., and Gomes Correia, A. (2001). "Influence of compaction and loading conditions on the dynamic properties of a silty sand." Proceedings: Fourth International Conference on Recent Advances in Geotechnical Earthquake Engineering and Soil Dynamics and Symposium in Honor of Professor W.D. Liam Finn, (March 26-31).

Hardin, B. O., and Drnevich, V. P. (1972). "Shear modulus and damping in soils." Journal of the Soil Mechanics and Foundations Division, 98(7), 667–692.

Hartzell, S., Bonilla, L. F., and Williams, R. A. (2004). "Prediction of nonlinear soil effects." Bulletin of the Seismological Society of America, 94(5), 1609–1629.

Idriss, I.M., and Sun, J.I. (1992). User's manual for SHAKE91: a computer program for conducting equivalent linear seismic response analyses of horizontally layered soil deposits, Department of Civil & Environmental Engineering, University of California, Davis, California.

Isenhower, W. M., and Stokoe, K. H. (1981). "Strain-rate dependent shear modulus of San Francisco Bay mud." International Conferences on Recent Advances in Geotechnical Earthquake Engineering and Soil Dynamics.

Ishibashi, I., and Zhang, X. (1993). "Unified Dynamic Shear Moduli and Damping Ratios of Sand and Clay." Soils and Foundations, Japanese Society of Soil Mechanics and Foundation Engineering, 33(No. 1), 10.

Ishihara, K. (1996). Soil behavior in earthquake geotechnics. Clarendon Press, Oxford.

Jennings, A. T. (1994). "Dynamic Properties of Unsaturated Loess." Master's thesis, University of Idaho.

Jennings, A. T., Hardcastle, J. H., and Sharma, S. (1997). "Dynamic Properties of Unsaturated Loess." Engineering geology and geotechnical engineering:proceedings of the Symposium on Engineering Geology and Geotechnical Engineering ., 32, 465–476.

Jiang, Y., Chen, W., Wang, G., Sun, G., and Zhang, F. (2016). "Influence of initial dry density and water content on the soil???water characteristic curve and suction stress of a reconstituted loess soil." *Bulletin of Engineering Geology and the Environment*, Springer Berlin Heidelberg, 1–11.

Johnson, R., Parsons, R. L., and Dapp, S. (2007). Soil Characterization and P-Y Curve

Development for Loess. Ktran Report. Kansas Department Of Transportation. Topeka, Kansas. 2007. 214 P.

Kavazanjian, E., Jr., Matasović, T. Hadj-Hamou and Sabatini, P.J. (1997). "Geotechnical Engineering Circular No. 3, Design Guidance: Geotechnical Earthquake Engineering for Highways," Report No. FHWA-SA-97-076, Federal Highway Administration, Washington, D.C.

Kane, H. (1968). A Mechanistic Explanation of the Physical Properties of Undisturbed Loess. University of Iowa Research Project HR-126. Iowa State Highway Commission, Iowa City, 1968, 113 pp.

Karam, J. P., Cui, Y. J., Tang, A. M., Terpereau, J. M., and Marchadier, G. (2009). "Experimental Study on the Cyclic Resistance of a Natural Loess from Northern France." Soils and Foundations, 49(3), 421–429.

Kim, D. S., Stokoe, K. H., and Hudson, W. R. (1991). "Deformational characteristics of soils at small to intermediate strains from cyclic tests." Research Rep. 1177-3, Center for Transportation Research, Bureau of Engineering Research, Univ. of Texas at Austin, Austin, TX, 142.

Kim, D.S., Seo, W.S., and Kim, M.J. (2003). "Deformation characteristics of soils with variations of capillary pressure and water content." Japanese Geotechnical Society, Soils and Foundations, 43(4), 71–79.

Kramer, Steven L. (1996). "Geotechnical earthquake engineering." Prentice Hall, Upper Saddle River, NJ 07458.

Ladd, R. S. (1978). "Preparing Test Specimens Using Undercompaction." Geotechnical Testing Journal, 1(1), 16–23.

Lade, P. V. (2016). "Triaxial Testing of Soil." John Wiley & Sons, Ltd. UK.

Lambe, T. W., and R. V. Whitman (1979), " Soil Mechanics," 2d ed., John Wiley & Sons, Inc., New York, 553 pp.

Maleki, M., and Bayat, M. (2012). "Experimental evaluation of mechanical behavior of unsaturated silty sand under constant water content condition." Engineering Geology, Elsevier B.V., 141–142, 45–56.

Mancuso, C., Vassallo, R., and D'Onofrio, A. (2002). "Small strain behavior of a silty sand in controlled-suction resonant column- torsional shear tests." Canadian Geotechnical Journal, 39(1), 22–31.

Mitchell, J., & Soga, K. (2005). Fundamentals of Soil Behavior. John Wiley & Sons, Hoboken, New Jersey.

Moore, H.L. (1994). A Geologic Trip across Tennessee by Interstate 40, The University of Tennessee Press, Knoxville, TN.

Mosallamy, M. El, Fattah, T. T. A. El, and Khouly, M. El. (2014). "Experimental Study on the Determination of Small Strain-Shear Modulus of Loess Soil." HBRC Journal, 2015, 11.

Parsons, R. L., Johnson, R. M., Brown, D. A., Dapp, S., and Brennan, J. J. (2009). "Characterization of Loess for Deep Foundations." DFI Journal, 3(785), 14–24.

PEER, (2017). PEER Ground Motion Database, https://ngawest2.berkeley.edu/ (08-22-2017).

Pinto, P. A. (2012). "Study of constitutive models for soils under cyclic loading. Introducing a non-linear model with a spline-based backbone curve." Universidade Teccnica Lisboa.

Romero, SM, and Rix, GJ. (2001). "Ground motion amplification in the Upper Mississippi Embayment". GIT-CEE/GEO-01-1, Atlanta.

Royster, D. L. (1965). "Engineering Characteristics of the Loessial Soils of West Tennessee." Tennessee Highway Conference Proceedings, 12–38.

Salem, M. A. (2007). "Stiffness of unsaturated compacted clays at small strains." PhD Dissertation, University of Texas at Austin.

Sartori, M. (2000). "The Quaternary climate in loess sediments : Evidence from rock and mineral magnetic and geochemical analysis: The Quaternary climate in loess sediments: Evidence from rock and mineral magnetic and geochemical." Swiss Federal Institute of Technology Zürich.

Sawangsuriya, A., Edil, T. B., and Bosscher, P. J. (2008). "Modulus−suction−moisture relationship for compacted soils." Canadian Geotechnical Journal, 45(7), 973–983.

Schnabel, P. B., Lysmer, J., and Seed H. B. (1972). "SHAKE: A Computer Program for Earthquake Response Analysis of Horizontally Layered Sites." University of California—Berkeley, Earthquake Engineering Research Center, Report No. EERC 72-12, December.

Sheeler, J. B. (1968). "Summarization and Comparison of Engineering Properties of Loess in the United States." Highway Research Board, (No 212), 1–9.

Stokoe, K. H., II, Darendeli, M. B., Andrus, R. D. and Brown, L. T. (1999). "Dynamic soil properties: laboratory, field and correlation studies," Sêco e Pinto, (ed.), Proceedings, Second Int. Conf. on Earthquake Geotechnical Engineering, Lisbon. 21-25 June 1999, (3): pp. 811-845, Rotterdam, Balkema.

Tavakoli, B., Pezeshk, S., and Cox, R.T., (2010). “Seismicity of the New Madrid Seismic Zone Derived from a Deep-Seated Strike-Slip Fault.” Bulletin of the Seismological Society of America 100(4): 1646–58.

USGS, U.S. Geological Survey. (2009). “Earthquake Hazard in the New Madrid Seismic Zone Remains a Concern.” http://pubs.usgs.gov/fs/2009/3071/pdf/FS09-3071.pdf. (05-11-2017)

USGS, U.S. Geological Survey, (2017). USGS National Seismic Hazard Website, <https://earthquake.usgs.gov/hazards/interactive/> (08-22-2017).

USGS, U.S. Geological Survey. (2009). “Loess soil in the United states.” http://gec.cr.usgs.gov/archive/eolian/task2.shtml. (10-15-2016)

USRA (2010). "Palouse Loess", <http://epod.usra.edu/blog/2010/08/palouse-loess.html> (04-19-2017)

Verruijt, A. (2009). Soil dynamics. < http://geo.verruijt.net/software/SoilDynamicsBook.pdf> (02-06-2017)

Vucetic, M. (1994). “Cyclic Threshold Shear Strains in Soils.” Journal of Geotechnical Engineering, 120(12), 2208–2228.

Vucetic, M., and Dobry, R. (1991). “Effect of Soil Plasticity on Cyclic Response.” Journal of Geotechnical Engineering, 117(1), 89–107.

Wen, B. P., and Yan, Y. J. (2014). “Influence of structure on shear characteristics of the unsaturated loess in Lanzhou, China.” Engineering Geology, Elsevier B.V., 168, 46–58.

Wu, Zhenzhong. (2014). “Measuring Dynamic Properties of Wind Turbine Foundation Soil in Resonant Column - Issues and Challenges.” Master’s thesis, University of Wisconsin – Madison.

## APPENDIX A: SOIL CHARACTERIZATION TESTS

Disturbed and intact soil samples were obtained on May 20 and July 16, 2016 from a bluff in Fulton Wildlife Refuge and brought to the geotechnical laboratory. The disturbed samples were simply recovered from an excavation made with a shovel. An intact sample was also cut from the slope of the bluff using block sampling procedures. The block sample was then inserted in a wooden box and covered with layers series of wax and plastic wrap to prevent moisture loss. Sieve analysis, hydrometer analysis, Atterberg limit, water content, and compaction tests were performed on a portion of the disturbed sample to classify and characterize the soil.

### *Sieve and Hydrometer Analysis*

To determine the grain size distribution, mechanical sieving was performed according to ASTM D6913 - 04. All of the dry soil passed the #40 sieve. Then a wet sieve analysis was performed to determine the percent retained on the #200 sieve. Again all of the soil sample passed the #200 sieve, which shows the soil is only silt and clay sized. A Hydrometer test was done to determine the gradation of the soil as per ASTM D4221 - 11. Three tests were taken and Figure 11 presents the test results. The test results show that the soil consists of 17% clay and 83% silt as shown in Figure 11 and is considered as a clayey loess.

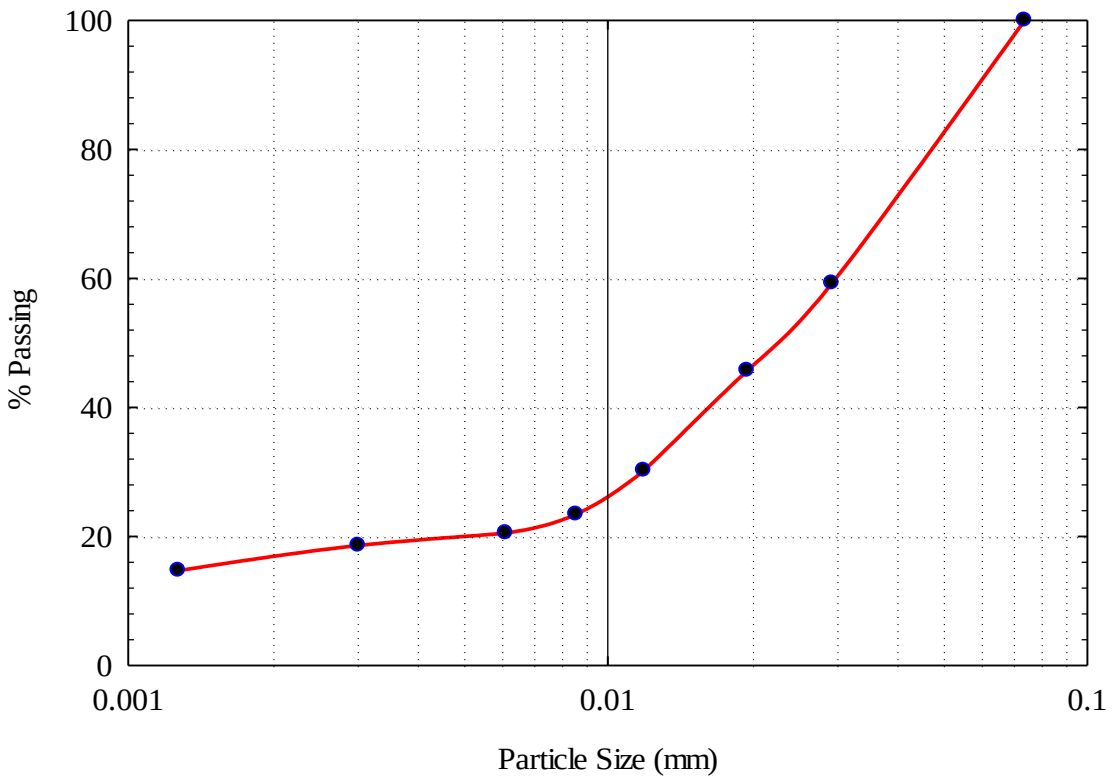


Figure A.1: Gradation of Fulton Loess

*Atterberg Limits*

Atterberg limit tests were performed in accordance with ASTM D 4318 to classify the soil. Table 5 provides a summary of the Atterberg limits. Based on the test results, the soil was classified as low plasticity clayey silt, ML, per the Unified Soils Classification System (USCS).

Table A.1: Atterberg limits test result of Fulton loess

| Average Moisture Content (%) | Liquid Limit (LL) | Plastic Limit (PL) | Plasticity Index (PI) |
|---|---|---|---|
| 28 | 30 | 29 | 1 |

*Compaction Test*

Standard Proctor compaction tests were performed per ASTM D698 – 12 to determine the optimum water content and maximum dry unit weight and obtain the relationship between

dry unit weight and water content of the soil. The test results are plotted in Figure 12 below. The optimum water content is 16.8%, and maximum dry density is 17.4 KN/$m^3$.

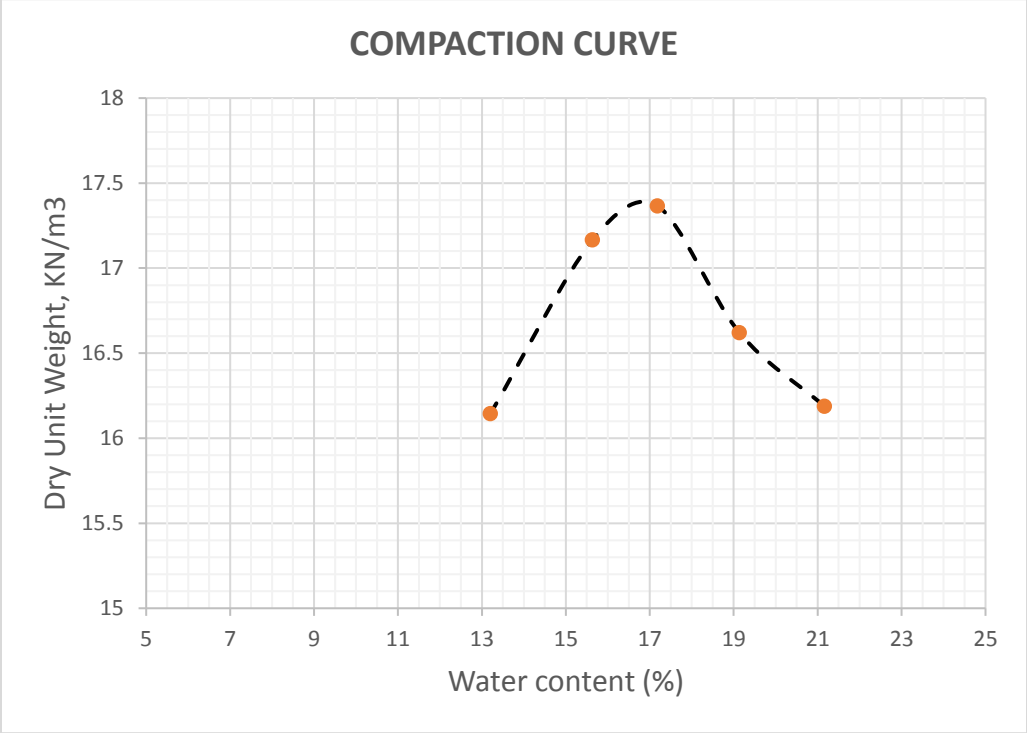


Figure A.2: Dry density and water content relationship of Fulton Loess

## APPENDIX B: TEST RESULTS

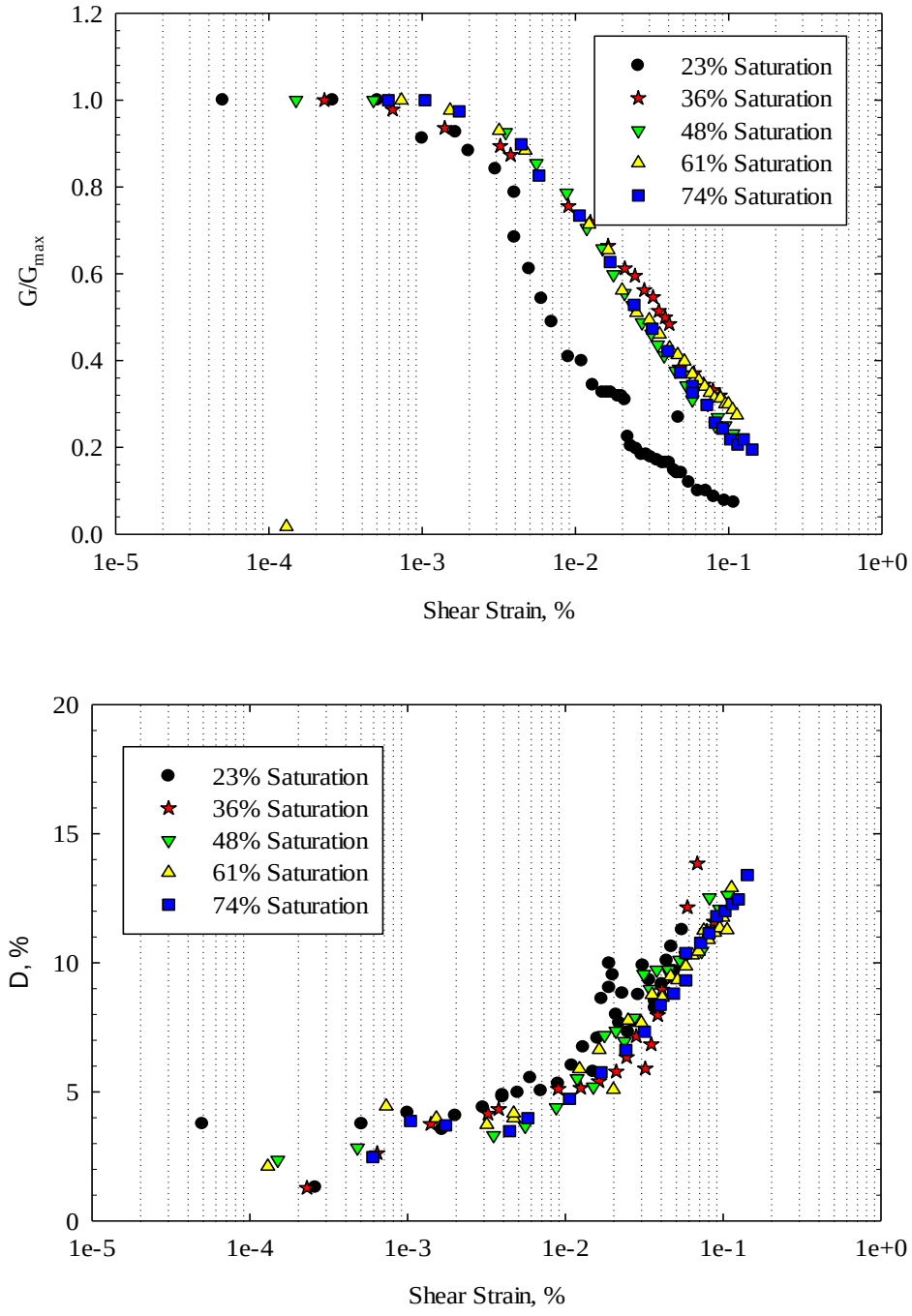


Figure B.1: Shear modulus degradation (top) and damping curve (bottom) of 0.87 void ratio specimen at 50 kPa confining stress

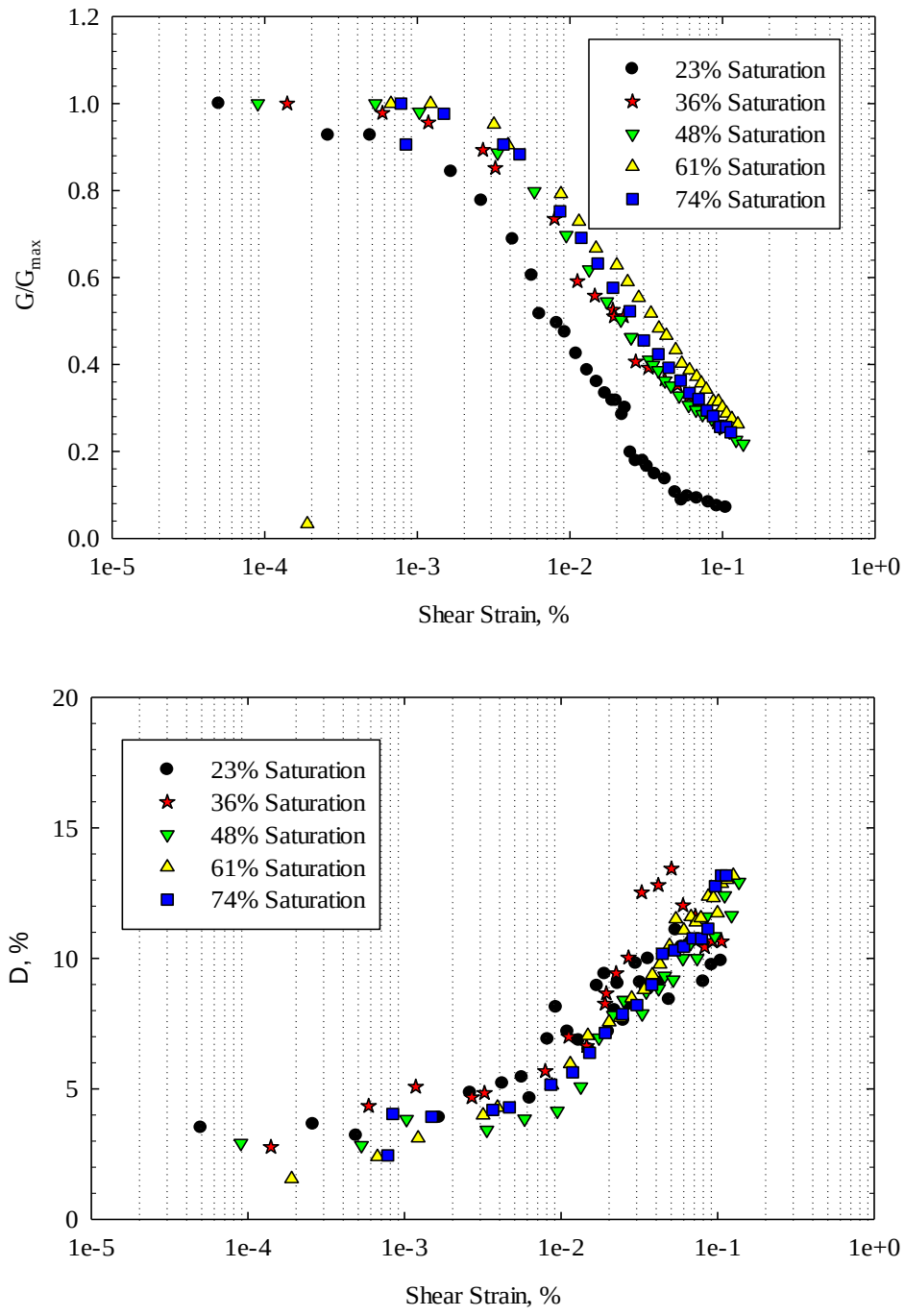


Figure B.2: Shear modulus degradation (top) and damping curve (bottom) of 0.87 void ratio specimen at 200 kPa confining stress

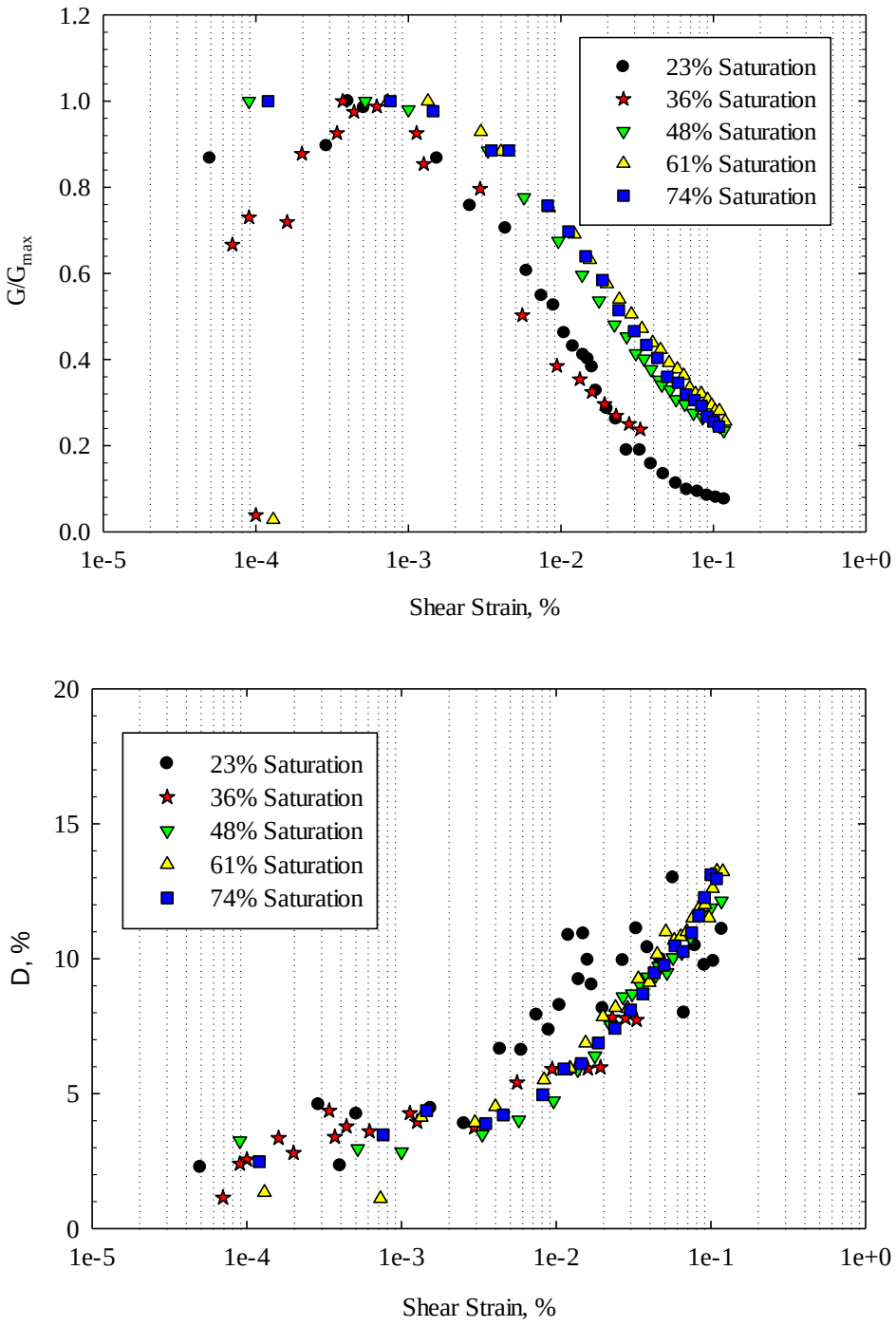


Figure B.3: Shear modulus degradation (top) and damping curve (bottom) of 0.87 void ratio specimen at 400 kPa confining stress

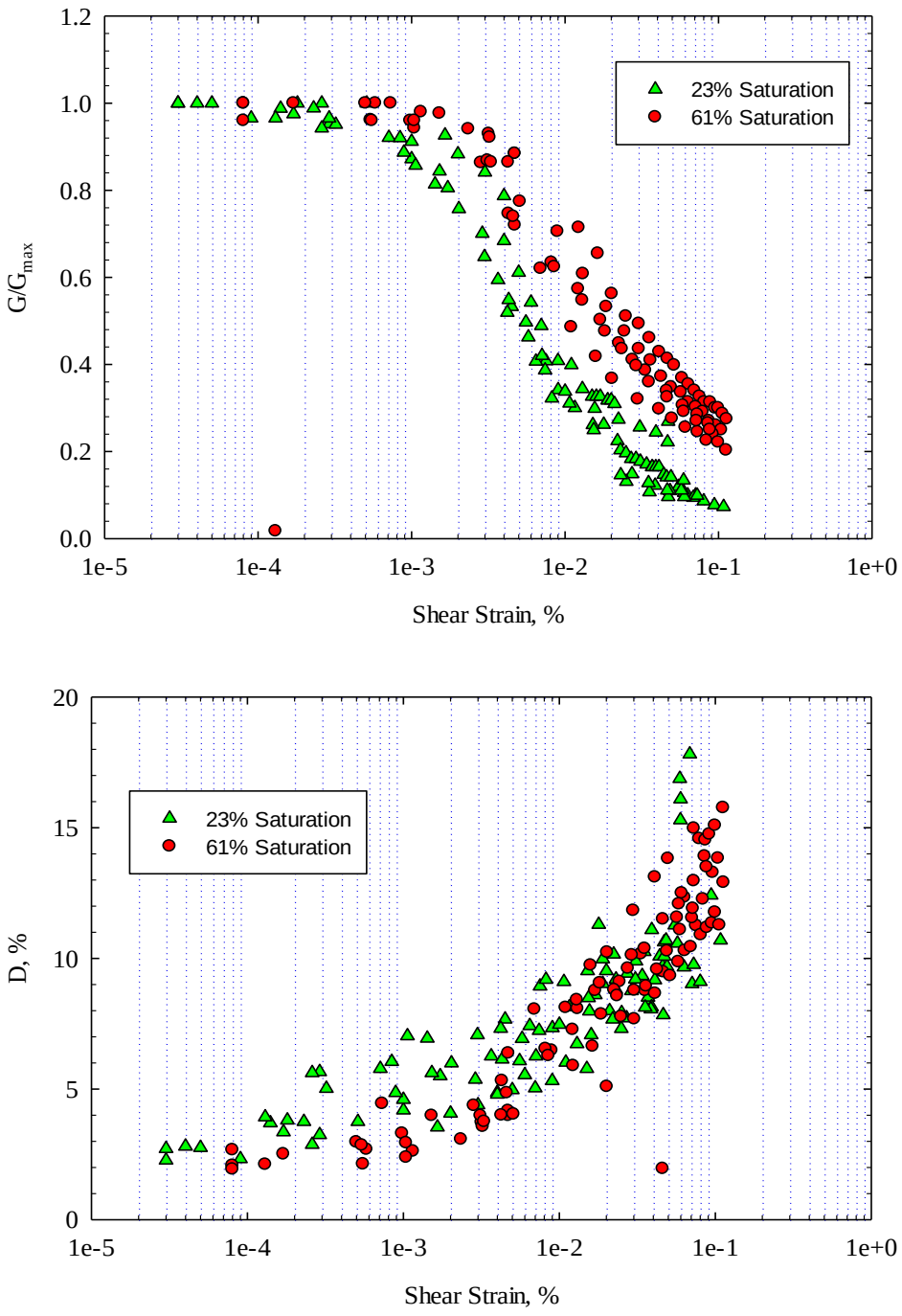


Figure B.4: Shear modulus degradation (top) and damping curve (bottom) of all specimens at 23% and 61% saturation and 0.87 void ratio tested at 50 kPa confining stress

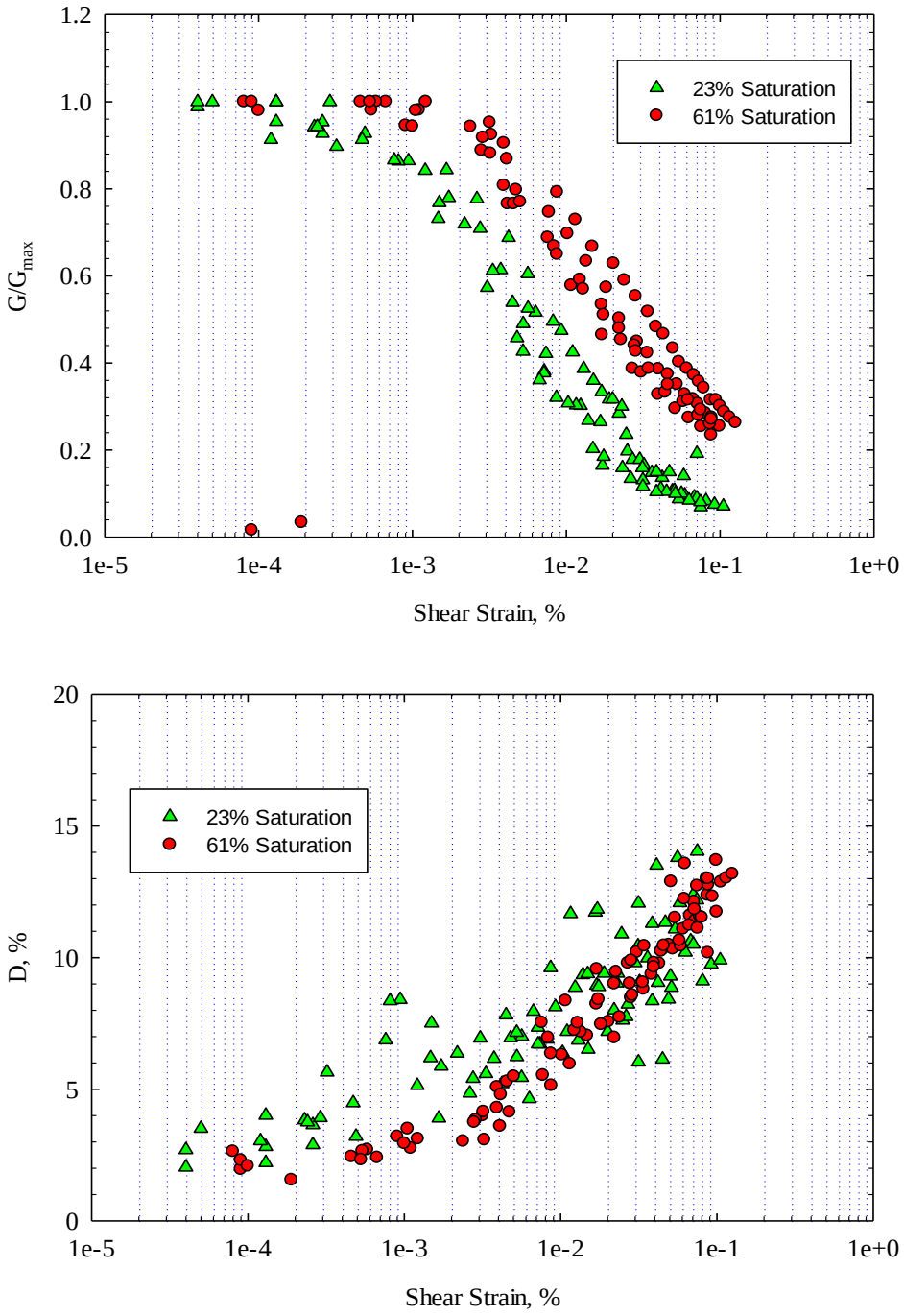


Figure B.5: Shear modulus degradation (top) and damping curve (bottom) of all specimens at 23% and 61% saturation and 0.87 void ratio tested at 200 kPa confining stress

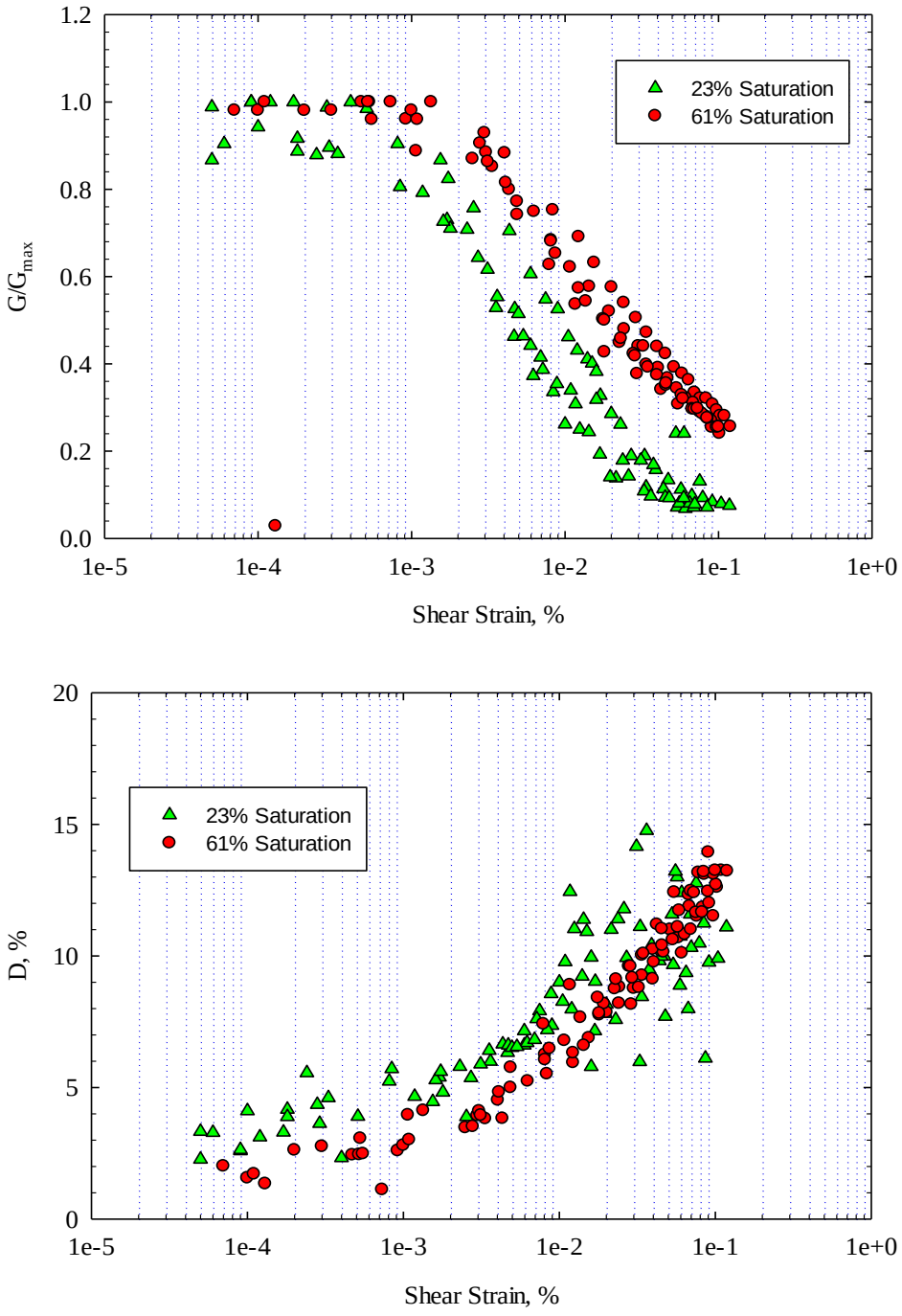


Figure B.6: Shear modulus degradation (top) and damping curve (bottom) of all specimens at 23% and 61% saturation and 0.87 void ratio tested at 400 kPa confining stress

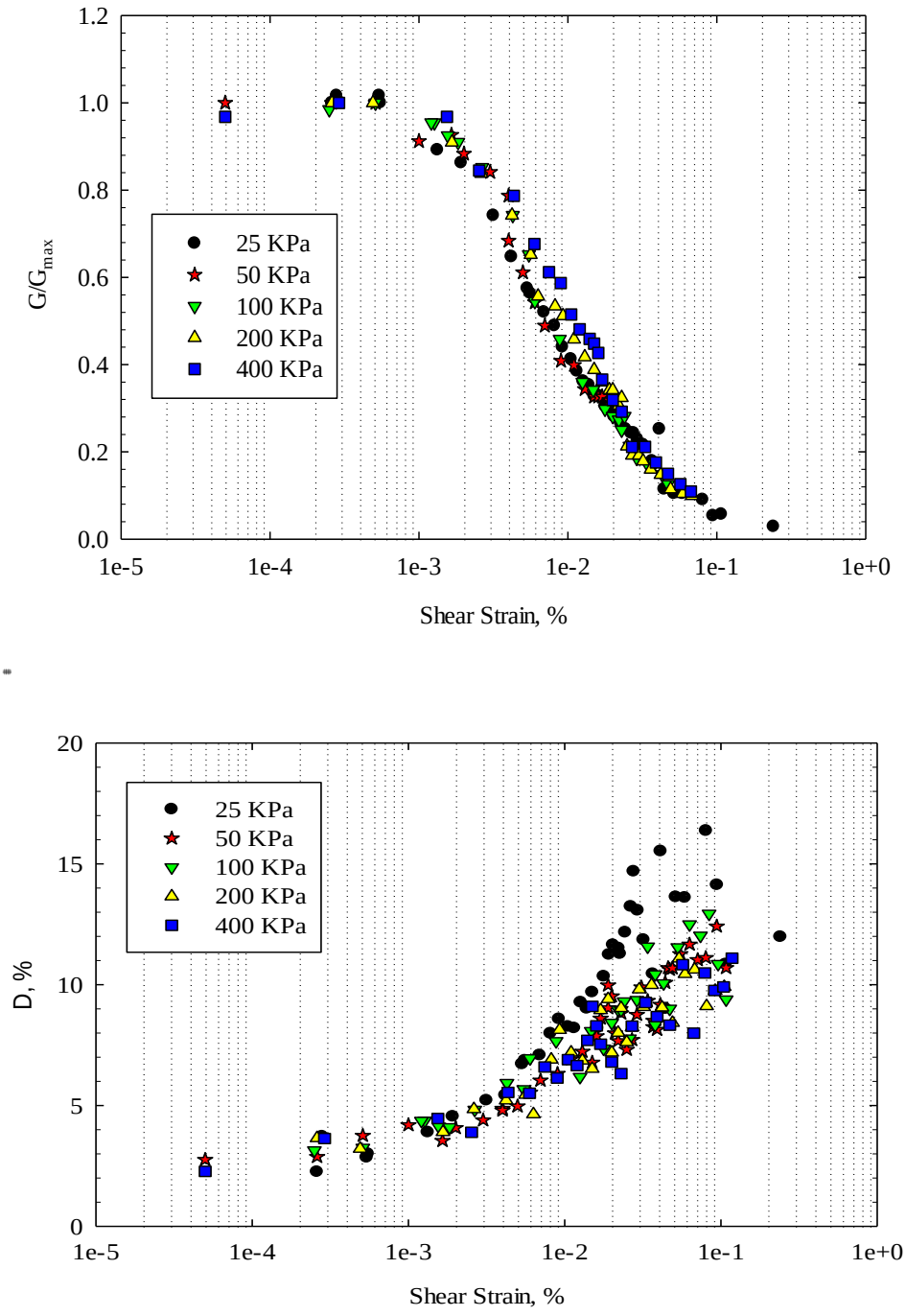


Figure B.7: Effect of confining stress on shear modulus degradation (top) and damping ratio (bottom) for a specimen prepared at 0.87 void ratio and 23% saturation

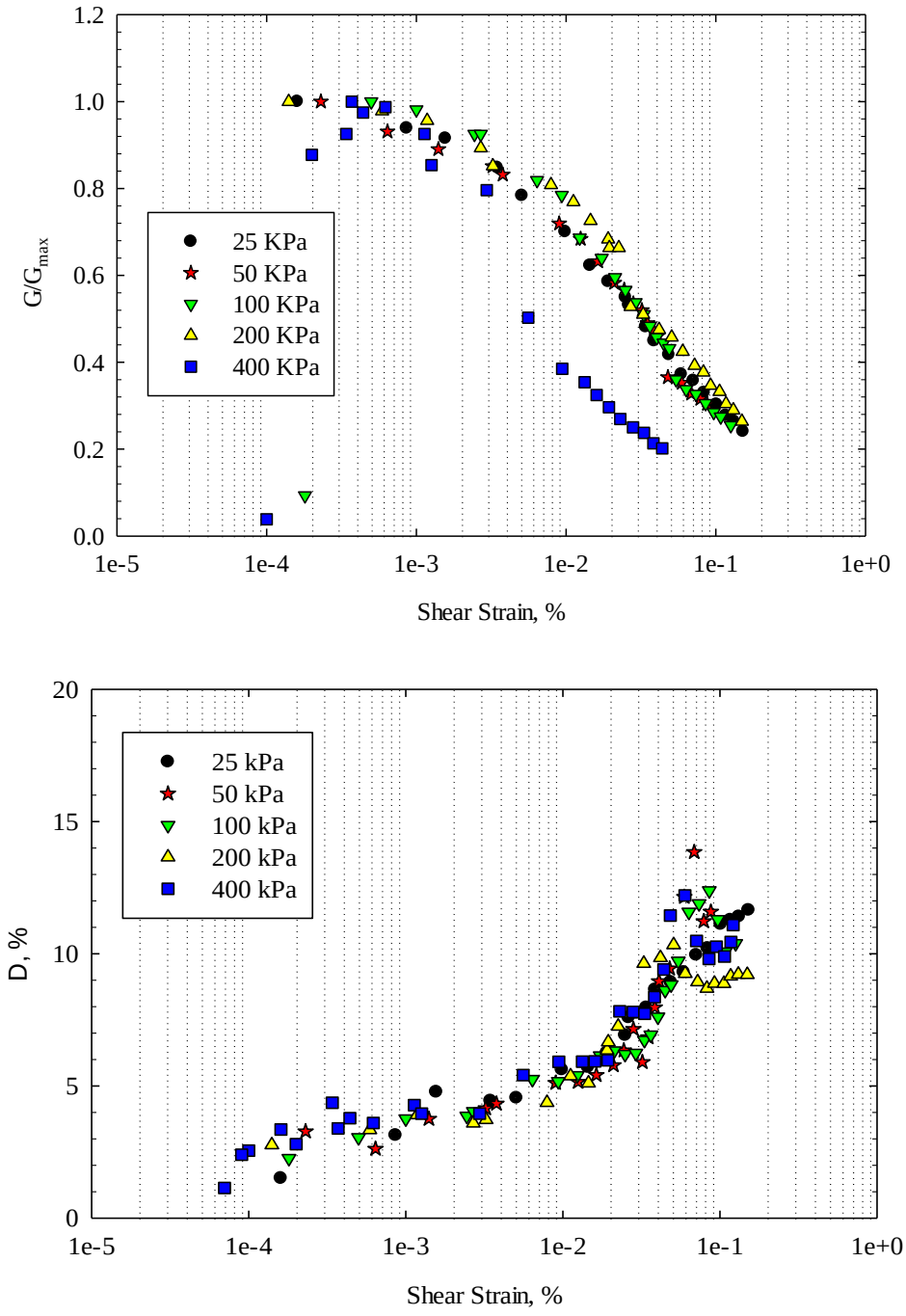


Figure B.8: Effect of confining stress on shear modulus degradation (top) and damping ratio (bottom) for a specimen prepared at 0.87 void ratio and 36% saturation

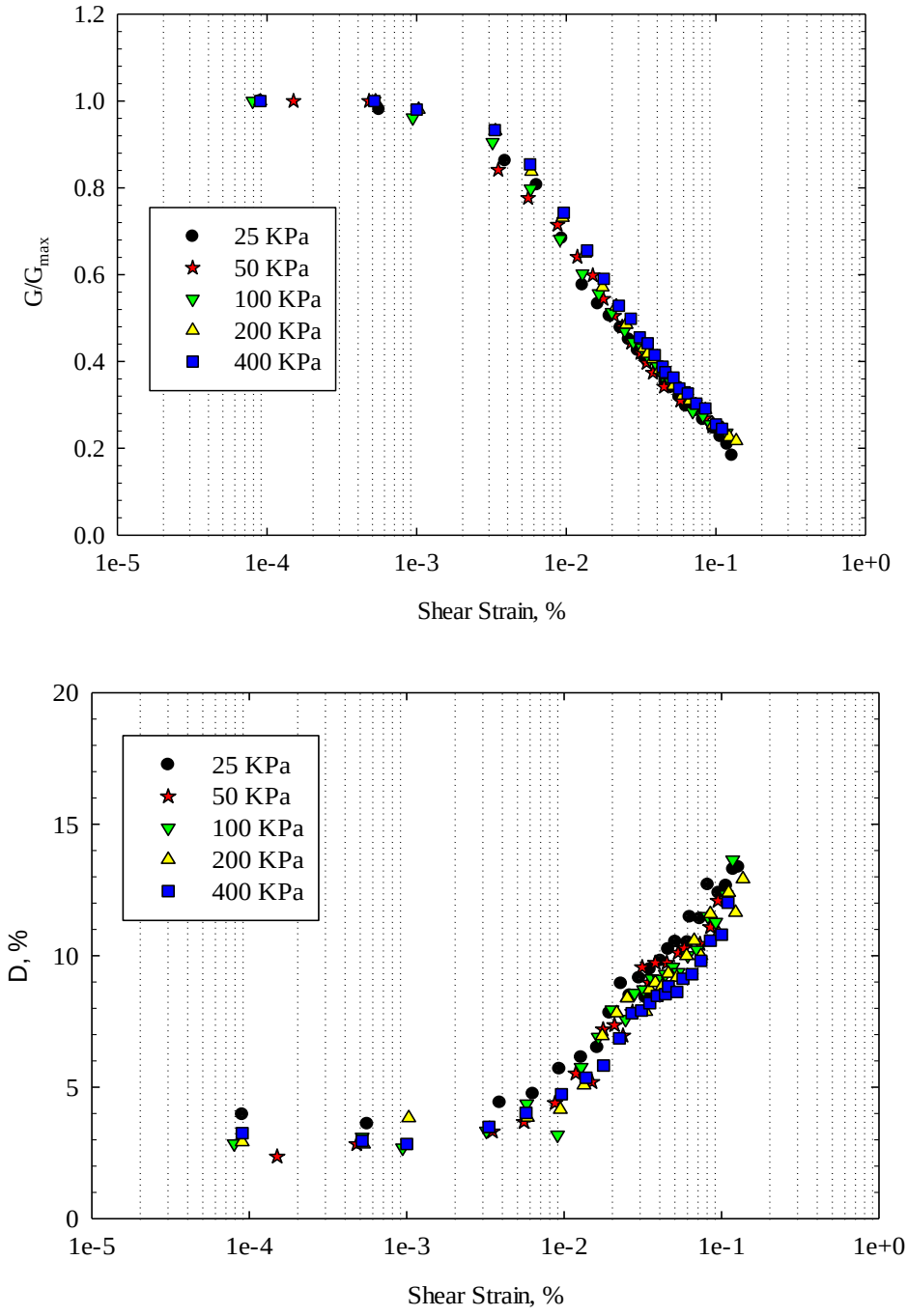


Figure B.9: Effect of confining stress on shear modulus degradation (top)and damping ratio (bottom) for a specimen prepared at 0.87 void ratio and 48% saturation

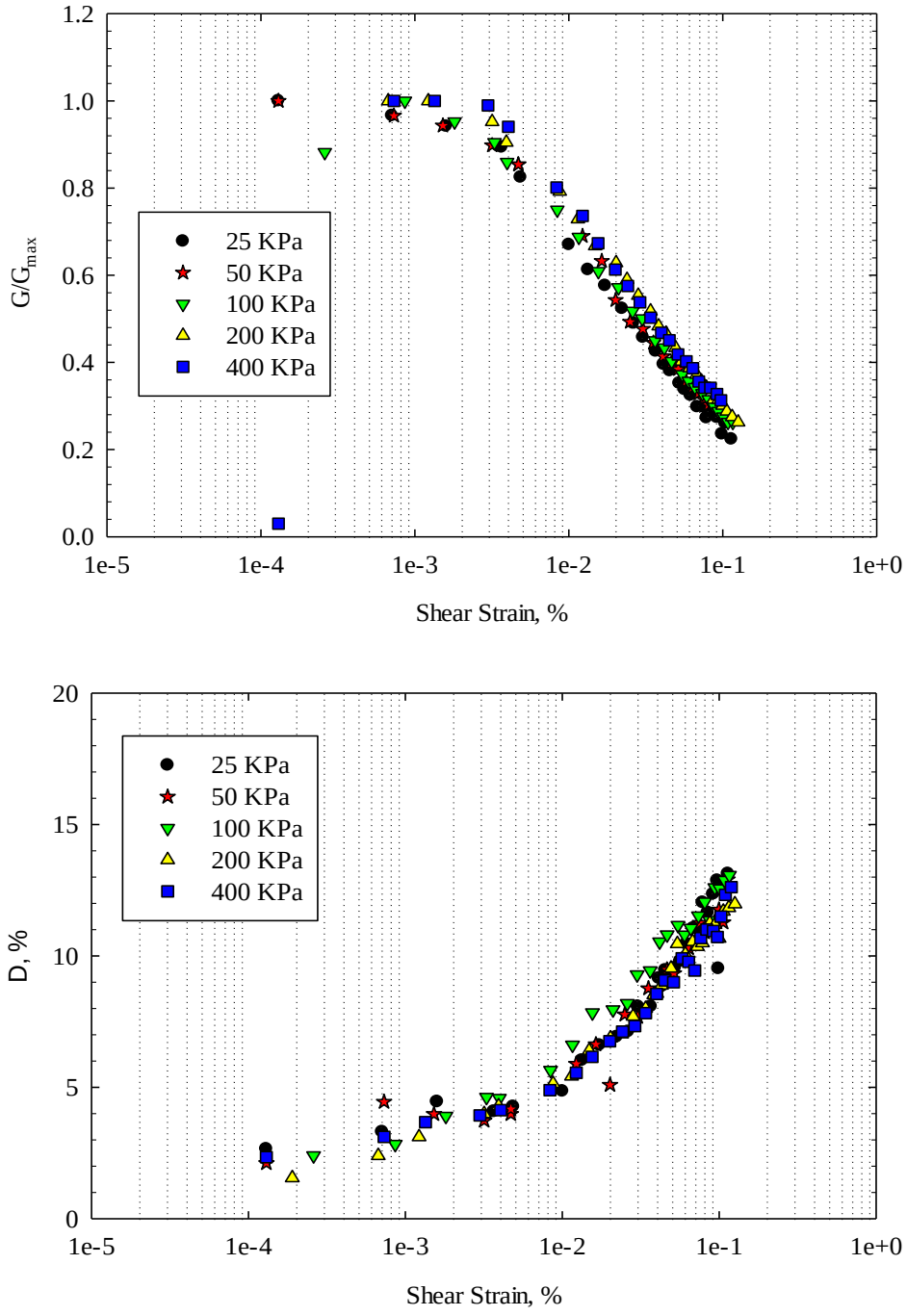


Figure B.10: Effect of confining stress on shear modulus degradation (top) and damping ratio (bottom) for a specimen prepared at 0.87 void ratio and 61% saturation

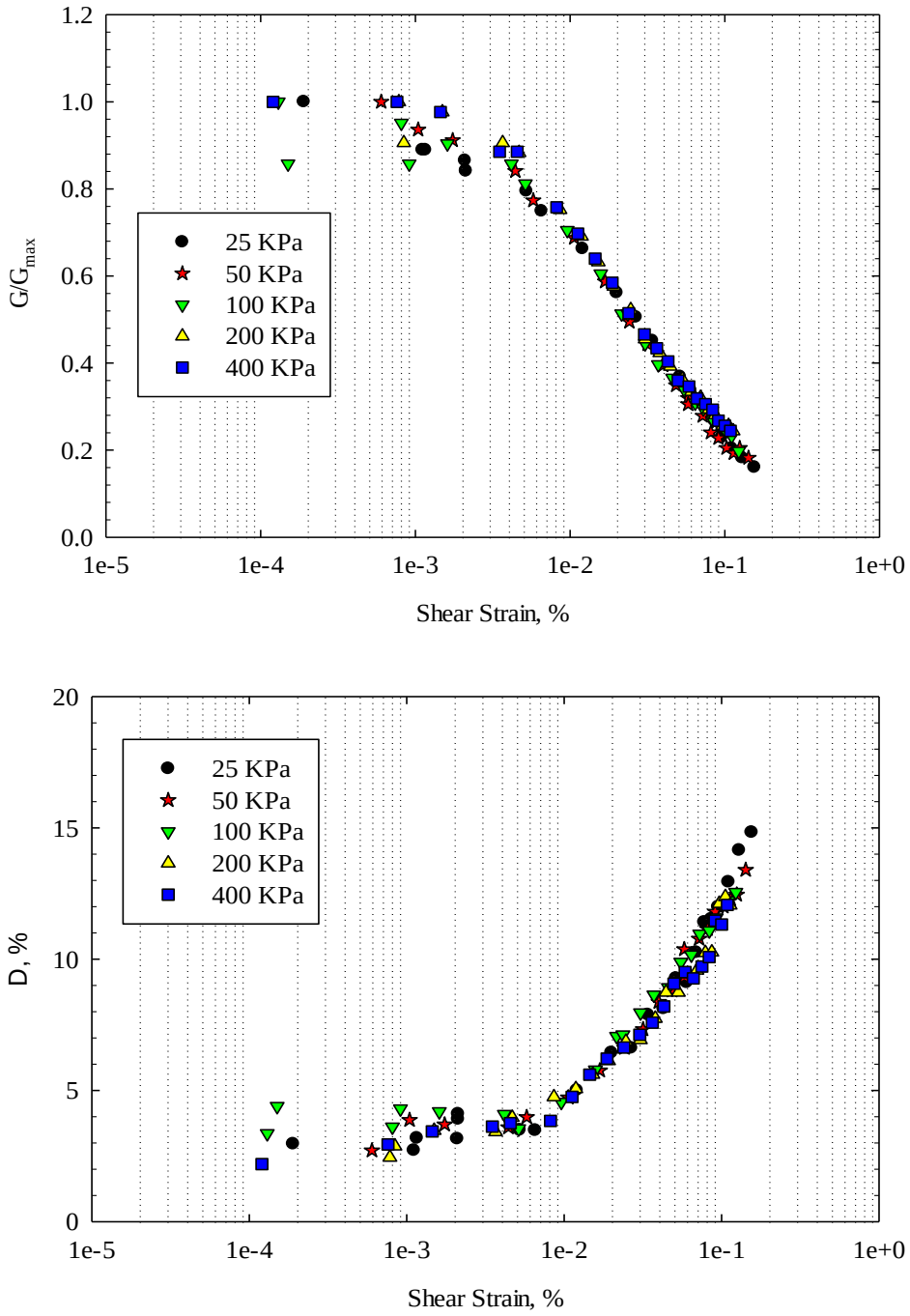


Figure B.11: Effect of confining stress on shear modulus degradation (top) and damping ratio (bottom) for a specimen prepared at 0.87 void ratio and 74% saturation

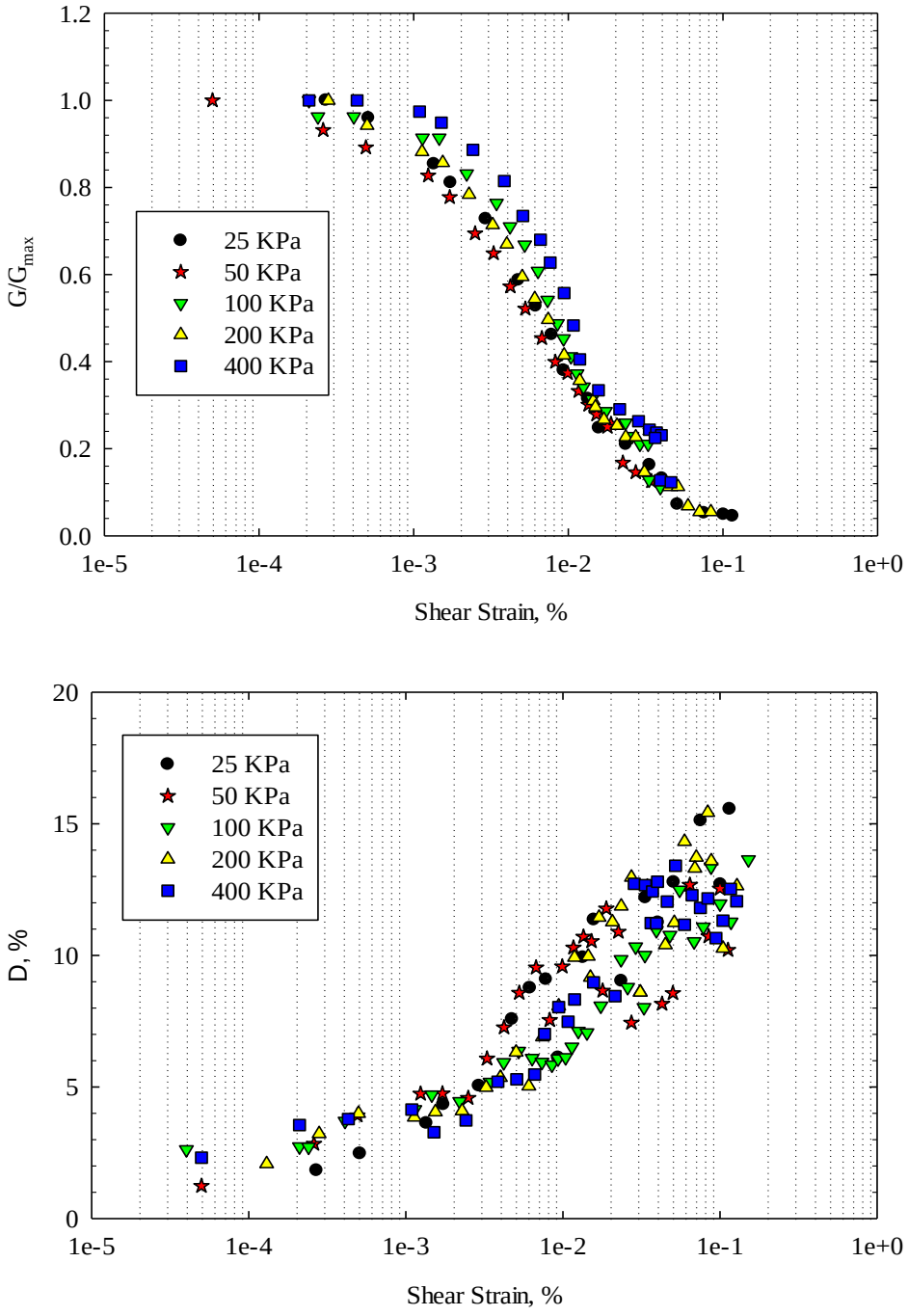


Figure B.12: Effect of confining stress on shear modulus degradation (top) and damping ratio (bottom) for a specimen prepared at 0.7 void ratio and 60% saturation

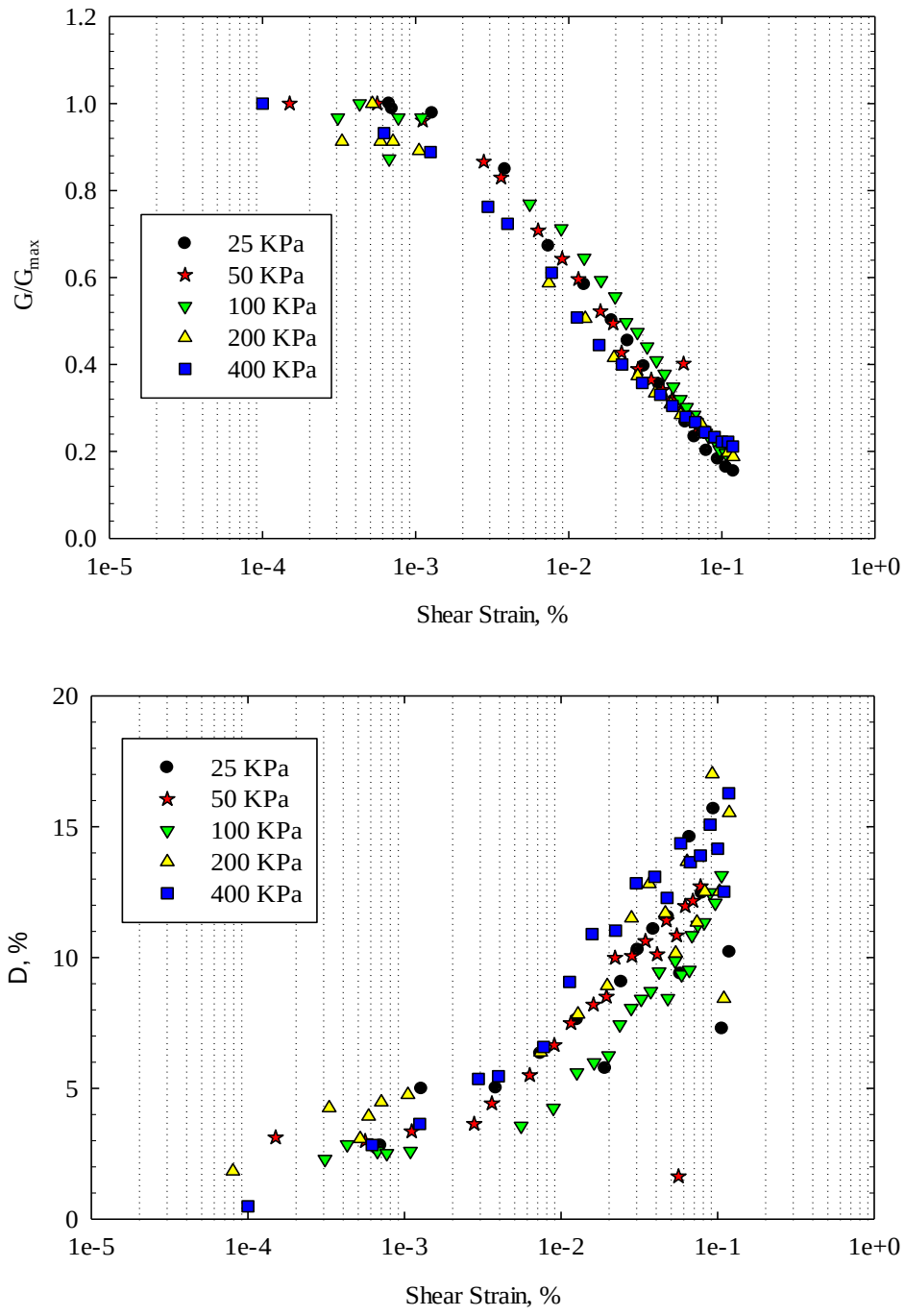


Figure B.13: Effect of confining stress on shear modulus degradation (top) and damping ratio (bottom) for a specimen prepared at 0.7 void ratio and 76% saturation

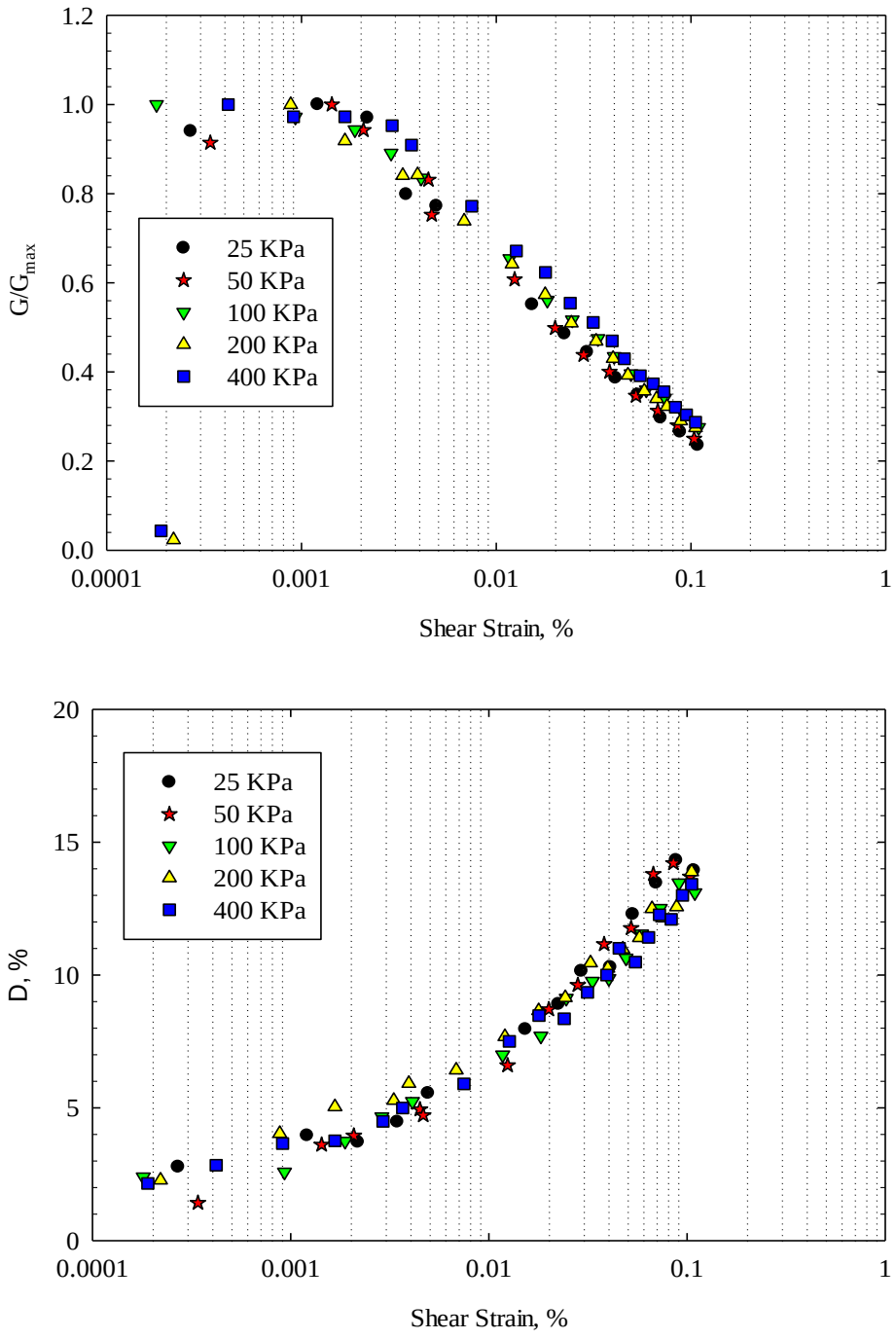


Figure B.14: Effect of confining stress on shear modulus degradation (top) and damping ratio (bottom) for an intact specimen at 1.21 void ratio and 61% saturation

## APPENDIX C: DESIGN EXAMPLE OF A CANTILEVER RETAINING WALL

To investigate the effect of the results of this study a design example of a cantilever retaining wall is provided here. The example uses a simplified ASD design procedure and calculates the factor of safety. The Mononobe-Okabe method of analysis, which is a pseudo-static method, is used to model the seismic earth pressure on the wall. The cantilever retaining wall shown in Figure C.1 is used as a design example. Table 10.1 presents design assumptions for the retain soil and concrete.

Table C.1: Assumptions summary for preliminary design for design example of a cantilever retaining wall

| **Design Assumptions** | **Value** | **Unit** |
|---|---|---|
| Unit weight of retained soil, $\Upsilon_{soil}$ | 18 | $kN/m^3$ |
| Unit weight of concrete $\Upsilon_{conc}$ | 23.5 | $kN/m^3$ |
| Cohesion of retained soil, c | 0 | $kN/m^2$ |
| Friction angle of retained soil, $\phi$ | 29 | degrees |
| Friction angle of foundation soil, $\phi_f$ | 10 | degrees |
| Bearing capacity of foundation soil, $q_{ult}$ | 1000 | kPa |
| Slope of the back of the wall, $\beta$ | 0 | degrees |
| Slope of the surface of the backfill, $\omega$ | 0 | degrees |
| Friction angle between soil & concrete, $\delta$ | 6 | degrees |

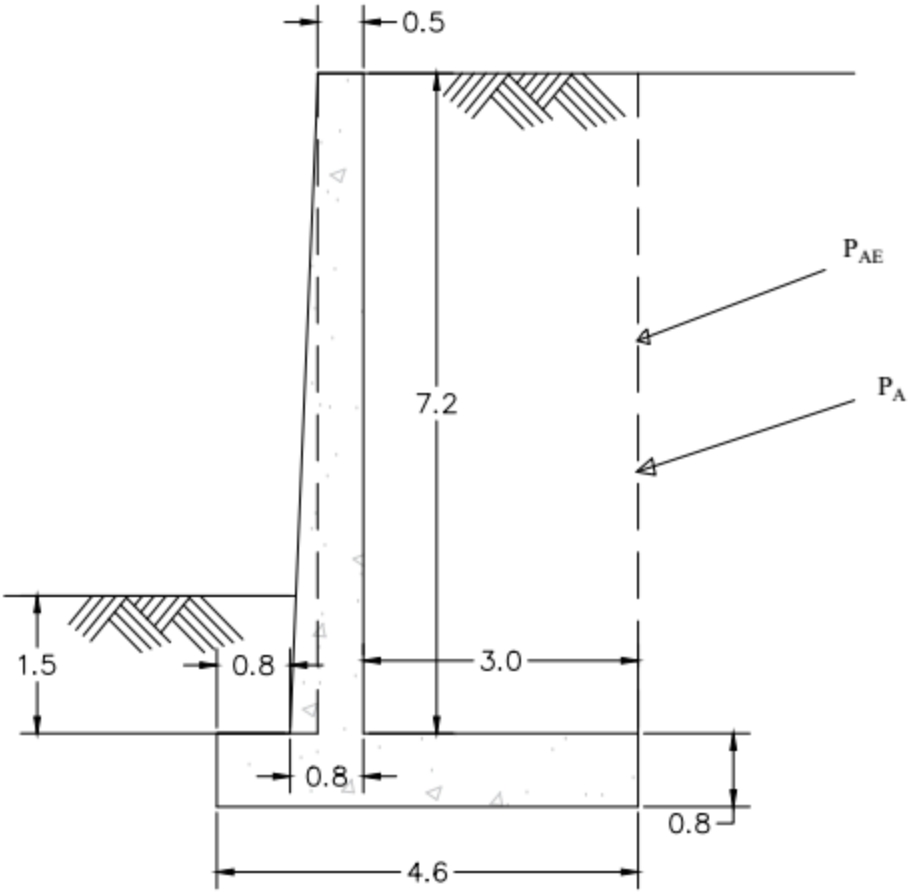


Figure C.1: Concrete cantilever wall example

The active static earth pressure is calculated using Rankine's method.

$$P_A = 0.5 * \Upsilon_{soil} * H^2 * K_A \tag{C.1}$$

where,

$$K_A = \frac{cos^2(\phi - \omega)}{cos^2\,\omega\, cos(\delta + \omega)\left(1 + \sqrt{\frac{sin(\phi + \delta)\, sin(\phi - \beta)}{cos(\delta + \omega)\, cos(\beta - \omega)}}\right)^2} \tag{C.2}$$

The active dynamic earth pressure is calculated using the Mononobe-Okabe method of analysis as (Kramer 1996).

The total active thrust is expressed as

$$P_{AE} = 0.5 * \gamma_{soil} * h^2 * K_{AE} * (1 - K_v) \quad \text{(C.3)}$$

where, H is the height of the wall, and $K_{AE}$ is the dynamic active earth pressure coefficient and is given by AASHTO (2017)

$$K_{AE} = \frac{cos^2(\phi - \theta - \omega)}{cos\,\theta\, cos^2\,\omega\, cos(\delta + \theta + \beta)\left(1 + \sqrt{\frac{sin(\phi + \delta)\, sin(\phi - \theta - \omega)}{cos(\delta + \theta + \omega)\, cos(\beta - \omega)}}\right)^2} \quad \text{(C.4)}$$

where,

$$\theta = tan^{-1}(\frac{k_h}{1 - k_v}) \quad \text{(C.5)}$$

$k_h$ is the horizontal peak ground acceleration,

$k_v$ is the vertical peak ground acceleration,

According to AASHTO (2017), walls and abutments that are free to translate or move during a seismic event may use a reduced horizontal acceleration coefficient, $k_h$, of 0.5 times the peak ground acceleration coefficient and a vertical acceleration coefficient, $k_v$, should be set equal to 0. The resultant force of the Mononobe-Okabe earth pressure distribution, as represented by ΔKae should be applied at 0.6H from the bottom of the pressure distribution.

The total active thrust, $P_{AE}$ (equation (C.3)), can be divided into a static component, $P_A$ (equation (C.1)), and a dynamic component, $\Delta P_{AE}$.

$$P_{AE} = P_A + \Delta P_{AE} \quad \text{(C.6)}$$

The static component, $P_A$, is known to act at H/3 above the base of the wall, whereas, the dynamic component, $\Delta P_{AE}$, is believed to act at 0.6H above the base of the wall. Therefore, the total active thrust, $P_{AE}$, will act at a height,

$$h = \frac{P_A(H/3) + \Delta P_{AE}(0.6H)}{P_{AE}} \quad \text{(C.7)}$$

Using equations, C.1 through C.7, a sample calculation was performed as follows.

*Step1: Calculate the earth pressure using the Mononobe-Okobe method*

Table C.2 shows the earth pressure result calculated using a spreadsheet. In this example calculation, a peak ground acceleration, PGA, of 0.416, determined from the site response analysis of 23% saturated specimens, is used.

Table C.2: Earth pressure calculation for cantilever retaining wall using spreadsheet

| **Parameter** | **value** |
|---|---|
| PGA | 0.416 |
| $K_h$ | 0.208 |
| $K_v$ | 0.00 |
| Ɵ | 11.75 |
| $K_{AE}$ | 0.483 |
| $K_A$ | 0.329 |
| $P_A$ | 189.6 |
| $P_{AE}$ | 278.4 |
| $\Delta P_{AE}$ | 88.8 |
| h | 3.35 |

*Step 2: Calculate the lateral forces and moments about the toe of the footing*

Table C.3 shows force and moment results calculated using a spreadsheet. The passive resistance may be ineffective near to the ground surface because of desiccation and cracking and disturbance during the excavation of the footing and has been ignored in the calculation.

Table C.3: Moment calculation for cantilever retaining wall

| Section | Width, m | Height, m | Area, $m^2$ | Force, kN/m | Moment arm, m | Moment about heel, kN.m/m |
|---|---|---|---|---|---|---|
| Soil on the front side of wall | 0.8 | 1.5 | 0.6 | 10.80 | 0.40 | 4 |
| Concrete wall (stem) | 0.5 | 7.2 | 3.6 | 84.6 | 1.35 | 114 |
| Sloped part of the concrete wall | 0.3 | 7.2 | 1.1 | 25.38 | 1.0 | 25 |
| Concrete footing of the wall | 4.6 | 0.8 | 3.7 | 86.48 | 2.3 | 199 |
| $P_{EV} = P_{AE} * \sin\delta$ | | | | 29 | 4.6 | 134 |
| Summation of vertical forces, $\sum V$ | | | | 625 | $\sum M_r$ | **1682** |
| $P_{EH} = P_{AE} * \cos\delta$ | | | | 277 | 3.35 | 927 |
| $\sum M_d$ | | | | | | **927** |

*Step 3: Calculate the sliding stability*

The factor of safety against sliding is given by,

$$FS_{Sliding} = \frac{\sum Resisiting\ force}{\sum Driving\ force} = \frac{\mu * \sum V}{P_{EH}} \quad \text{(C.8)}$$

where, μ is the interface friction angle between the concrete and the ground, which is considered equal to friction angle of the foundation soil, $\phi_f$. Then, the factor of safety against sliding is,

$FS_{Sliding} = 0.40$

Step 4: Calculate overturning stability

$$FS_{overturning} = \frac{\sum Resisiting\ moment}{\sum Driving\ moment} = \frac{\sum M_r}{\sum M_d} \quad \text{(C.9)}$$

$FS_{overturning} = 1.81$

*Step 4: Calculate bearing stability*

The point of load application from the toe, d, is,

$d = \frac{\sum M_r - \sum M_d}{\sum V} = 1.207\text{m}$

The eccentricity, e, is determined by,

$e = \frac{B}{2} - d$ = 1.09m

Then the maximum bearing pressure is calculated as,

$q_{max} = \frac{\sum V}{\mathrm{B}}\left(1 + \frac{6e}{\mathrm{B}}\right)$ = 329.5 kPa

$FS_{Bearing} = \frac{q_{ult}}{q_{max}}$ = 2.43

In summary, an example calculation for a retaining wall for the determination of factor of safety under earthquake loading has been provided. The sample calculation employs the Mononobe-Okabe earth pressure theory and determines the dynamic earth pressure using the PGA value from the site response analysis performed in this study.

## APPENDIX D: PROGRAM USED FOR DETERMINING BEST-FIT CURVE

*Best fit for Shear modulus degradation*

```
getwd()

setwd("C:/Users/----------/Best fit")

#open the csv file

dat <- read.csv("Efrem12.csv")

head(dat)

#Original Varaibles#

y = dat$y2;

x=dat$x1;

#transformed Variable#

x.t <- log10(x)

#Non- Linear Regression#

fit.nlin=nls(y~1/(1+(x/z)^a),start=list(z=0.01,a=0.85))

sfit.nlin<-summary(fit.nlin)

sfit.nlin

#plot

#install ggplot2 and plotly libraries first

install.packages("ggplot2")

library(ggplot2)

install.packages("plotly")

install.packages("plotly", repos="http://cran.rstudio.com/", dependencies=TRUE)

library(plotly)
```

```
#Append the predicted value to the original data, dat
dat$pred <- predict(fit.nlin)
head(dat)
#get the standard error of the model
se = summary(fit.nlin)$sigma

#Assuming normally distributed errors, 95% prediction intervals are given by
#cacluate the 95% confidence intervals
ci = as.data.frame(outer(dat$pred, c(outer(se, c(-1,1), '*'))*1.96, '+'))

#rename the column names
colnames(ci)<- c("lcl","ucl")

#use ggplot to plot the points and lines
ggplot() +
  geom_point(aes(x1,y2),dat) +
  geom_line(aes(dat$x1, dat$pred), col="blue",lwd=2) +
  geom_line(aes(dat$x1, ci$lcl), col="red", lty =2) +
  geom_line(aes(dat$x1, ci$ucl), col="red", lty =2)
```

*Best-fit for Damping Curve*

```
#Original Varaibles#
```

```
d = dat$y3;

x=dat$x1;

#transformed Variable#

x.t <- log10(x)


#Non- Linear Regression#

C1 <- -1.1143*a^2+1.8618*a+0.2523

C2 <- 0.0805*a^2-0.071*a-0.0095

C3 <- -0.0005*a^2+0.0002*a+0.0003

Dmasa <- 100/pi*((4*(x-z*log((x+z)/z))/(x^2/(x+z)))-2)

Dmas <- (C1*Dmasa)+(C2*Dmasa^2)+(C3*Dmasa^3)


fit.nlin=nls(d~(y*(1/(1+(x/z)^a))^0.1*Dmas+Dmin), start=list(Daran=0.5, Dmin=3))

sfit.nlin<-summary(fit.nlin)

sfit.nlin



#Append the predicted value to the original data, dat

dat$pred <- predict(fit.nlin)

head(dat)

#get the standard error of the model

se = summary(fit.nlin)$sigma
```

```
#Assuming normally distributed errors, 95% prediction intervals are given by

#cacluate the 95% confidence intervals

ci = as.data.frame(outer(dat$pred, c(outer(se, c(-1,1), '*'))*1.96, '+'))


#rename the column names

colnames(ci)<- c("lcl","ucl")


#use ggplot to plot the points and lines

ggplot() +

  geom_point(aes(x1,y3),dat) +

  geom_line(aes(dat$x1, dat$pred), col="blue",lwd=2) +

  geom_line(aes(dat$x1, ci$lcl), col="red", lty =2) +

  geom_line(aes(dat$x1, ci$ucl), col="red", lty =2)
```